LBL-31553

Lawrence Berkeley Laboratory

UNIVERSITY OF CALIFORNIA

Materials & Chemical Sciences Division

Magnetic Flux Noise in Copper Oxide Superconductors

M.J. Ferrari
(Ph.D. Thesis)

November 1991

LOAN COPY
Circulates
for 4 weeks
Bldg. 50 Library.
LBL-31553
Copy 2

Prepared for the U.S. Department of Energy under Contract Number DE-AC03-76SF00098

DISCLAIMER

This document was prepared as an account of work sponsored by the United States Government. Neither the United States Government nor any agency thereof, nor The Regents of the University of California, nor any of their employees, makes any warranty, express or implied, or assumes any legal liability or responsibility for the accuracy, completeness, or usefulness of any information, apparatus, product, or process disclosed, or represents that its use would not infringe privately owned rights. Reference herein to any specific commercial product, process, or service by its trade name, trademark, manufacturer, or otherwise, does not necessarily constitute or imply its endorsement, recommendation, or favoring by the United States Government or any agency thereof, or The Regents of the University of California. The views and opinions of authors expressed herein do not necessarily state or reflect those of the United States Government or any agency thereof or The Regents of the University of California and shall not be used for advertising or product endorsement purposes.

Lawrence Berkeley Laboratory is an equal opportunity employer.

DISCLAIMER

This document was prepared as an account of work sponsored by the United States Government. While this document is believed to contain correct information, neither the United States Government nor any agency thereof, nor the Regents of the University of California, nor any of their employees, makes any warranty, express or implied, or assumes any legal responsibility for the accuracy, completeness, or usefulness of any information, apparatus, product, or process disclosed, or represents that its use would not infringe privately owned rights. Reference herein to any specific commercial product, process, or service by its trade name, trademark, manufacturer, or otherwise, does not necessarily constitute or imply its endorsement, recommendation, or favoring by the United States Government or any agency thereof, or the Regents of the University of California. The views and opinions of authors expressed herein do not necessarily state or reflect those of the United States Government or any agency thereof or the Regents of the University of California.

LBL-31553

Magnetic Flux Noise in Copper Oxide Superconductors

Mark Joseph Ferrari

Department of Physics,
University of California
Berkeley, CA 94720

and

Materials Sciences Division
Lawrence Berkeley Laboratory
University of California
Berkeley, CA 94720

September 1991

This work was supported by the Director, Office of Energy Research, Office of Basic Energy Sciences, Materials Sciences Division of the U.S. Department of Energy under contract number DE-AC03-76SF00098.

Magnetic Flux Noise in Copper Oxide Superconductors

Copyright © 1991

by

Mark Joseph Ferrari

The U.S. Department of Energy has the right to use this thesis
for any purpose whatsoever including the right to reproduce
all or any part thereof

Magnetic Flux Noise in Copper Oxide Superconductors

by

Mark Joseph Ferrari

ABSTRACT

Magnetic flux noise and flux creep in thin films and single crystals of $YBa_2Cu_3O_{7-x}$, $Bi_2Sr_2CaCu_2O_{8+x}$, $Tl_2Ca_2Ba_2Cu_3O_x$, and $TlCa_2Ba_2Cu_3O_x$ are measured with a superconducting quantum interference device (SQUID). The noise power spectrum generally scales as $1/f$ (f is frequency) from 1 Hz to 1 kHz, increases with temperature, and decreases in higher-quality films. It is proportional to the magnetic field B in which the sample was cooled, at least in the range 0.1 mT < B < 3 mT. A model of thermally activated vortex motion is developed which explains the dependence of the noise on frequency, temperature, current, and applied magnetic field. The pinning potential is idealized as an ensemble of double wells, each with a different activation energy separating the two states. From the noise measurements, this model yields the distribution of pinning energies in the samples, the vortex hopping distance, the number density of mobile vortices, and the restoring force on a vortex at a typical pinning site. The distribution of pinning energies in $YBa_2Cu_3O_{7-x}$ shows a broad peak below 0.1 eV. The small ambient magnetic field, and the detection of noise even in the absence of a driving force, insure that the measured pinning energies are characteristic of isolated vortices near

thermal equilibrium. The observed vortex density in fields much less than 0.1 mT is too large to be explained by the ambient field, suggesting a mechanism intrinsic to the sample which produces trapped vortices. Vortex motion is shown to be one limitation on the sensitivity of practical SQUIDs and flux transformers fabricated from copper oxide superconductors, and a method involving a circulating supercurrent is introduced to improve this sensitivity. The success of this method implies that the two sites in each double well in the ensemble have nearly the same activation energy. Signals produced by the motion of a single vortex are also detected, from which the hopping distance and activation energy can be extracted.

Table of Contents

Table of Symbols iii
Table of Abbreviations ix
Acknowledgements x
I. Introduction 1
Abrikosov Vortices and Pinning 1
Copper Oxide Superconductors 5
Superconducting Magnetometers 6
II. The Apparatus 10
SQUID 10
Samples 13
McDLT Cryostat 18
Electronics 22
Experimental Procedure 25
III. Random Telegraph Signals 31
Observation of Random Telegraph Signals 32
Direct Noise Mechanism 34
Temperature Dependence of Lifetimes 38
Activation Energies for Vortex Motion 41
Noisy and Quiet Metastable States 46
IV. 1/*f* Noise 52
Dependence on Temperature and Sample Quality 52
Testing the Direct Noise Mechanism 61
V. 1/*f* Noise as a Superposition of Random Telegraph Signals 64
Extended Dutta-Dimon-Horn Model 65

Checking the Slope of the Noise Power Spectrum 68
Measuring the Distribution of Activation Energies 72
An *a*-Axis Sample 77
Why Not a Distribution of Attempt Times? 81
VI. Flux Transformers 83
Fabrication 84
Indirect Noise Mechanism 87
Testing the Indirect Noise Mechanism 91
Hybrid Magnetometer Performance 95
VII. Current Dependence 97
Reversible Suppression of $1/f$ Noise 97
Dutta-Dimon-Horn Model with Lorentz Force Terms 101
Two-Dimensional Pinning Model 105
Multiplicity and Distribution of Activation Energies 108
Hopping Distances and Restoring Forces 112
Excess Vortices 115
Current Dependence of a Random Telegraph Signal 117
VIII. Magnetic Field Dependence 121
Incoherent Vortex Motion 122
Excess Vortices Revisited 125
Flux Creep 126
Time Dependence of Field Cooled Noise 129
IX. Summary and Prospects 133
Conclusions 133
Unanswered Questions 136
References 139

Table of Symbols

a	Inner radius of SQUID
a_p	Temperature-independent pinning length
a_0	Mean distance between vortices, approximately $n_v^{-1/2}$
A	Total area of flux transformer segments
A_{eff}	Flux-focusing area of SQUID, $4ac$
A_ℓ	Area of circle between pinning sites in a switching process
A_p	Area enclosed by flux transformer pickup loop
A_s	Area of sample
B	Applied magnetic field
B_c	Thermodynamic critical field
B_{c1}	Lower critical field
B_{eff}	Areal density of vortices expressed as a magnetic field, $n_v\Phi_0$
B_0	Applied field necessary to produce one flux quantum in SQUID
c	Outer radius of SQUID
C	Heat capacity of hot side
C_t	Tank circuit capacitance
d	Distance between sample and SQUID
d_s	Thickness of sample
$D(\ell)$	Distribution of hopping distances in DDH ensemble
$D(U_0)$	Distribution of activation energies in DDH ensemble
$D(\tau_0)$	Distribution of correlation time prefactors in Scofield ensemble
e	Elementary charge
f	Frequency
F	Lorentz force

g	Factor by which flux transformer increases magnetic field responsivity of SQUID
G	Thermal conductance from hot side to cold side
h	Planck's constant
$\hbar$	Reduced Planck's constant, $h/2\pi$
$\boldsymbol{h}(r)$	Local magnetic field on a scale finer than the penetration depth
i	Integer which labels states of an RTS
I	Current in flux transformer
I_b	SQUID bias current
I_c	SQUID critical current, $2I_0$ for $\Phi = 0$
I_f	Current in field coil
I_0	Critical current of one Josephson junction
J_c	Critical current density
$k(T)$	Temperature-dependent pinning spring constant
k_B	Boltzmann's constant
k_0	Pinning spring constant at zero temperature, $k(0)$
$\boldsymbol{\ell}$	Vortex hopping distance
$\boldsymbol{\ell}_{cr}$	Length of crossunder
$\boldsymbol{\ell}_i$	Length of input coil
$\boldsymbol{\ell}_p$	Length of pickup loop
L	Self-inductance of SQUID
L_i	Self-inductance of flux transformer input coil
L_p	Self-inductance of flux transformer pickup loop
L_s	Self-inductance of sample ring
L_t	Tank circuit inductance
L_x	Self-inductance of an unknown structure

m	Slope of noise power spectrum, $S_\Phi(f) \propto 1/f^m$
M	Mutual inductance between feedback coil and SQUID
M_f	Mutual inductance between field coil and SQUID
M_i	Mutual inductance between input coil and SQUID
M_s	Mutual inductance between sample ring and SQUID
n	Exponent of coherence length in activated volume
n_s	Areal density of pinning sites
n_v	Areal density of vortices
N	Number of turns in flux transformer input coil
N_p	Number of switching processes in ensemble
N_v	Number of vortices
$p(\ell)$	Probability that sites separated by ℓ constitute a process
P_v	Number of bistable hopping processes per vortex
Q	Quality factor of tank circuit
r	Radial distance from center of vortex or pinning site
r_s	Position of pinning site
r_v	Position of vortex
R_f	Resistance of feedback current sense resistor
$S_B(f)$	Spectral density of field noise in magnetometer
$S_r(f)$	Spectral density of radial component of vortex motion
$S_V(f)$	Spectral density of feedback voltage noise
$S_\Phi(f)$	Spectral density of flux noise
$S_\Phi^{(in)}(f)$	Spectral density of indirect noise from flux transformer
$S_\Phi^{(S)}(f)$	Spectral density of flux noise intrinsic to SQUID
t	Reduced temperature, T/T_c
t	Time

t_0	Time at which $\Phi = 0$
T	Temperature
T_c	Superconducting transition temperature
T_m	Midpoint of temperature range for a random telegraph signal
T_{peak}	Temperature corresponding to a peak in $D(U_0)$
$u(r,T)$	Vortex potential energy due to single pinning site
$U(T)$	Temperature-dependent activation energy
$U^{(i)}(T)$	Activation energy in ith state of random telegraph signal
U_0	Activation energy at zero temperature, $U(0)$
$\tilde{U}_0(f,T)$	Zero-temperature activation energy of processes currently in experimental bandwidth
$U_{0,peak}$	Zero-temperature activation energy at which $D(U_0)$ peaks
V	Voltage across SQUID
V_{cal}	Feedback voltage corresponding to one flux quantum
V_f	Voltage across feedback current sense resistor
w	Width of SQUID washer at its narrowest
w_{cr}	Width of crossunder
w_i	Width of input coil
w_j	Width of generic segment of flux transformer
w_p	Width of pickup loop
w_s	Width of sample
α	Labusch parameter
α_i	Coefficient of inductive coupling between SQUID and input coil
α_s	Coefficient of inductive coupling between SQUID and sample
β	SQUID modulation parameter, $2LI_0/\Phi_0$

$\beta(T)$	Product of thermodynamic beta and normalized temperature dependence of activation energy, $U(T)/U_0 k_B T$
γ	Ratio of lifetimes of random telegraph signal, τ_1/τ_2
δ	Dimensionless misalignment parameter, $I\Phi_0 \ell \cos\theta / 2 w_j k_B T$
ΔI	Change in flux transformer current
ΔI_c	Difference of SQUID critical current for $\Phi = 0$ and for $\Phi = \Phi_0/2$
ΔM_f	Change in mutual inductance between field coil and SQUID at T_c
ΔU	Energy difference between minima of double well potential
ΔV	SQUID modulation amplitude measured at preamplifier output
$\Delta\Phi$	Amplitude of random telegraph signal
ε_ℓ	Self-energy per unit length of vortex
ζ	Dimensionless flux noise parameter in Eq. (6-3)
$\zeta^{(cr)}$	Value of ζ for direct noise from crossunder
$\zeta^{(i)}$	Value of ζ for direct noise from input coil
$\zeta^{(in)}$	Value of ζ for indirect noise from flux transformer
$\zeta^{(u)}$	Value of ζ for direct noise from unpatterned film
η	Coefficient of viscous damping of vortex motion
θ	Angle between Lorentz force and vortex trajectory
κ	Ginzburg-Landau parameter, λ/ξ
λ	Magnetic penetration depth
λ_{ab}	Penetration depth for screening currents in the *a-b* plane
μ_0	Permeability of free space
ν	Exponent in energy dependence of hopping distance, $\ell \propto U_0^\nu$
ξ	Ginzburg-Landau coherence length
ξ_{ab}	Ginzburg-Landau coherence length in *a-b* plane
ρ_n	Resistivity in normal state

τ	Correlation time of random telegraph signal, $(\tau_1^{-1} + \tau_2^{-1})^{-1}$
τ_{Ai}	Attempt time in ith state of random telegraph signal
τ_i	Lifetime of ith state of random telegraph signal
τ_0	Correlation time prefactor, $\tau_{Ai}/2$
Φ	Magnetic flux linking SQUID
Φ_ℓ	Maximum flux change caused by vortex hopping a unit distance
Φ_x	Magnetic flux linking an unknown structure
Φ_0	Magnetic flux quantum, $h/2e$
Φ_1	Logarithmic flux creep rate
ψ	Ginzburg-Landau order parameter

Table of Abbreviations

BCS	Bardeen, Cooper, and Schrieffer, Ref. [1]
BSCCO	$Bi_2Sr_2CaCu_2O_{8+x}$
DDH	Dutta, Dimon, and Horn, Ref. [2]
FET	Field effect transistor
FT	Flux transformer
GL	Ginzburg and Landau, Ref. [3]
McDLT	Flux noise apparatus described in this dissertation, or the eponymous McDonald's lettuce and tomato hamburger
RTS	Random telegraph signal
SQUID	Superconducting quantum interference device
TCBCO	$Tl_2Ca_2Ba_2Cu_3O_x$ or $TlCa_2Ba_2Cu_3O_x$
YBCO	$YBa_2Cu_3O_{7-x}$
YSZ	Yttrium-stabilized ZrO_2

Acknowledgements

I am very grateful to my research advisor, Prof. John Clarke, for giving me the opportunity to work on an exciting experiment in an exciting field. His insights guided my work from the construction of the apparatus to the analysis of the data. I can only hope I have picked up some of his ability to see to the heart of an issue.

It is a privilege to be paid to indulge one's curiosity. I gratefully acknowledge the National Science Foundation, the Department of Education, the California Competitive Technology Program, and the Department of Energy (through Lawrence Berkeley Laboratory) for the support which made my graduate work possible.

This dissertation describes measurements made on sixteen samples, all of them fabricated by others. In most cases my collaborators performed extensive measurements to characterize the samples. I am indebted to Kookrin Char and Todd Hylton for YBCO(1); Chang-Beom Eom for YBCO(2) and YBCO(6); Arun Inam, Lawrence Nazar, "Venky" Venkatesan, and Xin Di Wu for YBCO(3); Peter Rosenthal and Bob Hammond for YBCO(4) and YBCO(5); Jack Kingston and Fred Wellstood for YBCO(7), YBCO(8), YBCO(9), and the flux transformers; Dave Mitzi for the BSCCO crystals; and Wen Lee and Stuart Parkin for the TCBCO films. I would particularly like to thank Mac Beasley, Ted Geballe, and Aharon Kapitulnik, not only for their leadership of the Stanford group which produced almost half of the samples listed above, but also for inspiring conversations.

It would be difficult to overstate the importance of Fred Wellstood's contributions to the success of my experiment. The McDLT apparatus has its origins in Fred's concept of a scanning SQUID. In addition, Fred fabricated the SQUID, taught me how to use it, calculated the flux transformer noise, and generally responded thoughtfully and thoroughly to any question.

Important components of the apparatus were constructed by Mark Johnson, and Jørn Binslev Hansen assisted with an earlier version. I am grateful to Mark Johnson for the late nights he spent taking data, and to Nancy Missert and Tim Shaw for sharing their ideas and unpublished results. Philippe Lerch taught me about arrays of Josephson junctions.

I would like to thank Andrew Cleland, and especially John Schmidt, for making the second basement of Birge Hall an enjoyable and stimulating place to work. I will always remember our conversations, over a variety of beverages, about science and about life.

A number of people have irreversibly improved my understanding of physics, some with a few well-chosen words and others with an afternoon of patient explanation. It is a pleasure to acknowledge such discussions with John Clem on vortex dynamics, Shechao Feng on universal conductance fluctuations, Ronald Griessen on flux creep and the distribution of activation energies, Julia Hsu on ultrathin films, Roger Koch on SQUIDs and noise, Jochen Mannhart on pinning, Jon Pelz on $1/f$ noise and the perils of making models, and Kristin Ralls on interacting fluctuators. The two-dimensional pinning model introduced in Chapter VII was inspired by John Clem's unpublished and far more general work on self-similar pinning potentials.

I would never have been able to survive the rigors of graduate school without the friendship of Richard LaFreniere, and the love of Stacey Kern, who never doubted.

Finally, I thank my parents, Joseph and Barbara Ferrari, for all their years of faith, love, and support.

I. Introduction

> For we possess the heat of fire . . . but we want cold. . . . Instances of cold, therefore, should be searched for most diligently. . . . The condensations which take place in nature, by means of cold, should also be investigated, that by learning their causes, they may be introduced into the arts. . . .
>
> – Francis Bacon, *Novum Organum* (1620)

The magnetic flux noise measurements which are the subject of this dissertation were motivated by three factors: the advent of copper oxide superconductors, the resulting renewed interest in the dynamics of Abrikosov vortices, and the continuing search for new applications of superconducting magnetometers. Each of these motivations draws strength from the other two; for example, moving vortices probe the microstructure of the copper oxides, as well as affecting the sensitivity of devices fabricated from them. I will examine each of the three factors in turn.

Abrikosov Vortices and Pinning

Although many properties of superconductors, such as the transition temperature, energy gap, and isotope effect, require for their explanation the microscopic theory of Bardeen, Cooper, and Schrieffer (BCS) [1], the magnetic properties of superconductors are well described by the earlier, phenomenological theory of Ginzburg and Landau (GL) [3]. The GL theory introduced a complex order parameter ψ, interpreted as the

macroscopic wave function of the superconducting electrons, and the dimensionless parameter $\kappa = \lambda/\xi$, where λ is the penetration depth and ξ the coherence length. In 1957 Abrikosov [4] published a solution of the GL equations for the case $\kappa > 1/\sqrt{2}$, the regime of Type-II or "hard" superconductors. In this case the domain wall energy between normal and superconducting regions is negative. Thus, when the applied magnetic field B exceeds the critical value B_{c1} above which perfect diamagnetism (the Meissner state) is no longer energetically favorable, the superconductor will admit flux in a manner which maximizes the domain wall area (the mixed state). This mixed state is shown schematically in Fig. 1-1. It consists of a periodic array of current loops known as Abrikosov vortices, although they are sometimes called flux lines or fluxons. Each vortex encloses a single quantum of magnetic flux $\Phi_0 = h/2e$, the minimal amount consistent with a single-valued Cooper pair wave function. At the center of each vortex is a region (the "normal" core) where the order parameter of the superconductor is suppressed. The radius of the core is approximately the coherence length ξ. Extending beyond the core are a circulating supercurrent and its associated magnetic field, both of which fall off exponentially (for widely separated vortices) on the scale of the penetration depth λ.

For a number of reasons, superconducting thin films are usually unable to achieve the Meissner state, so I may safely assume that the samples described in this dissertation always contain some number of vortices. Geometrical effects [5] reduce the effective lower critical field for a thin film of width w_s and thickness d_s to approximately $B_{c1}\pi d_s/2w_s$ because the magnetic field at the edge of the sample greatly exceeds the

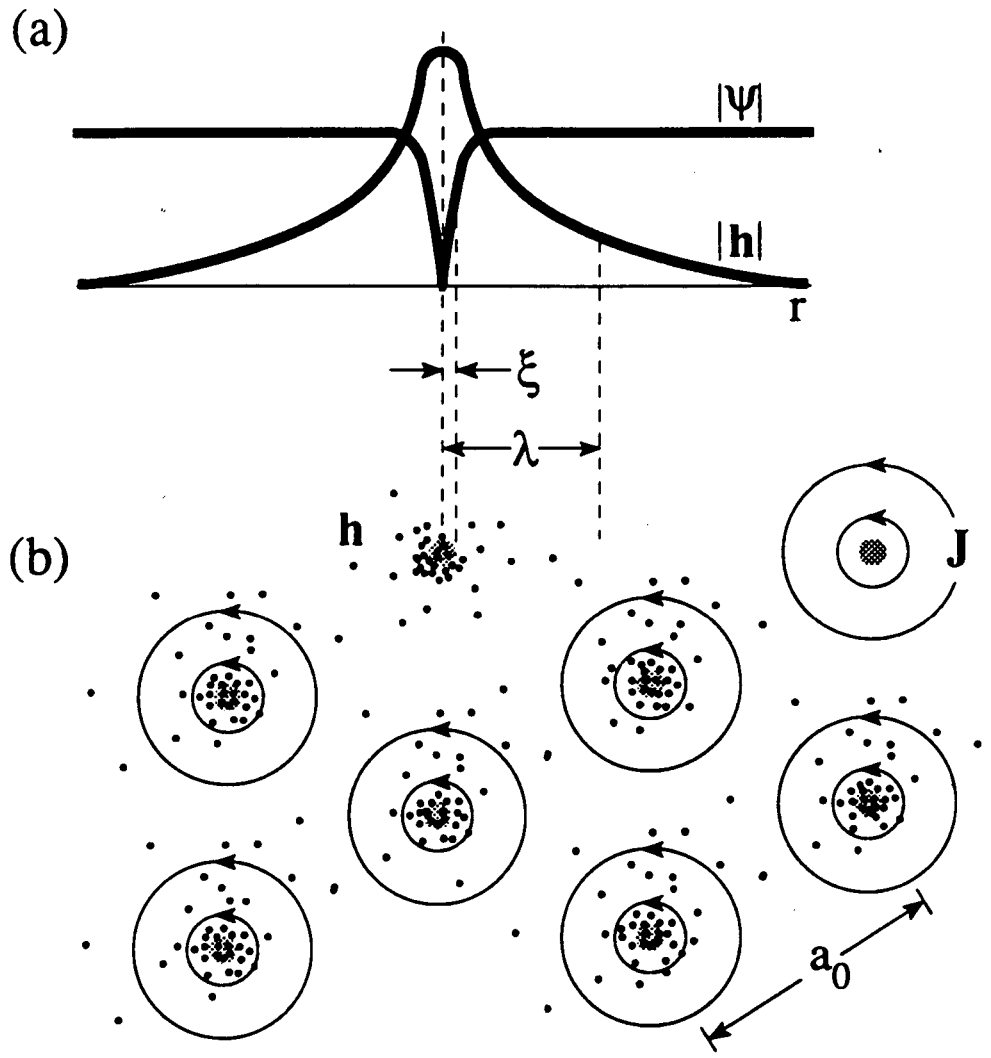

FIG. 1-1. Mixed state of a Type-II superconductor. (a) Amplitude of GL order parameter $|\psi(r)|$ and local field $|\boldsymbol{h}(r)|$ as functions of radius r around an isolated vortex, after Fig. 5-1 of Ref. [79]. I follow the convention of de Gennes [80] in using $\boldsymbol{h}$ to denote the microscopic value of the magnetic induction $\boldsymbol{B}$. (b) Sketch of triangular Abrikosov vortex lattice looking along direction of magnetic field, indicating flux density, circulating current $\boldsymbol{J}$, and lattice constant a_0.

applied field B. Even in the absence of an applied field, thermal fluctuations produce vortices for all temperatures $T > 0$, particularly in thin films where the vortex self-energy is low [6]. Only in the limits $T = 0$ and $B < B_{c1}\pi d_s/2w_s$ is the Meissner state a true equilibrium state, but even under these conditions the sample may be prevented from reaching equilibrium by the presence of pinning.

Pinning is a broad term for the effect of crystallographic or compositional defects in the sample which perturb the Abrikosov vortices from the periodic lattice illustrated in Fig. 1-1. In the presence of such material inhomogeneities, it is useful to think of the lattice not as a single periodic solution of the GL equations, but as an array of individual excitations subject to mutual repulsion and to pinning forces from the underlying crystal. Pinning of an isolated vortex can occur by a core interaction (the vortex core sheds some of its condensation energy by threading a defect where ψ is already suppressed), by a magnetic interaction (the defect permits a reduction in the circulating current), by an elastic interaction (the defect interacts with the altered density and elastic constants in the vortex core), by surface roughness (the vortex is attracted to thin regions of the sample in order to minimize its length) [7], and probably by other means as well. The identity of the defects which provide pinning in real materials is generally difficult to determine [8], except in unusual circumstances [9].

The mixed state and pinning are exhaustively reviewed in the 1972 monograph of Campbell and Evetts [10] and in Ullmaier's text [8]. Recent research just prior to the discovery of copper oxide superconductors is summarized by Brandt and Essmann [11].

Copper Oxide Superconductors

Superconductivity was discovered [12] in 1911, but not until 1987 did it appear on the cover of *Time* [13]. Interest in the field, both in the physics community and in the popular press, was sparked by the discovery of copper oxide superconductors with unprecedentedly high critical temperatures. The record superconducting transition temperature T_c had previously increased relatively slowly from 4.2 K in Hg (1911) [12] to 23 K in Nb_3Ge (1973) [14,15]. Then, in an astonishingly brief period, the highest reported T_c reached 35 K in $La_{2-x}Ba_xCuO_4$ (1986) [16,17], 90 K in $YBa_2Cu_3O_{7-x}$ (1987) [18], 110 K in $Bi_2Sr_2CaCu_2O_{8+x}$ (1988) [19], and has peaked as of the time of this writing at 125 K in $Tl_2Ca_2Ba_2Cu_3O_x$ (1988) [20,21]. The cuprate superconductors are of physical interest not only for their high transition temperatures, but also for other, presumably related properties: extreme anisotropy, short coherence length, and large upper critical field.

One consequence of the short in-plane coherence length, $\xi_{ab} \approx 2$ nm in $YBa_2Cu_3O_{7-x}$ (YBCO) [22,23], is that vortex pinning energies are of order 0.1 eV, much lower than in conventional superconductors [24]. Combined with the higher thermal energies available as a result of the increased T_c, this makes thermally activated vortex motion much more readily observable. Never before have so many physicists focused their attention on vortex dynamics. Experiments on high-T_c materials have revealed giant flux creep [25-31], dissipation in samples oscillated in a magnetic field [32,33], thermally activated resistivity [34-37], and a possible vortex-glass phase transition [38-42]. Anisotropy produces

distorted vortices [43] and vortex chains [44], and perhaps abets a Kosterlitz-Thouless unbinding transition [45-49].

The entertaining story of the discovery of copper oxide superconductors is told by Bednorz and Müller in their Nobel Prize lecture [50]. Good introductions to the high-T_c materials have appeared in the form of general review articles [51-53] and texts [54-56], as well as summaries of structural [57,58] and electronic [59,60] properties, but the field is progressing so rapidly that I fear these reviews will soon be superseded.

Superconducting Magnetometers

The superconducting quantum interference device (SQUID), first demonstrated by Jaklevic *et al.* in 1964 [61,62], is the most sensitive known detector of magnetic flux. There are two principal types of SQUIDs, the dc SQUID and the rf SQUID. The latter has not achieved the sensitivity of the former, and it will not be discussed here. As indicated in Fig. 1-2, a dc SQUID is a superconducting loop interrupted by two Josephson junctions [63,64]; ideally, these have the same critical current I_0. Shunt resistors are generally placed in parallel with the junctions in low-T_c SQUIDs to render their current-voltage characteristics nonhysteretic. To operate the SQUID, one applies a constant current $I_b \gtrsim 2I_0$ and monitors the voltage V across it. This voltage is an oscillatory function of the flux Φ linking the SQUID, with period Φ_0. For this reason, the SQUID is often described as a flux-to-voltage transducer.

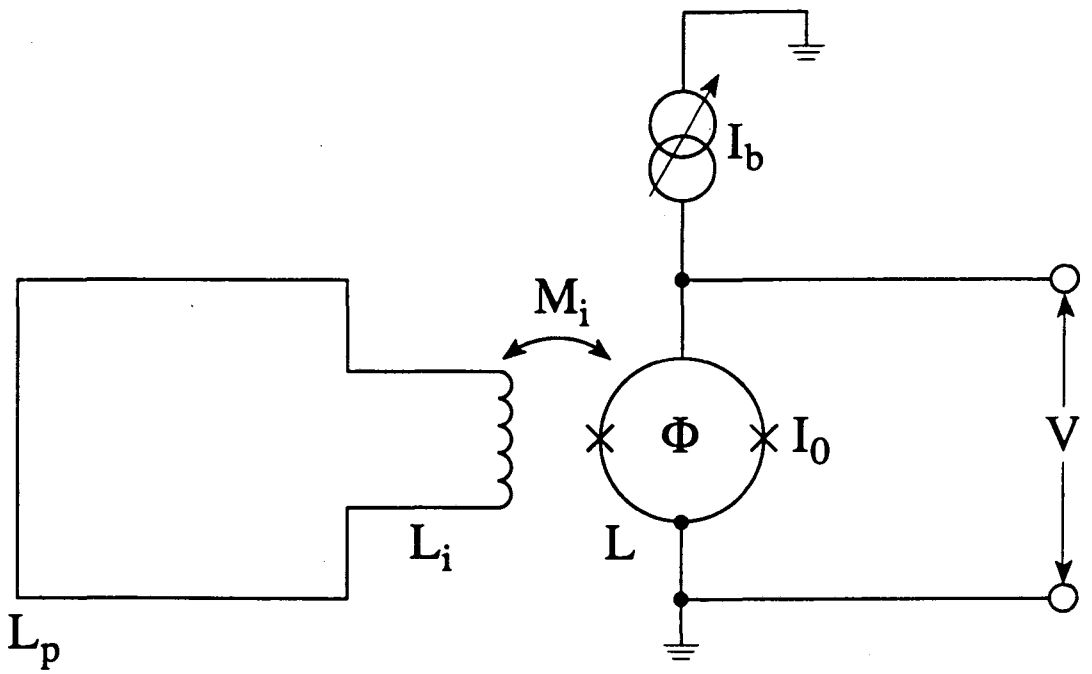

FIG. 1-2. Schematic of dc SQUID of inductance L coupled to superconducting flux transformer. Flux through SQUID is Φ and critical current of each Josephson junction is I_0. Input coil of inductance L_i has mutual inductance M_i with SQUID; pickup loop inductance is L_p.

In practice, it is commonly used as a null detector in a feedback loop which extends its dynamic range, as described in the next chapter.

The first device made from a thin film of copper oxide superconductor was the YBCO dc SQUID of Koch *et al.* [65]. Unlike low-T_c SQUIDs whose intrinsic noise usually exhibits a well-understood [66,67] white power spectrum at frequencies $f \gtrsim 1$ Hz, these devices were plagued with large amounts of $1/f$ noise over the entire measured bandwidth. More sensitive devices were later fabricated from $Tl_2Ca_2Ba_2Cu_3O_x$ films [68], but their $1/f$ noise remained higher than that in low-T_c SQUIDs. Knowing that vortex motion had been suggested as a source of such excess noise [69], I was motivated to study it in the copper oxides; this dissertation describes the progress I have made in extracting information about vortex dynamics from noise measurements. Recent results of Kawasaki *et al.* [70] suggest that the noise sources in high-T_c devices are actually fairly diverse, and I hope that I have shed light on at least one of them.

Although the SQUID is a sensitive detector of magnetic flux, its small size implies a relatively poor magnetic field sensitivity. Superconducting magnetometers generally overcome this deficiency by the use of a flux transformer [71,72] as shown in Fig. 1-2, although other coupling schemes have been successfully employed [73]. The need for a flux transformer is particularly acute in the case of SQUIDs fabricated from copper oxide superconductors since these devices operate at higher temperatures than conventional SQUIDs, and therefore have smaller inductances. To the best of my knowledge, complete YBCO thin-film magnetometers consisting of a grain boundary dc SQUID and a multilayer flux transformer have been demonstrated at the time of this writing by two

groups, Miklich *et al.* [74] and Oh *et al.* [75], who reported field sensitivities of 0.6 pT $Hz^{-1/2}$ and 12 pT $Hz^{-1/2}$, respectively, at 10 Hz and 77 K. The sensitivity in both cases was limited by the $1/f$ noise in the SQUID.

Clarke [76] has recently reviewed the theory and diverse applications of SQUIDs, as have Ryhänen *et al.* [77] with particular emphasis on low-frequency applications. Issues arising from the application of copper oxide superconductors to the fabrication of SQUIDs are considered by Clarke and Koch [78].

II. The Apparatus

It was a miracle of rare device,
A sunny pleasure dome with caves of ice!

– Samuel Taylor Coleridge, *Kubla Khan* (1798)

An obvious impediment to identifying intrinsic sources of noise in a high-T_c SQUID, or indeed in any sensor, is that the device generating the noise and the one detecting it are the same. Within the sensor there are generally a number of different noise sources, and perhaps more than one mechanism by which a given source couples to the output. Changing a parameter of the device, such as temperature, in an attempt to probe one of these sources or couplings often affects them all. Motivated by the large flux noise measured in high-T_c SQUIDs [65,68], I sought to disentangle the measurement of flux noise from its generation. This chapter describes the experimental apparatus, constructed by Mark Johnson and myself, which allows a low-T_c SQUID to detect the flux noise in a high-T_c sample.

SQUID

The experiments described in this dissertation are essentially measurements of the fluctuating magnetization of superconducting samples. A superconducting quantum interference device (SQUID) [76] was chosen as the magnetometer because of its high sensitivity and its

efficient coupling to the sample. The SQUID is shown schematically in Fig. 2-1. It is a Type L dc SQUID in the nomenclature of Wellstood, to whose dissertation [81] the interested reader is referred for a comprehensive discussion of the fabrication and operation of these devices. Briefly, the SQUID was fabricated on a sapphire substrate as follows: Photoresist was patterned to define two shunt resistors, a 30 nm layer of AuCu was evaporated, and then the photoresist was lifted off. Next, a 200 nm Nb layer was sputtered onto the entire substrate, then photolithographically patterned and reactive-ion etched to form the base electrode and contacts. Two 200 nm SiO layers were deposited, each containing two slits 2 μm wide patterned by liftoff. The slits in the lower SiO layer were perpendicular to those in the upper layer, forming two 4 μm^2 windows which defined the junctions. Photoresist was patterned for the counterelectrode, which in this case formed the SQUID body as well. The junctions were cleaned by ion milling and plasma oxidized to form the tunnel barrier, then 200 nm of PbIn was evaporated and lifted off. No final passivation layer was used.

The resulting SQUID (Fig. 2-1) possesses a square washer geometry with an inner diameter of $2a = 200$ μm and an outer diameter of $2c = 1000$ μm. Its self inductance is $L \approx 0.4$ nH and its total critical current is $2I_0 \approx 9$ μA. Two such SQUIDs were fabricated by Fred Wellstood in October 1987, and all of the data presented here were taken with one of these. This SQUID was still functioning in July 1991, with only a factor-of-two decrease in its critical current, when it succumbed to mechanical damage.

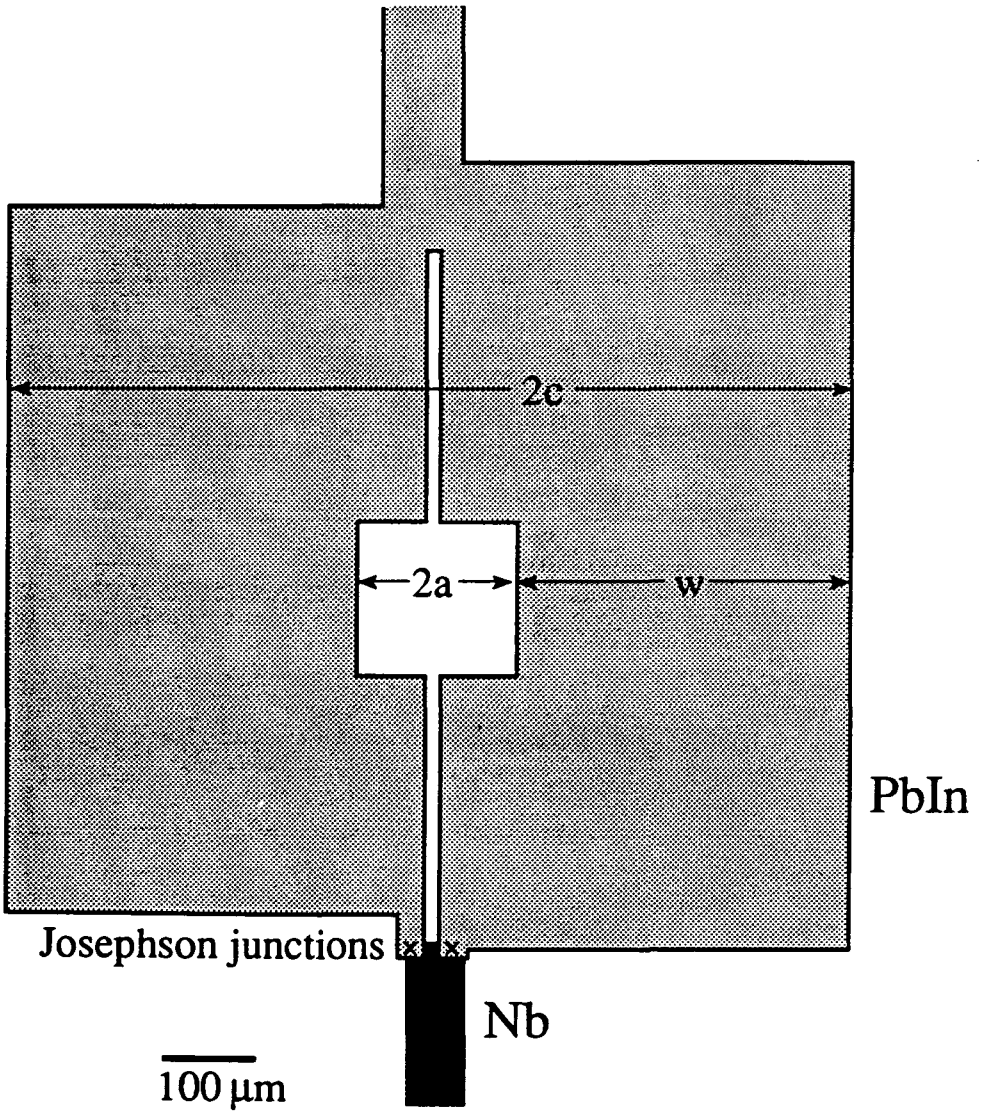

FIG. 2-1. Schematic of thin-film dc SQUID used for flux noise measurements. PbIn square washer has inner radius *a*, outer radius *c*, and width $w = c-a$. Resistive shunts not shown. After Fig. 1.15 of Ref. [81].

Samples

I was fortunate to have a large number of collaborators skilled in the deposition and characterization of copper oxide superconductors, who provided me with the samples listed in Table 2-1. The BSCCO samples are single crystals, the TCBCO samples are unpatterned films, and the YBCO samples include unpatterned films, single layers patterned into rings, and multiple layers patterned into flux transformers. I will now survey the materials properties of the various samples.

The sample name in Table 2-1 indicates chemical composition. The films denoted YBCO are $YBa_2Cu_3O_{7-x}$. The flux transformers T0, T1, and T2 contain two $YBa_2Cu_3O_{7-x}$ films with an intermediate $SrTiO_3$ layer; their fabrication will be described in detail in Chapter VI. The samples denoted BSCCO are $Bi_2Sr_2CaCu_2O_{8+x}$ with possible intergrowths of second phases, detected both by x-ray diffraction and by noise measurements discussed in Chapter III. Sample TCBCO(1) is $Tl_2Ca_2Ba_2Cu_3O_x$ and TCBCO(2) is $TlCa_2Ba_2Cu_3O_x$.

The second column in Table 2-1(a) indicates the method by which the sample was deposited or grown, according to the following abbreviations: cosputter, three sputter sources (Y, Ba, and Cu); sputter, single sputter source (or two identical sources); laser, laser ablation of a stoichiometric target; coevaporate, electron-beam evaporation from three sources; melt, single crystal grown from melt. The third column lists the substrate for the thin-film samples; TCBCO(1) and TCBCO(2) were deposited on yttrium-stabilized ZrO_2 (YSZ). The last column gives a reference for further details of the fabrication process.

Sample	Deposition	Substrate	d_s (μm)	Pattern	Name	Ref
YBCO(1)	Cosputter	$SrTiO_3$	0.2	Ring	087131B3	[89]
YBCO(2)	Sputter	MgO	0.4	Film	187A4	[90]
YBCO(3)	Laser	$LaAlO_3$	0.3	Film	M031589A	[91,92]
YBCO(4)	Coevaporate	$SrTiO_3$	0.2	Ring	G8835C5	[93]
YBCO(5)	Coevaporate	$SrTiO_3$	0.5	Ring	G8819A2	[93]
YBCO(6)	Sputter	$SrTiO_3$	0.4	Film	M049C7	[94]
YBCO(7)	Laser	MgO	1	Film	23	[95]
YBCO(8)	Laser	MgO	0.4	Film	76	[95]
YBCO(9)	Laser	MgO	0.4	Film	365	[95]
T0	Laser	MgO	0.3	FT	188	[96]
T1	Laser	MgO	0.3	FT	215	[96]
T2	Laser	MgO	0.3	FT	204	[96]
BSCCO(1)	Melt	None	40	Flake	--	[97]
BSCCO(2)	Melt	None	150	Flake	--	[97]
TCBCO(1)	Sputter	YSZ	2	Film	--	[98]
TCBCO(2)	Sputter	YSZ	2	Film	--	[98]

TABLE 2-1(a). Deposition parameters of all samples. From left to right, the columns give the sample name used in this dissertation, the method by which the sample was fabricated, the substrate on which it was deposited, the sample thickness d_s, the form into which it was patterned, the original name assigned by the fabricator of the sample, and the number of the reference describing the fabrication technique. See text for explanation of abbreviations.

Sample	Orientation	T_c (K)	J_c(4.2 K) (A/cm^2)	S_Φ(1 Hz,40 K) (Φ_0^2/Hz)
YBCO(1)	>90% *c*	85	5×10^6	2×10^{-8}
YBCO(2)	*c*	84.4	4×10^7	2×10^{-9}
YBCO(3)	*c*	89.8	2×10^7 [(a)]	$< 10^{-9}$
YBCO(4)	*a* and *c*	85	2×10^4	1×10^{-7}
YBCO(5)	polycrystalline	47	--	3×10^{-4}
YBCO(6)	>90% *a*	81	1×10^6	4×10^{-7}
YBCO(7)	--	85 [(a)]	--	6×10^{-8}
YBCO(8)	--	88 [(a)]	--	$\sim 10^{-9}$ [(b)]
YBCO(9)	--	82	--	2×10^{-6}
T0	--	71	2×10^4	$< 10^{-6}$
T1	--	77	3×10^5	1×10^{-6}
T2	--	59	3×10^4	2×10^{-6}
BSCCO(1)	*c*	90	$\sim 10^6$	1×10^{-7}
BSCCO(2)	*c*	93	$\sim 10^6$	6×10^{-7}
TCBCO(1)	*c*	119	$\sim 10^5$	4×10^{-8}
TCBCO(2)	*c*	102	$\sim 10^5$	4×10^{-7}

[(a)] Transport measurement. [(b)] Measured at $T = 4.2$ K.

TABLE 2-1(b). Measured parameters of all samples. From left to right, the columns give the sample name used in this dissertation, the crystalline orientation, the superconducting transition temperature, the critical current density at 4.2 K, and the flux noise power at 1 Hz and 40 K. For flux transformers, noise measured by SQUID is multiplied by $\zeta^{(u)}/(\zeta^{(in)}+\zeta^{(cr)}) \approx 3$ (see Table 6-1) to refer it to an unpatterned film.

The thickness d_S of the sample is given in the fourth column of Table 2-1(a). For the single-layer samples d_S is the film thickness exclusive of the substrate, for the multiple-layer samples (flux transformers) it is the thickness of one typical YBCO layer, and for the single crystals it is the total thickness. The thicknesses are only approximate, since d_S was generally estimated from the deposition parameters, and not measured directly.

The fifth column in Table 2-1(a) denotes the patterning, if any, performed on the sample. The word "film" indicates an unpatterned thin film. "Flake" is a cleaved single crystal, typically a few square millimeters in area. "Ring" is a thin film which was been patterned by photolithography and a dilute nitric acid etch into a square washer with 200 μm inner diameter and 1000 μm outer diameter, to match the dimensions of the SQUID. The motivation for this pattern, which I eventually realized was unnecessary, will be discussed at the end of this chapter. Finally, "FT" is a multilayer flux transformer as described in Chapter VI. The sixth column lists the name assigned to the sample by the group which fabricated it.

Table 2-1(b) summarizes the measurements performed to characterize the samples. X-ray diffraction was employed to determine the crystalline orientation of the grains constituting the samples. The second column lists the crystallographic axis oriented along the thinnest dimension of the sample: normal to the substrate for the thin films, and out of the plane of the flake for the single crystals. Although x-ray measurements were not performed on YBCO(7), YBCO(8), YBCO(9), and the flux transformers, results from samples deposited under similar conditions in the same system lead me to expect good *c*-axis orientation. The transition

temperature T_c was determined inductively as described later in this chapter (see Fig. 2-5). The critical current density J_c of the thin films was determined from the width of magnetic susceptibility hysteresis loops, measured prior to patterning, if any, and analyzed according to the Bean model [82]. The exception is sample YBCO(3), for which J_c was obtained from a transport measurement. For the flux transformers, J_c was determined by measuring the maximum supercurrent which the transformer could support and dividing by the cross section of the narrowest segment (the input coil). If the transformer critical current were limited by isolated defects such as grain boundaries formed where the upper film climbs an edge, as has been observed to occur [83,84], then the listed J_c would underestimate the bulk value.

The last column in Table 2-1(b) gives the flux noise power measured at 1 Hz and 40 K, except for YBCO(8) which was measured only at 4.2 K. I chose $T = 40$ K because it is below the transition temperature T_c of all samples and near $T_c/2$ for most of them. The noise also tends to be less strongly temperature dependent near 40 K. The measurements were made when the sample exhibited $1/f$ noise as described in Chapter IV; some samples occasionally produced random telegraph signals (see Chapter III) which, when active, could increase the noise power by orders of magnitude above the tabulated value. A thorough investigation of the flux noise will be the subject of the remaining chapters of this dissertation.

McDLT Cryostat

In order to measure the flux noise produced by a sample, it was necessary to find a way to couple it inductively to the SQUID, so that its magnetization linked flux into the SQUID, while keeping the two thermally isolated, so that the temperature of the sample could be varied without affecting the performance of the SQUID. These two seemingly incompatible goals were realized with the apparatus depicted in Figs. 2-2 and 2-3. Named the McDLT after a now-discontinued McDonald's sandwich [85], the apparatus is divided into a hot side and a cold side, as was the sandwich. A small amount of vacuum grease is used as an adhesive to attach the SQUID substrate to a sapphire plate as shown in Fig. 2-2. The two electrical leads to the SQUID are affixed with pressed In contacts. The sapphire plate is attached by means of a clamp and a Cu disk to a Cu tab which is brazed to the brass flange of the vacuum can containing the apparatus (Fig. 2-3). This arrangement, which is unnecessarily complicated for historical reasons, provides thermal conductivity from the SQUID to the liquid ^{4}He bath surrounding the vacuum can.

The sample is similarly attached with vacuum grease to a Si plate on the hot side. Epoxied to the opposite side of the Si plate are a Pt resistance thermometer and a 1 kΩ metal film resistor which functions as a heater. The Si plate is attached to a $\cup$-shaped piece of fiberglass, which is stood off from the sapphire plate on spacers made of Si, macor, or quartz, and bristles from a horsehair or nylon brush. The bristles lie flat between the spacers and decrease the thermal conductivity from the hot side to the cold side. Since the thickness of the sample substrate varies from sample to

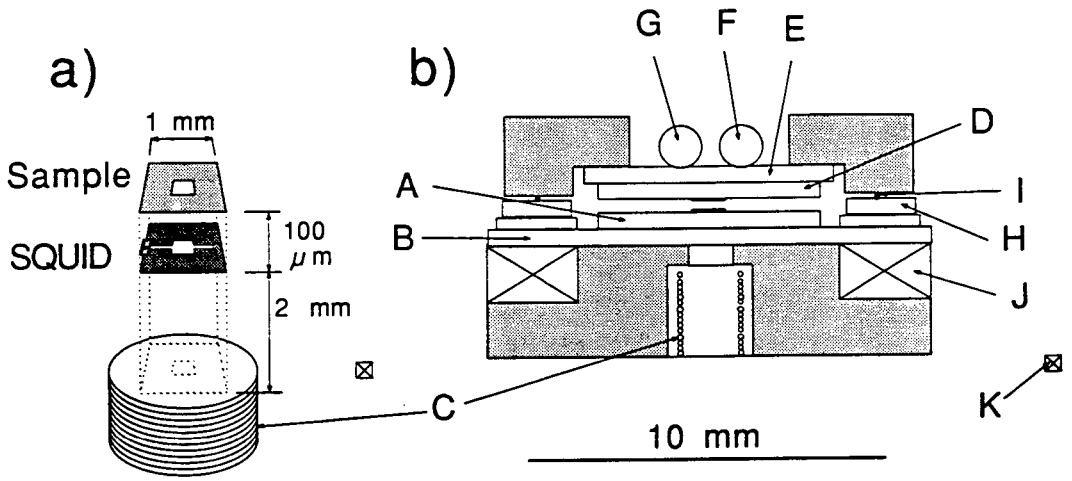

FIG. 2-2. Schematic of apparatus used to measure flux noise. (a) Essential elements of McDLT arrangement. Copper oxide sample, here patterned in "ring" geometry of Table 2-1, supported parallel to Nb-PbIn SQUID coupled to Nb feedback coil. Sample and SQUID are inductively coupled but thermally isolated. Substrates not shown. (b) Front view illustrating mounting arrangement. A is the SQUID substrate, B is the sapphire plate, C is the modulation and feedback coil, D is the sample substrate, E is the Si plate, F is the heater, G is the thermometer, H is a spacer, I is a bristle, J is the field coil, and K is the big coil. Mechanical support provided by fiberglass components (shaded). Hot side is the portion above the bristles, cold side the portion below.

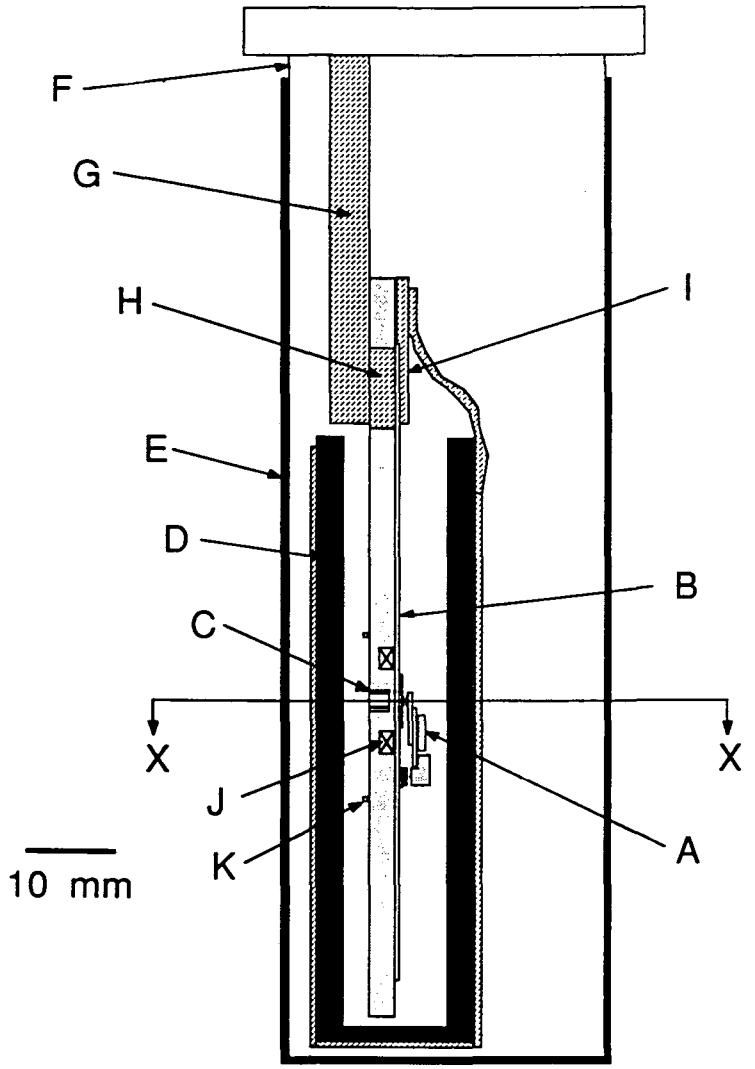

FIG. 2-3. Side view of apparatus. View in Fig. 2-2(b) represented here by section X-X. A is the hot side, B is the sapphire plate, C is the modulation and feedback coil, D is the inner Pb shield, E is the outer Pb shield, F is the vacuum can, G is the Cu tab, H is the Cu disk, I is the clamp, J is the field coil, and K is the big coil. Space constraints allow either the inner Pb shield or the big coil to be mounted, but not both as drawn here.

sample, new spacers and bristles are chosen for each run. I use a micrometer to determine the thickness of each spacer and bristle individually, insuring that their total height produces a gap between the SQUID and the sample of 100 μm. The apparatus is assembled as described above, and then two pieces of dental floss are tied tightly around it to hold the hot side and cold side together.

On the opposite side of the sapphire plate from the SQUID is a small 10-turn Nb coil which allows me to operate the SQUID in a flux-locked loop as described in the next section. The mutual inductance between this feedback coil and the SQUID is 0.1 nH when the sample is normal. Two additional Nb coils, prosaically named the field coil and the big coil, allow the application of magnetic fields to the apparatus. Both are indicated in Fig. 2-2. The field coil has more turns than the big coil (452 versus 10), and can store a persistent current; it therefore provides a stronger and more stable field. The big coil has a larger inner diameter (19 mm versus 8 mm) and therefore provides a more uniform field, which is important for experiments on large samples such as flux transformers. To produce a field of 1 μT at the SQUID requires a current of 20 μA in the field coil or 2 mA in the big coil.

Two superconducting Pb shields attenuate magnetic noise from external sources, as illustrated in Fig. 2-3. The inner shield surrounds the hot side and cold side, while the outer shield encloses the entire vacuum can except for its upper flange. After I added the big coil to the apparatus, however, it was necessary to omit the inner shield, since it would not fit over the big coil. No increase in background noise was observed. The entire dewar is located within a cylindrical mu-metal shield 39 cm in

diameter and 122 cm in height, insuring that the apparatus is cooled in a small magnetic field. I tested this shield before inserting the apparatus by surveying the volume to be occupied by the vacuum can with a fluxgate magnetometer. The largest radial dc component of the magnetic field (in the plane of Fig. 2-2) was 0.31 μT, and the largest axial component (out of the plane) was 0.11 μT. Under ordinary daytime conditions, the ac magnetic field in the shield was dominated by an axially-directed 60 Hz signal with a peak-to-peak amplitude of 0.03 μT.

Note that the only normal metal objects within 1 cm of the SQUID are of small volume: the metal film heater resistor, the Pt wire thermometer, the In contacts, and the manganin and Cu wires to the hot side and to the SQUID. This minimizes excess Johnson noise [86]. Nevertheless, such noise appeared at high frequencies when a flux transformer was mounted on the hot side, as described in Chapter VI, because of the increased field sensitivity provided by the transformer.

Electronics

The feedback electronics for the SQUID, which I appropriated without significant modification from earlier designs [69,72], are shown in Fig. 2-4. Their essential purpose is to provide a voltage V_f proportional to the flux Φ applied to the SQUID over a fairly wide range (typically $-70\Phi_0 < \Phi < 70\Phi_0$). The SQUID bias current I_b is supplied by a simple resistive divider, and adjusted to give maximum response. A 100 kHz square-wave oscillator applies ac flux modulation to the SQUID through

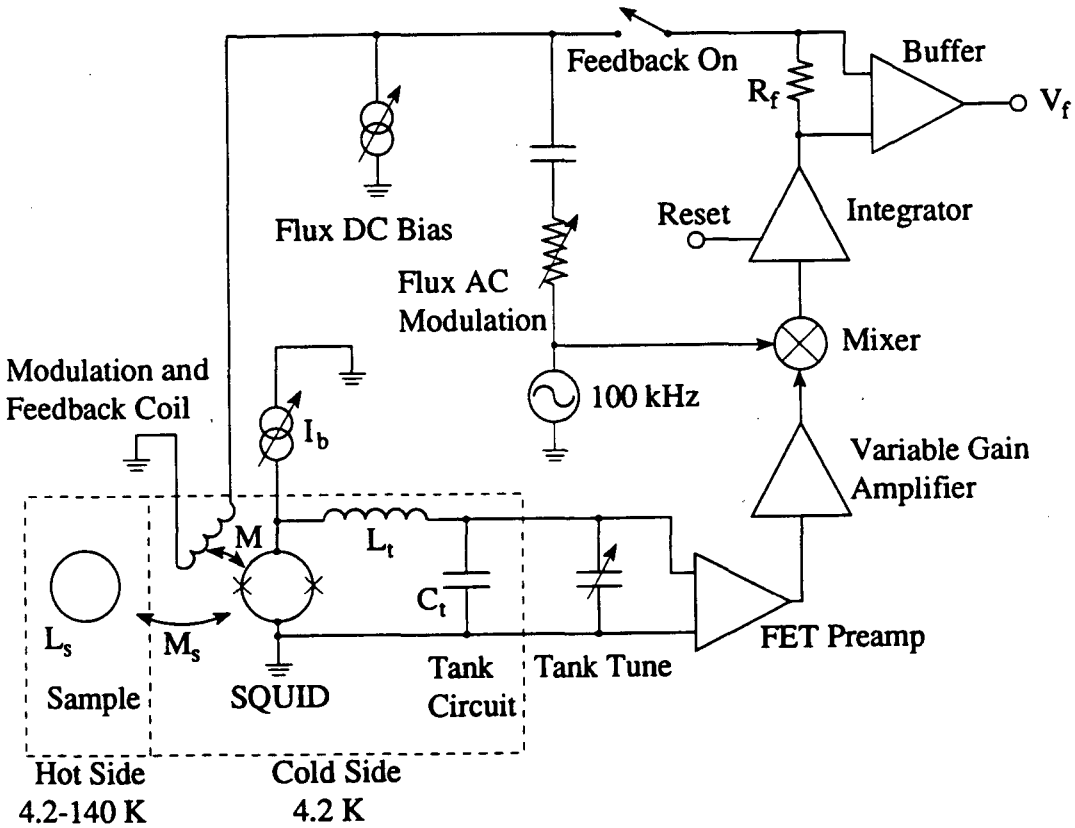

FIG. 2-4. Schematic of SQUID modulation and feedback electronics. Mutual inductance M between SQUID and feedback coil defined to include effect of shielding by sample (M_s). Tank circuit composed of superconducting Nb inductor $L_t = 0.54$ mH, mica capacitor $C_t = 4.7$ nF, and room-temperature tuning capacitor. Output voltage V_f measured by unity-gain buffer amplifier across feedback sense resistor $R_f = 10$ kΩ.

the modulation and feedback coil. I adjust the peak-to-peak amplitude of the square wave to $\Phi_0/2$ so that, when the quasistatic flux linking the SQUID is displaced from an integer (or half-integer) number of flux quanta, the resulting error signal is as large as possible. The voltage across the SQUID is coupled to a room-temperature FET preamplifier through a cooled tank circuit resonant at 100 kHz with quality factor $Q \approx 60$. A superconducting Nb coil forms the inductor of the tank circuit, which is tuned by means of an additional room-temperature capacitor. The tank circuit increases the effective impedance of the SQUID by a factor of approximately Q^2; the optimal source impedance of the preamplifier is of order 10 kΩ. The output of the preamplifier can be monitored on an oscilloscope without disturbing the SQUID in order to measure the modulation amplitude ΔV with the feedback loop open.

The voltage which appears across the SQUID is amplified, mixed with the output of the ac modulation oscillator, and integrated. In this way, the applied flux Φ is lock-in detected. When the feedback switch is closed, the output of the integrator is fed back to the modulation and feedback coil through a sense resistor R_f to cancel the applied flux. A buffer amplifier measures the voltage drop V_f across the sense resistor, which is proportional to Φ. Measuring flux noise in the SQUID is thus reduced to measuring the power spectral density $S_V(f)$ of voltage noise across the buffer. The dc flux bias provided to the modulation and feedback coil by an additional current supply allows the offset of the buffer to be zeroed.

All of the electronics in Fig. 2-4 are powered by automobile batteries for noise immunity, as are the current sources for the field and big

coils, the heater, and the field coil heat switch. The apparatus is located in a shielded room constructed from Cu mesh, although the electrical environment in the second basement of Birge Hall is sufficiently quiet that leaving the door of the screen room open had no discernable effect on the performance of the SQUID. The mu-metal cylinder provides most of the shielding from low-frequency sources. The voltage noise across the buffer is measured with a Hewlett-Packard 3561A spectrum analyzer located outside the shielded room, and the spectra are stored and processed by a computer. A digital voltmeter in parallel with the spectrum analyzer facilitates zeroing the buffer voltage and measuring V_{cal} as described below.

Experimental Procedure

Each experimental run begins with the mounting of the sample on the hot side and the assembly of the McDLT apparatus as described above. The vacuum can and outer Pb shield are attached and the can is evacuated with a mechanical pump. I precool the apparatus by immersing the vacuum can in liquid N_2 while monitoring the temperature of the hot side, which typically takes one or two minutes to decrease from room temperature to 0°C, indicative of good thermal isolation. The cryostat is then inserted into a dewar of liquid ^{4}He at atmospheric pressure, surrounded by the mu-metal shield, where it remains for the duration of the run. The hold time of the dewar is three days; a fill tube on the insert allows me to transfer additional cryogen as needed.

After the initial cooldown, and after each transfer, I raise the temperature of the sample to well above T_c, open and close the heat switch on the field coil to release any trapped flux, and set a heater current corresponding to the temperature at which I wish to make a noise measurement. This insures that the sample is cooled through T_c in a magnetic field of less than 1 μT. Presumably as a result of temperature-dependent thermal conductivity, the ultimate temperature T of the hot side is roughly linear in the heater current, with 4 mA (16 mW heater power) producing $T = 100$ K. This value is only typical, as the thermal conductance $G \approx 170$ μW/K from the hot side to the cold side changes with each run when the spacers and bristles are replaced. The rate at which I can take data is limited by the equilibration time after a change in heater current. I crudely estimate the heat capacity of the hot side at 100 K to be $C \approx 0.3$ J/K, giving a thermal time constant $C/G \approx 1800$ s, similar to what I observe experimentally. Even at 100 K, almost all of the heat flow from the hot side takes place by conduction, not radiation.

After waiting one or two hours for the temperature to stabilize, I begin the process of "taking a point." I adjust the tank tune capacitor, the dc flux bias, the ac flux modulation, and the bias current I_b to produce the maximum preamplifier modulation amplitude ΔV, which I record. The optimum value of I_b decreases with increasing hot side temperature, providing a measure of the temperature of the SQUID. I record the resistance of the Pt thermometer and place the SQUID in feedback. I calibrate the output of the buffer amplifier by first applying flux to the SQUID with the dc flux bias until an offset of a few hundred mV appears across the buffer, then pressing the integrator reset button which causes the

buffer voltage to jump nearer to zero. Since the feedback loop is stable only at lockpoints separated by an integer number of flux quanta, the observed jumps are multiples of some voltage V_{cal} which I can determine by repeating the above process for different initial offsets. As a result I know that one flux quantum applied to the SQUID will cause the buffer voltage to increase by V_{cal}.

Having optimized and calibrated the apparatus, I am now ready to measure the noise. I adjust the dc flux bias to minimize the buffer voltage, in order to obtain the maximum sensitivity on the spectrum analyzer, and begin averaging. Generally I average for 200 s with a bandwidth of 100 Hz (50 averages), followed by 20 s at 4 kHz (200 averages). My experimental bandwidth is limited at low frequencies to ~1 Hz by the averaging time, and at high frequencies by a resonance at a few kHz in the feedback electronics. When noise processes are occurring on a very long time scale, such as the random telegraph signal in BSCCO(2) described in Chapter III, I can decrease the low-frequency limit to a few mHz and increase the averaging time to hours. When the averaging is complete and the spectra are stored in the computer, I remeasure the Pt thermometer to gauge the temperature drift. Then I take another set of spectra, measure the temperature a third time, and change the heater current. After the equilibration time, I repeat the process.

I determine the transition temperature of the sample from the temperature dependence of the calibration V_{cal}, essentially a dc susceptibility measurement. Figure 2-5 plots the mutual inductance $M = \Phi_0 R_f / V_{cal}$ between the feedback coil and the SQUID, which increases dramatically when the sample, YBCO(1) in this case, is heated through T_c

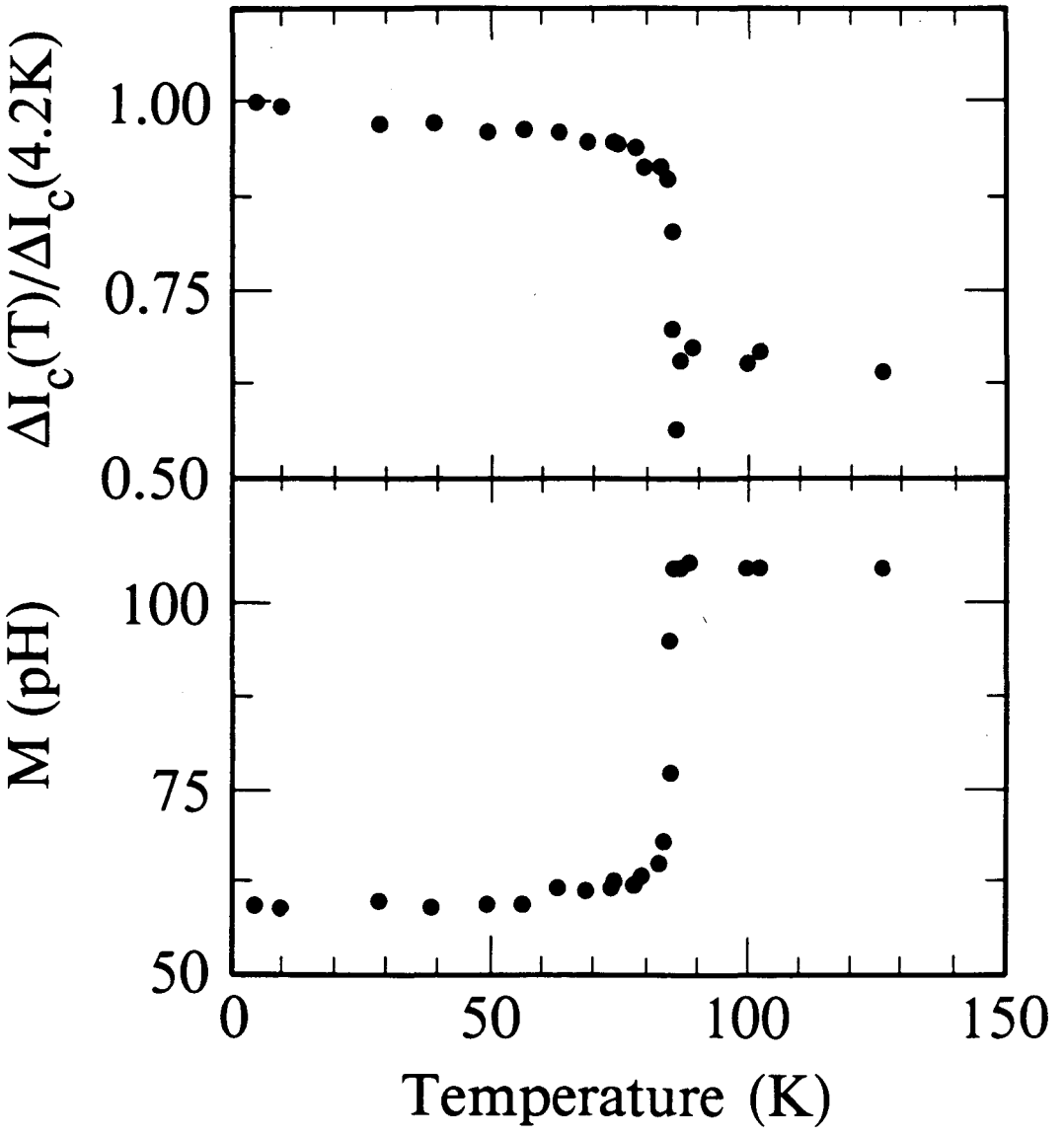

FIG. 2-5. Temperature dependence of SQUID parameters for sample YBCO(1). Upper graph, normalized modulation amplitude $\Delta I_c(T)/\Delta I_c(4.2\text{ K})$; lower graph, mutual inductance M between the SQUID and the feedback coil.

and therefore no longer shields the SQUID. I define T_c to be the greatest temperature at which M is depressed below its constant high-temperature value. This definition should correspond to the onset temperature for a susceptibility measurement or to the zero-resistance temperature for a transport measurement. The small jump in M near 60 K in Fig. 2-5 is reproducible, and probably results from a small amount of the oxygen-deficient phase [87,88] of YBCO with $T_c \approx 60$ K. The sharpest inductive transition I observed was in sample YBCO(3), plotted in Fig. 4-3(a), with a width of less than 1 K.

For the samples which were patterned into rings, I determined the mutual inductance $M_s = \alpha_s(LL_s)^{1/2}$ between the SQUID and the sample from the modulation depth of the critical current of the SQUID. Here, the self-inductance of the sample ring is $L_s \approx L = 0.4$ nH, and α_s is the coefficient of inductive coupling between the SQUID and the sample. The modulation depth ΔI_c is defined to be the difference between the maximum and minimum values measured for the critical current as the flux through the SQUID is varied. Fortunately ΔI_c is proportional to the voltage modulation ΔV, which is readily measured as described above. Above T_c the SQUID is not shielded by the sample, and I estimate the modulation parameter $\beta = 2LI_0/\Phi_0 \approx 2$. Below T_c the SQUID inductance is reduced to $L' = L(1-\alpha_s^2)$ by the diamagnetic screening of the sample, and the modulation parameter to $\beta' = \beta(1-\alpha_s^2)$. From the observed increase in ΔI_c with decreasing temperature illustrated in Fig. 2-5, I can calculate β' according to Fig. 4 of Ref. [66], and thereby deduce L' and α_s. The coupling coefficient α_s ranged from 0.6 to 0.7 for the "ring" samples. I will show in Chapter III that the coupling of flux from a vortex into the

SQUID is approximately the same for "film" and for "ring" samples, so the above procedure is sensible even when the inductance of the sample is not well defined.

From the measured feedback voltage noise $S_V(f)$, the flux noise in the SQUID is easily calculated to be

$$S_\Phi(f) = \left(\frac{\Phi_0}{V_{cal}}\right)^2 S_V(f) \ . \tag{2-1}$$

To facilitate comparison of the flux noise in the sample to noise in devices, such as low-T_c or high-T_c SQUIDs, I will generally use instead the noise referred to the sample:

$$S_\Phi(f) = \left(\frac{\Phi_0}{\alpha_s V_{cal}}\right)^2 S_V(f) \ . \tag{2-2}$$

Since α_s is of order unity, Eqs. (2-1) and (2-2) differ only slightly. When the symbol $S_\Phi(f)$ is used in the remainder of this dissertation, the definition in Eq. (2-2) is assumed unless explicitly stated otherwise.

III. Random Telegraph Signals

> "They [the Templars] were remarkable, no doubt about it" was Belbo's summation. "But tell me, Casaubon, do you love them?"
>
> "I'm doing my thesis on them. If you do your thesis on syphilis, you end up loving even the Spirochaeta pallida."
>
> – Umberto Eco, *Foucault's Pendulum* (1988)

The noise generated by the samples in my experiment can be divided into two types, based on its power spectrum: $1/f$ noise and Lorentzian noise. The latter is produced by random telegraph signals (RTSs) and, although less common than $1/f$ noise in the samples I have measured, it is simpler to analyze, and will therefore be considered first. An RTS is produced by the motion of a single vortex, and is thus the more fundamental of the two types of noise. In Chapter V, I will develop a theory which explains $1/f$ noise as a superposition of many RTSs.

A comprehensive review of random telegraph signals is provided by Kirton and Uren [99]. Random telegraph signals in the voltage noise from YBCO have been reported by several groups [100-102]. The results in this chapter, some of which have appeared previously [103], are to my knowledge the only systematic study of RTSs in flux noise, although such events have been seen by others [104,105].

Observation of Random Telegraph Signals

Figure 3-1 illustrates random telegraph signals generated by three different samples. At most temperatures, these samples produced only $1/f$ noise, which will be discussed in Chapter IV and subsequent chapters. However, in certain narrow ranges of temperature, RTSs appeared. As shown in Figs. 3-1(a) and (b), when the temperature of sample YBCO(3) was between 88.4 K and 88.6 K, the flux Φ linking the SQUID switched back and forth between two discrete levels at a rate that increased markedly with temperature. I interpret this signal as the hopping of one vortex between two pinning sites; it is possible that several vortices are moving together as a bundle, but I will argue against this interpretation below. The amplitude of the signal in Figs. 3-1(a) and (b) is $\Delta\Phi = 1.3 \times 10^{-3}\Phi_0$. The magnitude of the fluctuations about each level is also roughly the same: this noise may be due to the motion of the vortex (or bundle) in its metastable state, or more likely to the motion of other vortices in the film. Processes similar to this one were detected in 11 of the 16 samples in Table 2-1.

The process in Fig. 3-1(d) was observed in BSCCO(2). The magnetically determined transition temperature of this sample was 93 K; however, the existence of large levels of flux noise at higher temperatures indicates the presence of a small fraction of a second superconducting phase with $T_c \approx 110$ K, known to exist [19] in BSCCO. In the temperature range from 95 K to 101 K, the flux switches among a number of values, approximately equally spaced by $\Delta\Phi = 6.5 \times 10^{-3}\Phi_0$. A likely explanation for this behavior is that a fixed number of flux quanta occupy

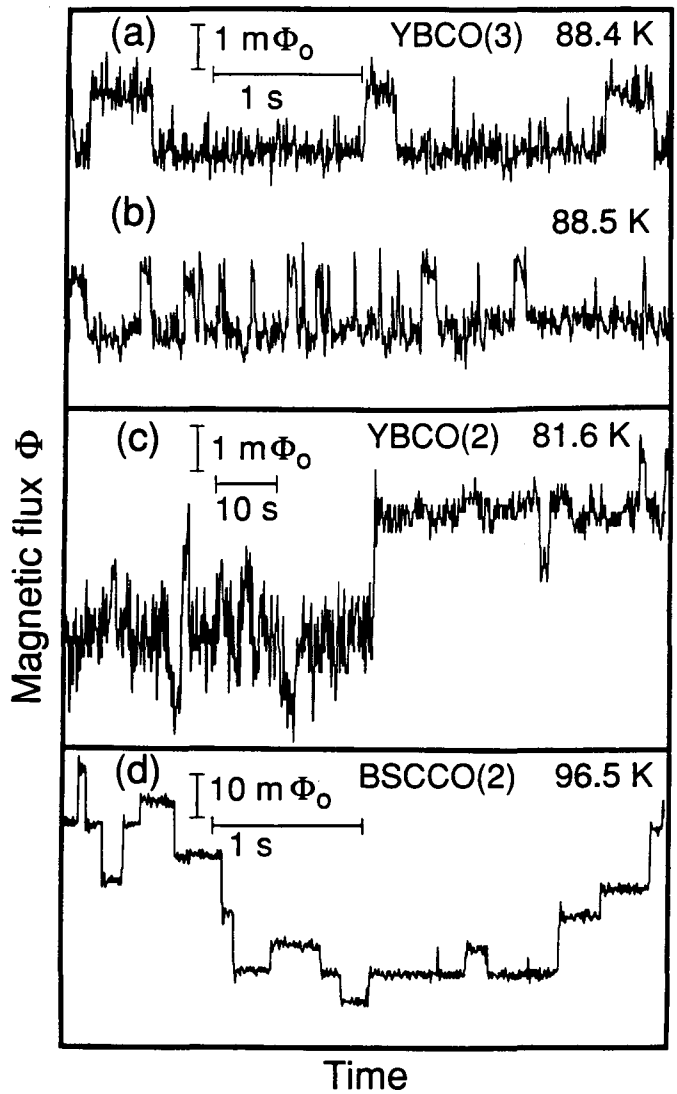

FIG. 3-1. Flux through SQUID vs. time generated by (a) laser-deposited YBCO(3) at 88.4 K, (b) same film at 88.5 K, (c) sputtered YBCO(2) at 81.6 K, and (d) BSCCO(2) flake at 96.5 K. Note changes of scale in (c) and (d). Zeros of axes are arbitrary.

two pinning sites, the various flux levels correspond to differing occupancies of these sites, and the hopping of vortices between the sites is uncorrelated. I will adopt this interpretation in the analysis which follows. Another initially plausible explanation is that above its inductively determined transition temperature, the sample contains a superconducting portion which is multiply connected and traps a flux Φ_X. The switching in Fig. 3-1(d) would then correspond to thermally activated transitions among the states $\Phi_X = 0, \pm\Phi_0, \pm 2\Phi_0$, and so on. However, the variance of Φ_X from its mean would provide a measure of the self inductance L_X of the hypothetical multiply connected structure according to $<\Phi_X^2>/L_X \approx k_B T$, and this yields the unreasonably large value $L_X \approx 6$ nH.

Direct Noise Mechanism

I will now consider the mechanism by which the motion of one vortex in the sample produces an RTS. This mechanism is called direct noise because the flux from the moving vortex directly links the SQUID. It is distinguished from another form of coupling, indirect noise, which will be introduced in Chapter VI. The direct noise mechanism is illustrated schematically in the inset to Fig. 3-2. Because the magnetic field lines from a vortex must close around the sample, and the gap between the sample and the SQUID is small on the scale of the sensing area of the SQUID [106], a vortex near the center of the sample couples a large fraction of a flux quantum $\Phi \approx \alpha_S \Phi_0$ into the SQUID, where $\alpha_S \approx 0.7$ as estimated in Chapter II. If this vortex were to be displaced towards

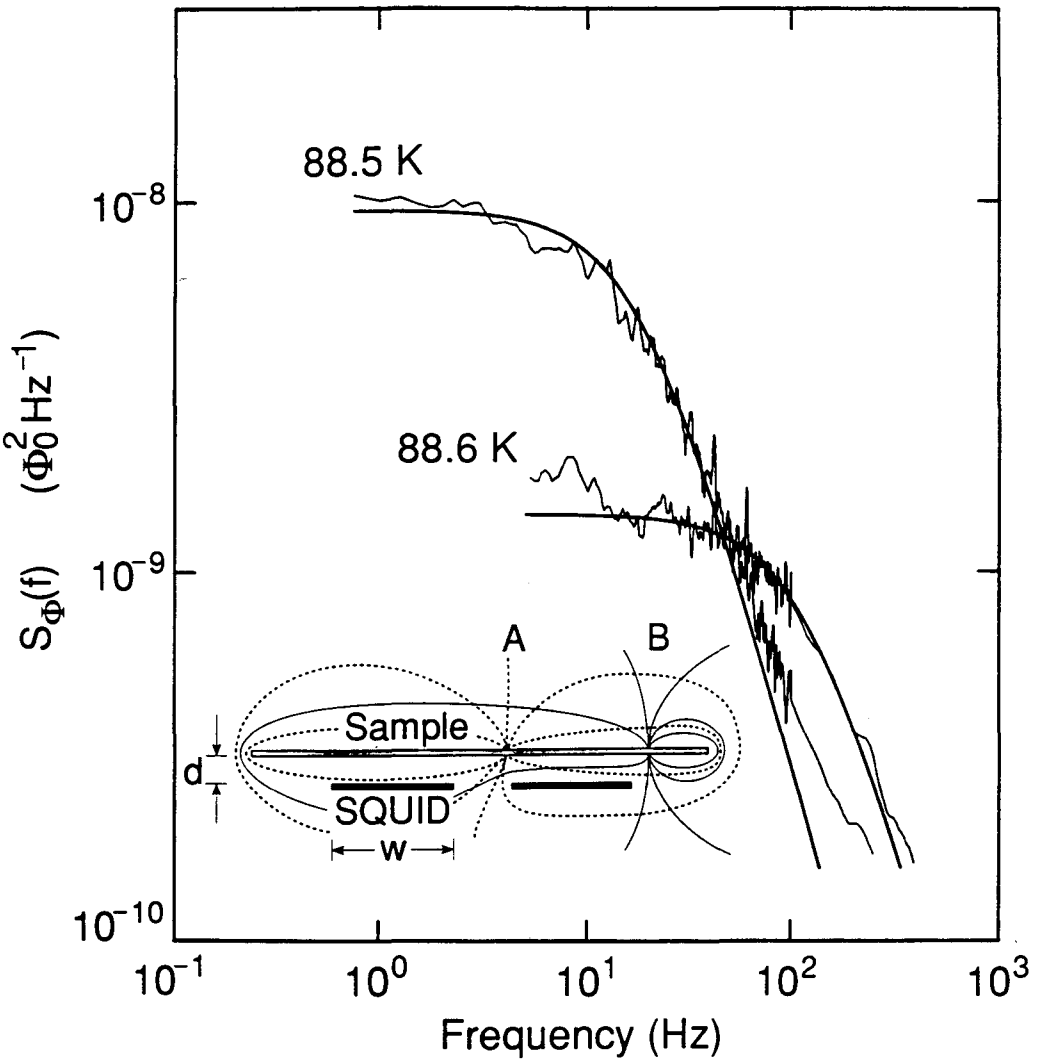

FIG. 3-2. Spectral densities of random telegraph signals from YBCO(3) at two temperatures. Light curves are power spectra of noise measured in SQUID [Eq. (2-1)]. Heavy curves are Eq. (3-2) with $\Delta\Phi = 1.3 \times 10^{-3}\Phi_0$ and $\gamma = 4.5$, as determined from time domain data, and $\tau_1 =$ 48 and 7.3 ms, respectively. Departures at high frequencies are caused by noise from other vortices in the film and from the measuring system itself. Inset: Schematic cross section of sample and SQUID placed distance *d* apart. Width of the SQUID at its narrowest is *w*. Vortex pinned at site A couples flux $\Phi \approx \alpha_s\Phi_0$ (dotted field lines) into the SQUID, while one at site B couples negligible flux (solid field lines).

the edge of the sample, the flux Φ linking the SQUID would decrease. Note that if a hole were opened in the sample above the hole in the SQUID (a change from "film" to "ring" geometry in Table 2-1), flux quantization implies that the field lines in the inset to Fig. 3-2 would be only slightly distorted. For this reason, the geometry of the sample has little bearing on my analysis of the noise.

I will approximate the decrease in Φ with distance to be linear across the width $w = 400$ μm of the SQUID. A better approximation due to Fred Wellstood appears in Ref. [107], and John Clem has calculated the coupling exactly for specific geometries [108]. A vortex which hops radially a distance ℓ causes the flux through the SQUID to change by $\Delta\Phi \approx \alpha_s \Phi_0 \ell / w$. If the vortex were to move in a direction other than radial, $\Delta\Phi$ would be reduced; it follows that $\ell \geq w\Delta\Phi/\alpha_s\Phi_0$. These lower limits on the hopping distance are listed in Table 3-1 for RTSs in five samples. The process observed in BSCCO(2) in the range 95 K < T < 101 K occurred when the majority of the sample was in the normal state, and therefore no longer providing a superconducting groundplane as depicted in the inset to Fig. 3-2, so the inferred hopping distance may considerably underestimate the actual value.

Changing the temperature of the sample by a fraction of a degree often causes the RTS to vanish, but when I could observe the same process over a range of temperatures I saw no variation in ℓ, implying that the vortex continues to hop between the same two sites. Of course, if the vortex bundle actually contains not one but N_V flux quanta, ℓ should be reduced to ℓ/N_V. Because $\Delta\Phi$ remains constant over observational times of hours and also as the temperature is varied, I believe that the hopping

Sample	T (K)	ℓ (μm)
YBCO(2)	78.4	0.80
	81.1	2.7
YBCO(3)	85.6	0.16
	88.4 [a]	0.76
YBCO(4)	50.9	5.8
T2	45.3	6 [b]
BSCCO(1)	89.9	26
	90.5	32
	91.1	10
BSCCO(2)	35.3	5.1
	50.6	5.2
	95.1 [a]	3.7
TCBCO(1)	4.2	3.5
	78.1	5 - 10 [c]

[a] Process observed over a range of temperatures.

[b] According to Eq. (6-1) with $w_j = 20$ μm.

[c] More than one process observed at this temperature.

TABLE 3-1. Vortex hopping distances for different RTSs observed in seven samples at various temperatures. These values are lower limits.

process involves a single vortex, and I will make that assumption in the remainder of this chapter. A hopping distance of micrometers, observed in several samples (see Table 3-1), is quite long, suggesting that the vortex is moving along a path of weak superconductivity, such as a twin or grain boundary. In Chapter VII, I will demonstrate that the hopping distances of vortices producing RTSs are orders of magnitude greater than those involved in $1/f$ noise.

Temperature Dependence of Lifetimes

Since the switching rate in Figs. 3-1(a) and (b) increases with temperature, a trend observed in other RTSs as well, it is natural to ask whether the processes are thermally activated. This would imply that the lifetimes $\tau_1(T)$ and $\tau_2(T)$ in each of the two potential wells are given by

$$\tau_i(T) = \tau_{Ai} \exp[\, U^{(i)}(T)/k_B T\,] \;, \quad i = 1,2 \;. \tag{3-1}$$

Here, the lower state is labeled by $i = 1$ and the upper state by $i = 2$, τ_{Ai}^{-1} is the attempt frequency in the ith state, and $U^{(i)}(T)$ is the temperature-dependent energy barrier for hopping out of that state. The lifetime ratio $\gamma = \tau_1/\tau_2$ is exponentially sensitive to the difference in activation energies $U^{(1)}(T)-U^{(2)}(T)$. The temperature dependence of γ obtained from the time traces of the process in YBCO(3) is plotted in Fig. 3-3(a). Note that the measured values of γ are consistent with a constant value of 4.5±1.0, even though τ_1 and τ_2 change by two orders of magnitude over the same

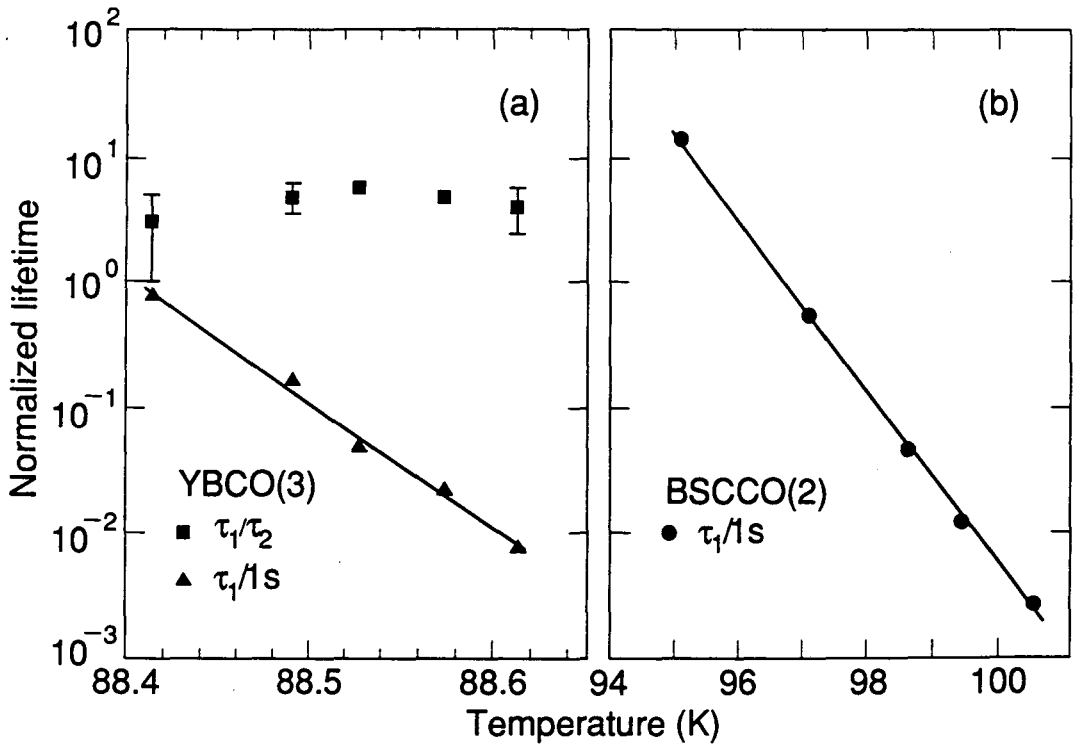

FIG. 3-3. Lifetimes vs. temperature for (a) YBCO(3) and (b) BSCCO(2). Solid lines are least-squares fits of Eq. (3-1) to $\tau_1(T)$ assuming $U(T) = U_0(1-t^4)$ and $\tau_{A1} = 10^{-11}$ s. Fitting parameters are given in Table 3-2.

temperature range. I conclude that the states 1 and 2 have very nearly the same activation energy.

One often reads in the literature [109] that the observability of an RTS necessarily implies a small difference in activation energies $U^{(1)}(T)-U^{(2)}(T) \lesssim 2k_BT$, on the grounds that a large energy difference would make it impossible for both τ_1^{-1} and τ_2^{-1} to be in the measured bandwidth at the same temperature, according to Eq. (3-1). However, this is true only if the attempt times τ_{Ai} are comparable. Thus there is no reason *a priori* that the measured values of γ should be temperature independent. This measurement allows me to take the activation energies in the two states of the RTS to be exactly equal in order to simplify the following discussion, and to attribute the asymmetry in the lifetimes to different attempt frequencies τ_{A1}^{-1} and τ_{A2}^{-1}, but the data in Fig. 3-3(a) are fit nearly as well by the assumption of equal attempt frequencies and slightly different activation energies $U^{(1)}(T)-U^{(2)}(T) \approx 11$ meV.

The power spectrum of a random telegraph signal is a Lorentzian of the form [110]

$$S_\Phi(f,T) = \frac{4(\Delta\Phi)^2}{(\tau_1+\tau_2)[(\tau_1^{-1}+\tau_2^{-1})^2+(2\pi f)^2]}, \qquad (3\text{-}2)$$

and in Fig. 3-2 I plot $S_\Phi(f)$ measured in YBCO(3) at two temperatures. The solid curves are obtained from Eq. (3-2) with fixed values of γ and $\Delta\Phi$, as determined from the time traces; τ_1 is the only fitting parameter. From fits of this kind, I obtain τ_1 versus temperature, shown plotted as triangles in Fig. 3-3(a). The data for BSCCO(2) imply $\gamma \approx 1$, since Φ is distributed symmetrically about its mean, and an analysis similar to that applied to YBCO(3) yields the values of τ_1 plotted in Fig. 3-3(b).

Equation 3-2 implies that the noise plateau below the Lorentzian knee frequency $S_\Phi(f \rightarrow 0)$ should be proportional to $(\Delta\Phi)^2\gamma(\gamma+1)^{-3}\tau_1$. For the switching processes in YBCO(3) and BSCCO(2), $S_\Phi(f \rightarrow 0)$ plotted on logarithmic axes as a function of τ_1 exhibits a slope very close to unity, as shown in Fig. 3-4. This implies that the temperature dependence of the noise power spectrum can be attributed solely to $\tau_1(T)$. Other parameters, such as the number of vortices involved in the process, the lifetime ratio γ, the hopping distance ℓ, and the SQUID-sample coupling α_s, do not change significantly over this temperature range.

Activation Energies for Vortex Motion

From the temperature dependence of the lifetime $\tau_1(T)$, the zero-temperature vortex pinning energy U_0 can be extracted. Since the measurements were made within a few degrees of T_c, some estimate of the functional form of $U(T)$ is required, but the temperature intervals over which values of $\tau_1(T)$ exist are too small to enable me to determine this unambiguously. If I were to assume that $U(T)$ is well approximated by a temperature-independent U_0 as proposed, for example, in Ref. [34], then a least-squares fit of Eq. (3-1) to the data from YBCO(3) would yield U_0 = 16 eV and $\tau_{A1}^{-1} \approx 10^{900}$ Hz. Since this attempt frequency is unphysically high, I conclude that a temperature-independent pinning energy is inconsistent with the data. Previous workers [10,35,111] seeking a general functional form for $U(T)$ have taken it to be proportional to the product of the condensation energy density and an activated volume

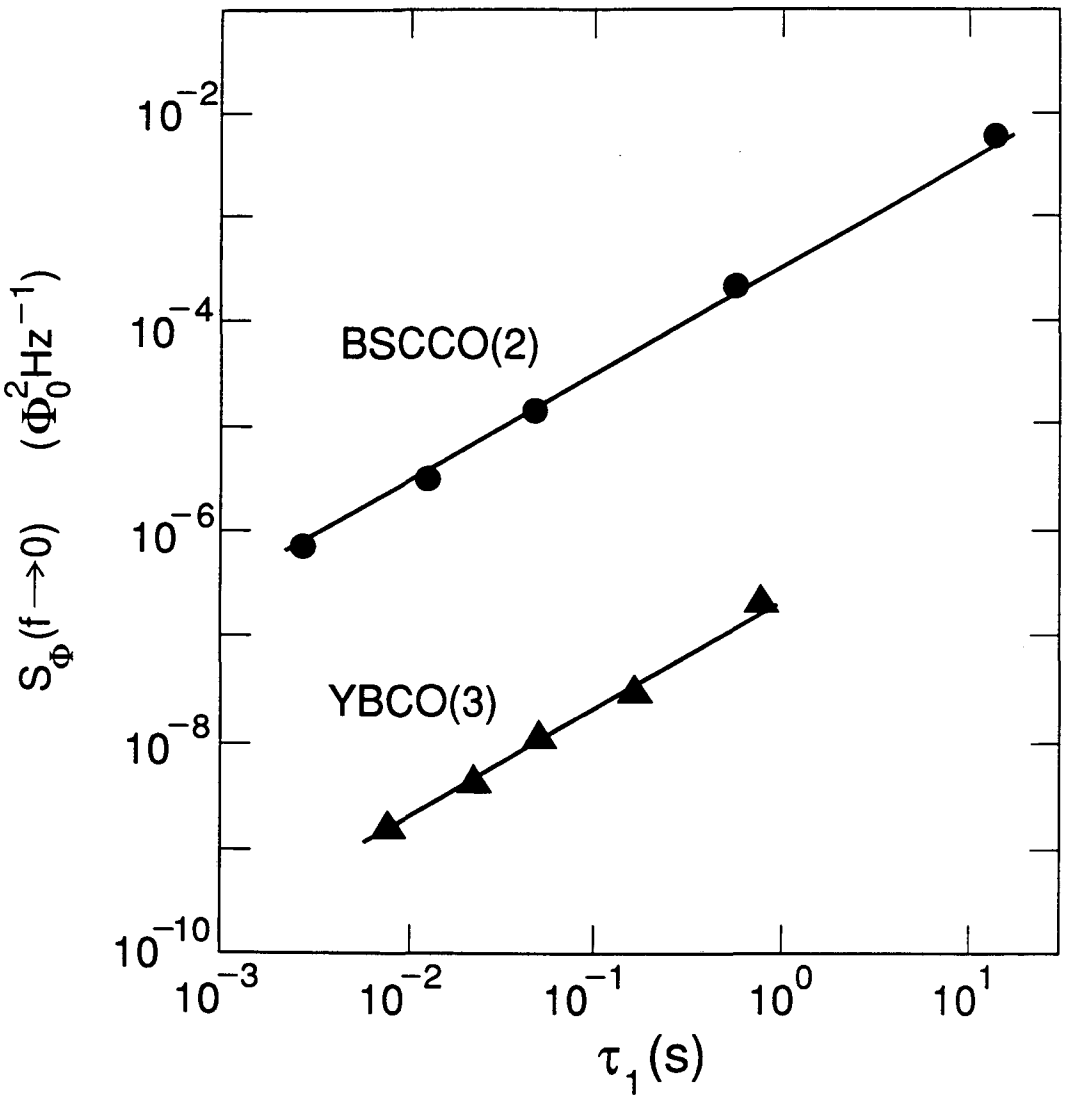

FIG. 3-4. Noise power on low-frequency plateau $S\Phi(f \rightarrow 0)$ vs. down-state lifetime τ_1 for two samples. Triangles, YBCO(3); circles, BSCCO(2). Noise in SQUID computed according to Eq. 2-1. Lines are least-squares fits with unit slope.

$[B_c^2(T)/2\mu_0]\xi^n(T)a_p^{3-n}$, where a_p is a temperature-independent pinning length and $n = 3$, 2, or 1. I regard T_c as a fitting parameter, since the small region in which the vortex moves may have a transition temperature different from that measured for the sample as a whole; nevertheless, the fitted values of T_c determined below are in reasonable agreement with the measurements. I restrict τ_{A1} to the physically meaningful range [79] 10^{-12} s $\leq \tau_{A1} \leq 10^{-5}$ s. Fitting Eq. (3-1) to the measured values of $\tau_1(T)$ gives the values of U_0 and T_c listed in Table 3-2, using the following temperature dependences of $U(T)$:

n = 3. This value gives $U(T) = U_0(1+t^2)(1-t^4)^{1/2}$, where $t = T/T_c$ and I have used the standard results [79] $\Phi_0 = 2\sqrt{2}\pi\lambda(T)\xi(T)B_c(T)$, $B_c(T)/B_c(0) = 1-t^2$, and $\lambda(T)/\lambda(0) = (1-t^4)^{-1/2}$. The temperature dependence of the penetration depth $\lambda(T)$ follows from the empirical two-fluid model, which agrees well with the theoretical result for a strong-coupled BCS superconductor [112,113] and with the values measured for YBCO [114,115].

n = 2. Using this value, I obtain

$$U(T) = U_0(1-t^4) \ , \tag{3-3}$$

the temperature dependence of which arises solely from $\lambda(T)$. Fits to Eq. (3-1) for $\tau_{A1} = 10^{-11}$ s are shown in Fig. 3-3. Fits of similar quality are obtained for all values of τ_{A1} and n, so it is difficult to determine the proper values for these parameters from the RTS data. However, I will argue below that the choices $\tau_{A1} = 10^{-11}$ s and $n = 2$ are the most physically reasonable.

	$n = 1$		$n = 2$		$n = 3$		
τ_{A1} (s)	U_0 (eV)	T_c (K)	U_0 (eV)	T_c (K)	U_0 (eV)	T_c (K)	$U(T_m)$ (eV)
			Sample YBCO(3)				
10^{-5}	33	89.1	4.0	88.9	0.37	88.7	0.07
10^{-10}	23	89.8	4.1	89.4	0.56	89.0	0.16
10^{-11}	21	90.0	4.1	89.5	0.59	89.0	0.17
10^{-12}	21	90.1	4.1	89.6	0.63	89.0	0.19
			Sample BSCCO(2)				
10^{-5}	0.93	107	0.39	104	0.12	101	0.08
10^{-10}	0.81	117	0.47	110	0.20	104	0.18
10^{-11}	0.81	120	0.48	112	0.22	105	0.20
10^{-12}	0.80	122	0.49	113	0.23	105	0.22

TABLE 3-2. Zero-temperature activation energies U_0 and local transition temperatures T_c deduced for RTSs in two samples for different values of the attempt time τ_{A1} and different models of the temperature dependence of $U(T)$. The models are labeled by n, the power of the coherence length in the activated volume. A typical activation energy in the temperature range where the switching was observed is $U(T_m)$, where T_m = 88.5 K for YBCO(3) and 97.8 K for BSCCO(2).

$n = 1$. This model has been applied successfully to high-field transport data [116], giving $U(T) = U_0(1-t^2)(1-t^4)^{1/2}$.

Table 3-2 indicates that U_0 increases as n decreases from 3 to 1. The $n = 1$ values for YBCO(3) are so high as to be physically unlikely; since the model is derived from the shear energy of a strongly interacting vortex lattice [116], it is probably inappropriate to my low-field experiment. The RTS data provide no basis for preferring the $n = 2$ values over the $n = 3$ values; both activation energies correspond to a single vortex pinned over a length less than or equal to the sample thickness. However, most types of pinning interactions for isolated vortices [8] give energies proportional to the vortex self-energy [117]

$$\varepsilon_\ell(T) = \frac{\Phi_0^2 \ln\kappa}{4\pi\mu_0 [\lambda_{ab}(T)]^2} = \varepsilon_\ell(0)\,(1-t^4) \ , \qquad (3\text{-}4)$$

which depends on temperature in the same manner as Eq. (3-3) for $n = 2$. Here, λ_{ab} is the penetration depth when the screening current flows in the a-b plane, as appropriate for vortices parallel to the c axis. In addition, Hagen and Griessen have found that only $n = 2$ is consistent with flux creep data analyzed according to their model [111].

The lifetime of the random telegraph signals analyzed here provides useful information about the activation energy, even without knowledge of its precise temperature dependence. Table 3-2 gives values of $U(T_m)$, where T_m is the midpoint of the temperature range over which switching was observed, and these energies depend on τ_{A1} but not on n. An estimate of τ_{A1} follows from the fact that the effective mass of a vortex is generally negligible except in artificially structured samples [118,119], so that the response of pinned vortices is determined by the competition between

viscous and restoring forces. In the copper oxides, where the normal-state resistivity ρ_n is quite large, one expects a weak coefficient of viscous damping [79] $\eta = \Phi_0^2/2\pi\xi^2\rho_n$, which decreases the characteristic time [120]. This is confirmed by several experiments [34,111,121] which found the attempt times for vortex motion in high-temperature superconductors to be quite small, in the range 10^{-12} s $\leq \tau_{A1} \leq 10^{-10}$ s. Over this range, Table 3-2 yields $U(T_m) = 0.175 \pm 0.015$ eV for YBCO(3) and $U(T_m) = 0.20 \pm 0.02$ eV for BSCCO(2). Thus, I can estimate reliably the pinning energy in the temperature range where the random telegraph signals appear, but I have no meaningful way to extrapolate it to $T = 0$ without a model of $U(T)$ from another source.

Noisy and Quiet Metastable States

So far in this chapter I have considered processes in which the noise power is dominated by switching between readily identified metastable states. The spectral density of fluctuations about the mean value in each state could be neglected. Figure 3-1(c) depicts one event from a more complex process in sample YBCO(2) in which the flux switches between two states separated by $2.8 \times 10^{-3}\Phi_0$. In contrast to the process seen in YBCO(3) and BSCCO(2), the noise in state 1 (the lower level) is much higher than in state 2. I interpret this event as the hopping of a vortex between a pinning site where it is relatively mobile (state 1), producing a high noise level, and another site where it is much more restricted spatially. A more dramatic example of such a process appears in

Fig. 3-5(a). These data, obtained from sample TCBCO(1), indicate three metastable states for the vortex, each producing a different amount of noise. Presumably the spatial gradient of the pinning potential is greatest in the relatively quiet middle state. This process persisted for many minutes, with hopping among the same three states occurring every few seconds.

Noise processes such as these, in which the state of one fluctuator influences the noise power of another, have been observed in other systems such as metal-oxide-semiconductor diodes [122] and metallic constrictions [123]. Those data have generally been interpreted as the result of interactions among several reconfiguring defects, rather than as the motion of a single degree of freedom (analogous to vortex position) in a complicated potential. In the absence of microscopic information about the fluctuators, both explanations are tenable, but in the case of flux noise the low vortex density makes the single-vortex interpretation more plausible. However, vortices in the sample need not be uniformly distributed, therefore I can not rule out the possibility that the processes in Figs. 3-1(c) and 3-5(a) represent the interaction of one slowly hopping vortex with one or more rapidly moving vortices.

I have found that under certain circumstances it is possible to activate and deactivate single RTSs. Note that when the feedback switch is open in Fig. 2-4, the output of the integrator goes to either the positive or the negative rail (±15 V), depending on its initial perturbation. Thus, closing the feedback loop applies a small magnetic field step (approximately 0.8 μT) of known sign to the SQUID and sample. The effect of this step is shown in Figs. 3-5 and 3-6. After closing the feedback loop

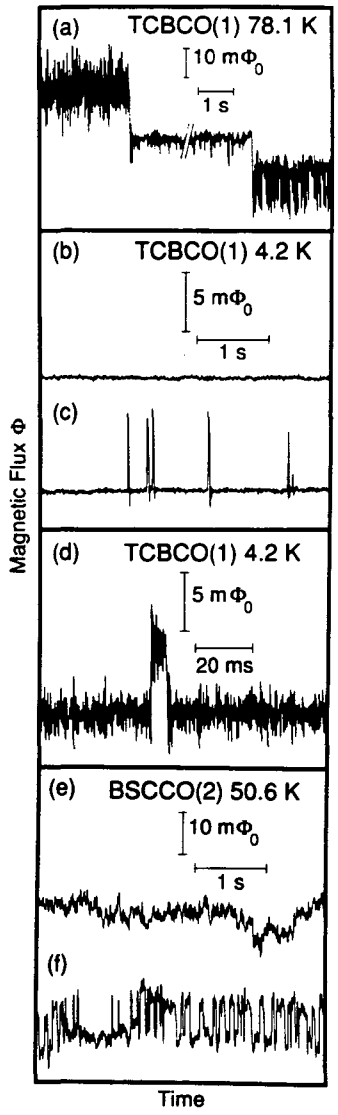

FIG. 3-5. Flux through SQUID vs. time generated by switching processes. (a) Sample TCBCO(1) at 78.1 K with three metastable states. Several seconds of data have been omitted as indicated by broken segment, during which time the fluctuator remained in the middle state. (b) TCBCO(1) at 4.2 K after negative-going magnetic field increment. (c) Same as (b), except switching has been induced by positive-going magnetic field increment. (d) Single event from (c) with time resolution increased by a factor of 40. High-frequency noise is also increased because of larger bandwidth. (e) BSCCO(2) at 50.6 K after positive field increment. (f) Same as (e), except switching induced by negative field increment. Zeros of axes are arbitrary.

with a negative-going field step, I observed from sample TCBCO(1) at 4.2 K the relatively featureless flux noise in Fig. 3-5(b). However, when closing the feedback loop caused a positive-going field step, two dramatic changes occurred. An RTS appeared in the time domain, evident as spikes in Fig. 3-5(c); both states in the process are clearly resolved on the expanded time scale in Fig. 3-5(d). Furthermore, the time-averaged flux $\langle\Phi\rangle$ was larger by $0.1\Phi_0$ when the RTS was active compared to its value in the absence of the RTS. The amplitude of the RTS is too small to explain this increase, which I believe corresponds to an actual change in the magnetization of the sample, caused by the trapping or displacement of a single vortex.

I observed similar behavior in sample BSCCO(2) at 50.6 K. Following a positive field step, noise was observed as in Fig. 3-5(e), while Fig. 3-5(f) shows additional noise from an RTS after a negative field step. The average flux $\langle\Phi\rangle$ is $0.02\Phi_0$ less when the RTS is present than when it is not. The noise power spectra under these two conditions are plotted in Fig. 3-6(a). In the absence of the RTS, the noise exhibits a featureless $1/f$ spectrum, of the type to be discussed in Chapter IV. The negative field step causes a weak knee to appear in the frequency domain near 10 Hz. The difference spectrum in Fig. 3-6(b) is well described by Eq. (3-2), as shown, indicating that the effect of the field step is to superpose a single RTS on $1/f$ noise from another source, presumably the motion of other vortices not involved in the RTS.

I found that the RTSs in Figs. 3-5(c) and (f) could be reliably activated by positive and by negative field steps, respectively, and deactivated by a step of the opposite polarity. It seems likely that the

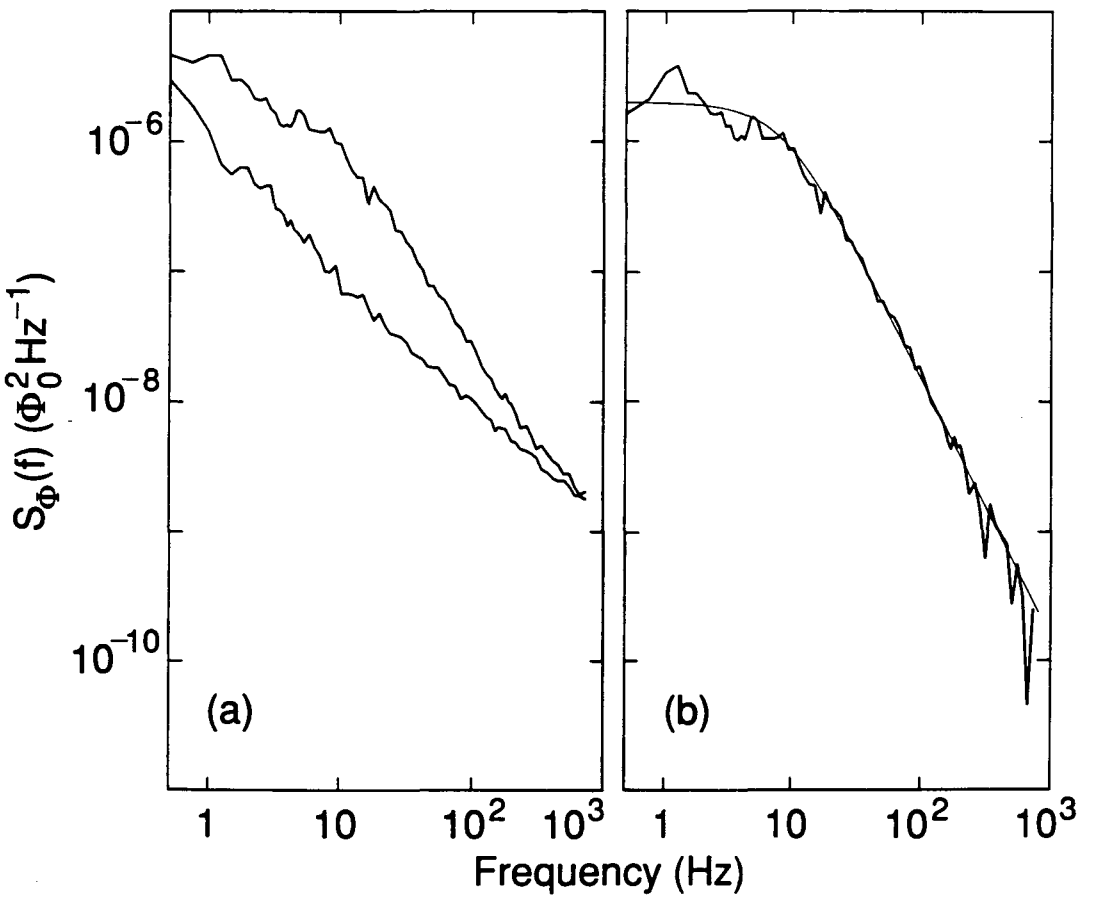

FIG. 3-6. Spectral densities of noise from BSCCO(2) at 50.6 K, referred to sample as in Eq. (2-2). (a) Total noise after positive-going (lower spectrum) and negative-going (upper spectrum) magnetic field increment. (b) Heavy curve, difference of spectra in (a); light curve, Lorentzian from Eq. (3-2) fitted with two free parameters: $\tau = (\tau_1^{-1}+\tau_2^{-1})^{-1} = 18$ ms and $(2\tau\Delta\Phi)^2/(\tau_1+\tau_2) = 2 \times 10^{-6}\ \Phi_0^2$/Hz.

shielding currents induced by the changes in the applied magnetic field exert Lorentz forces which push a vortex into or out of a noisy configuration, depending on the sign of the perturbation. Chapter VII will provide further examples of the deliberate control of individual noise processes by the application of magnetic fields. The flux creep data in Chapter VIII will show vortices passing through noisy and quiet configurations as they make their way out of the sample.

IV. 1/*f* Noise

All is flux, nothing stays still.

– Heraclitus (c. 500 B.C.), in Diogenes Laertius

The random telegraph signals discussed in Chapter III yielded readily to analysis because they possess clear features: an amplitude $\Delta\Phi$ in the time domain and a knee frequency τ^{-1} in the frequency domain. These features exist because a single hopping process dominates the noise. As might be expected, this situation is unusual. Typically there are of order 10^4 to 10^6 mobile vortices in the sample (as determined in Chapter VII), and the noise they produce is almost featureless, scaling as $1/f$ over the entire bandwidth of the measurement, as already shown in Figs. 3-5(e) and 3-6(a). This chapter draws upon earlier work [124,125] to survey the phenomenology of the $1/f$ noise in the samples, and I will develop a model for the analysis of the noise in Chapter V.

Dependence on Temperature and Sample Quality

An example of $1/f$ noise from YBCO(5), the noisiest sample I measured, is shown in Fig. 4-1. At 4.2 K, $S_\Phi(f)$ varies approximately as $1/f$ over the bandwidth of the measurement, 1 Hz to 1 kHz. When I increased the temperature to 44 K, the noise power at all frequencies increased by a factor of about 600. Immediately two features demand

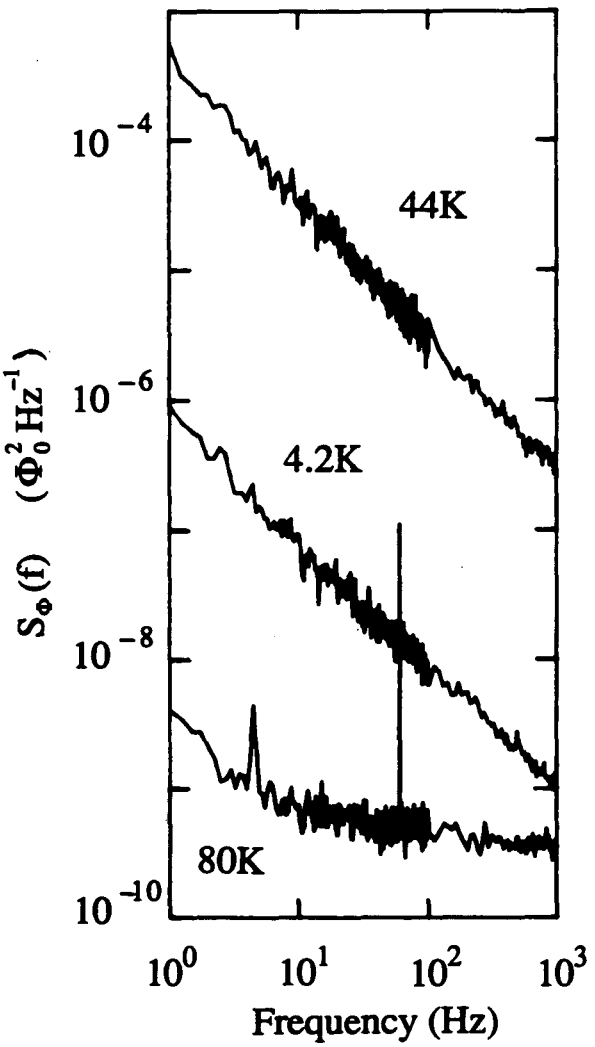

FIG. 4-1. Power spectra of total flux noise measured in sample YBCO(5) at three temperatures. The spectrum at 80 K shows noise from the SQUID, 60 Hz pickup, and a mechanical resonance at 4.5 Hz.

explanation: the frequency dependence of the noise, and the fact that the noise energy is not linear in the thermal energy k_BT. These issues will be addressed in Chapter V. At temperatures well above $T_c = 47$ K, noise from the sample is negligible. The spectrum at 80 K in Fig. 4-1 shows only broadband noise from the SQUID itself, a spike at 60 Hz from the ubiquitous power-line field, and a microphonic at 4.5 Hz. This last peak could be excited by gentle taps on the dewar, and presumably results from a mechanical mode of the apparatus moving in the residual magnetic field. Because the apparatus was never assembled exactly the same way twice, the sensitivity and characteristic frequency of these microphonics varied from run to run, and usually they were completely absent.

Figure 4-2 plots the spectral density of the noise at 1 Hz as a function of temperature for the three samples which were patterned into rings as described in Chapter II. The noise power generally increases with temperature, rising steeply just below T_c. Just above T_c, the noise drops very quickly with increasing temperature, and its spectral density is no longer $1/f$. The detailed behavior of each sample is different; for example, in YBCO(5) I observed a knee frequency in some spectra consistent with a Lorentzian superimposed on a $1/f$ background. At point A in Fig. 4-2 this knee frequency is near 10 Hz, at point B it is near 100 Hz, and at point C the noise is white over the bandwidth of the measurement. I interpret this as a single process dominating the noise because its hopping distance is unusually large, perhaps because the sample has separated into weakly coupled superconducting regions. Sample YBCO(3) exhibited quite different behavior close to T_c, as shown in Fig. 4-3. The noise power rises by five orders of magnitude in less than 1 K, peaks exactly at the inductive

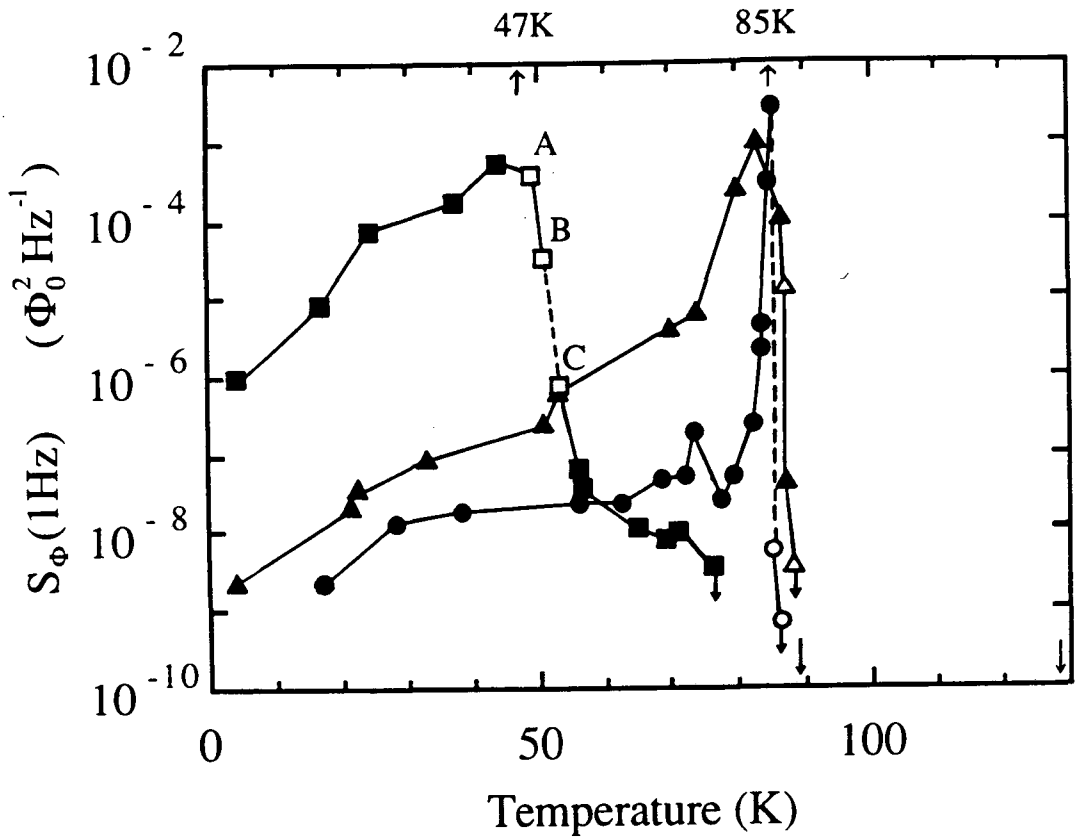

FIG. 4-2. Spectral density of flux noise at 1 Hz vs. temperature for three "ring" samples: squares, YBCO(5); triangles, YBCO(4); circles, YBCO(1). SQUID noise has been subtracted. Solid symbols imply that the spectral density is $1/f$ at 1 Hz, open symbols that it is white or nearly white. Dashed lines indicate temperature ranges where the noise prevented flux-locked operation of the SQUID. Downward arrows above T_c indicate upper limits on the noise from the samples. Small errors in the calibration of the thermometer and the subtraction of background noise have been corrected since the original appearance of this figure in Ref. [124].

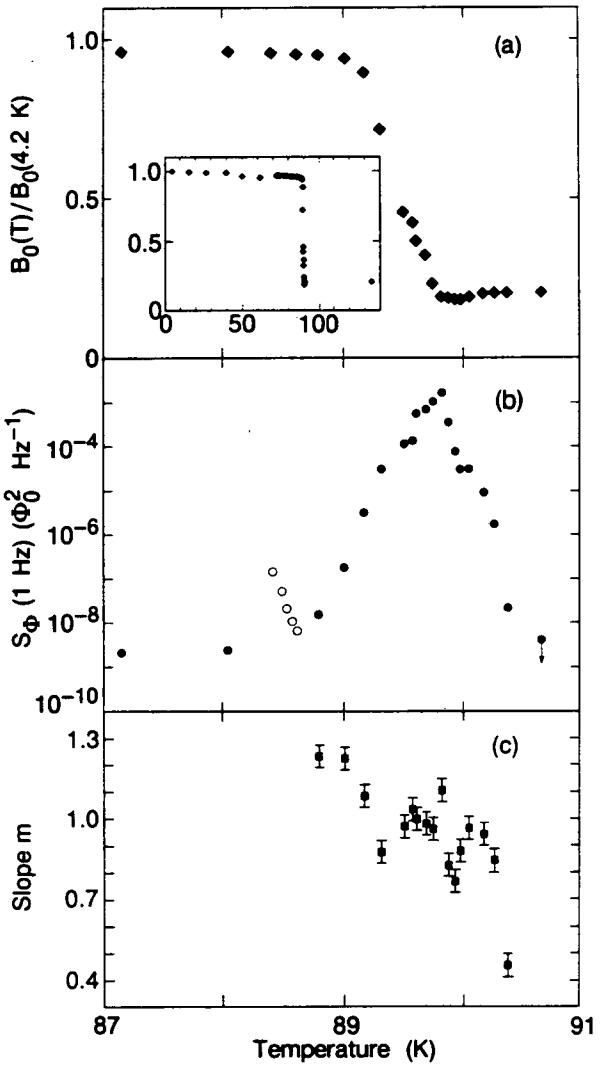

FIG. 4-3. Sample YBCO(3) within a few degrees of $T_c = 89.8$ K. (a) Normalized applied magnetic field B_0 required to generate one flux quantum in the SQUID vs. temperature. The drop in B_0 reflects vanishing diamagnetic screening as the film becomes normal. This plot is essentially the reciprocal of the mutual inductance measurement described in Fig. 2-5. Inset shows B_0 over a wider temperature range. (b) Noise power at 1 Hz vs. temperature. Solid symbols, $1/f$ spectra; open symbols, Lorentzian spectra from RTSs analyzed in Chapter III; downward arrow, upper limit on noise. (c) Slope m of noise power spectrum vs. temperature.

T_c, and then falls just as rapidly. Throughout this temperature range, the power spectrum scales roughly as $1/f$, but its slope tends to decrease with increasing temperature.

From the data in Fig. 4-2 it is evident that noise decreases as sample quality improves, and that the noise well below T_c is less temperature dependent for the quieter films. I will present additional measurements below which support these generalizations. As Table 2-1(a) indicates, the parameters used to measure sample quality generally vary together, so that low-noise films tend to have high critical currents, high transition temperatures, and good epitaxial orientation. Since I have not varied these independently, I lack sufficient data to completely identify the material parameters which control the noise; an exception is the *a*-axis sample YBCO(6) discussed in Chapter V. Clearly there are three factors which need to be disentangled:

Number of vortices. I assume that the $1/f$ noise can be understood as the superposition of noise from many vortex hopping events. This model will be developed in detail in Chapter V. It implies that a sample which contains fewer vortices will tend to be less noisy. I will present evidence in Chapter VII that the number of vortices is intrinsic to the sample, and not generated by the applied magnetic field, at least for very small values of the field.

Hopping distance. As we saw in Chapter III, the noise power from a single RTS is proportional to ℓ^2, the square of the hopping distance. Thus a sample in which the vortices are hopping shorter distances will be less noisy, all other things being equal.

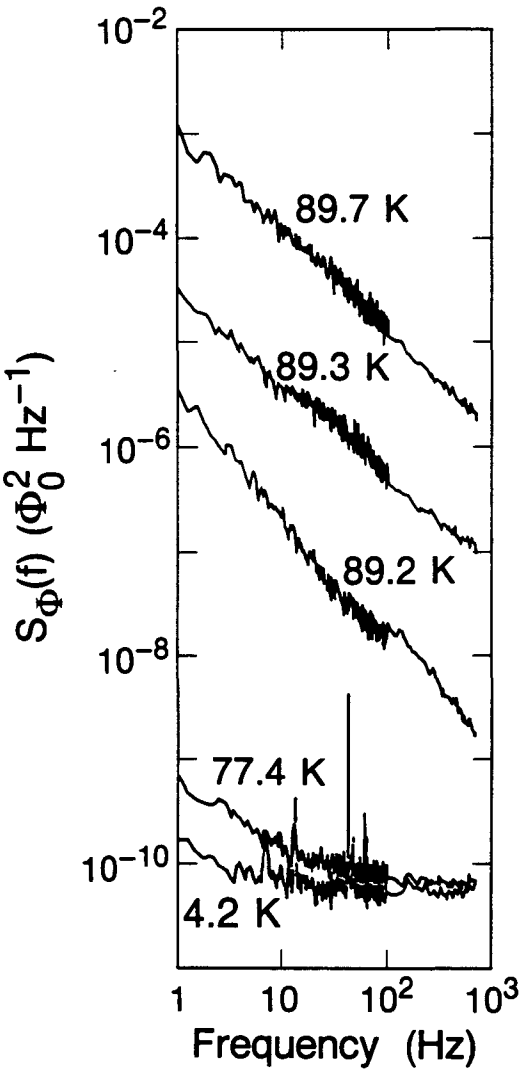

FIG. 4-4. Spectral density $S_\Phi(f)$ of flux noise in YBCO(3) at five temperatures. At 4.2 K, the observed noise can be attributed to the SQUID measuring system; the SQUID contribution is significant at temperatures up to 87 K. Spikes are from 60 Hz pickup and microphonics.

Activation energy. The power spectrum for each vortex hopping process is a Lorentzian [Eq. (3-2)] with a knee frequency $\tau^{-1} = \tau_1^{-1} + \tau_2^{-1}$. If τ^{-1} is far outside the bandwidth of the noise measurement, the process will not be detected. According to Eq. (3-1), τ depends sensitively on the activation energy $U(T)$ and less sensitively on the attempt time. A sample in which $U(T)$ is large will be less noisy, all other things being equal. Very small values of $U(T)$ might also lead to low measured noise, because the vortices would be moving too quickly to detect, but in that case the sample would have a vanishingly small critical current density [126,127].

The least noisy film on which I made measurements was the laser ablated *in situ* film YBCO(3). Figure 4-4 shows the spectral density of the flux noise $S_\Phi(f)$ at five temperatures. At 4.2 K the noise is nearly white and is dominated by noise in the SQUID. At 77.4 K the spectral density of the measured low-frequency noise has increased by a factor of approximately four compared to the 4.2 K value. The spectra at higher temperatures scale as $1/f^m$, where $m \approx 1$, and increase rapidly in magnitude with temperature. Explaining the temperature dependence of m for this and other samples will be a major thrust of the theory to be developed in Chapter V. Figure 4-5 plots the temperature dependence of S_Φ(1 Hz) for YBCO(3). The noise increases slowly as temperature is raised from 4.2 K to 87 K, then peaks sharply at T_c. This peak is plotted on an expanded temperature scale in Fig. 4-3(b). It is quite interesting to me that the maximum noise power at $T \approx T_c$ is always of order $10^{-3}\ \Phi_0^2$/Hz at 1 Hz in YBCO, regardless of the sample. This suggests an intrinsic mechanism generating the noise in this temperature range, independent of materials properties [128]. I will speculate further on this topic in Chapter V.

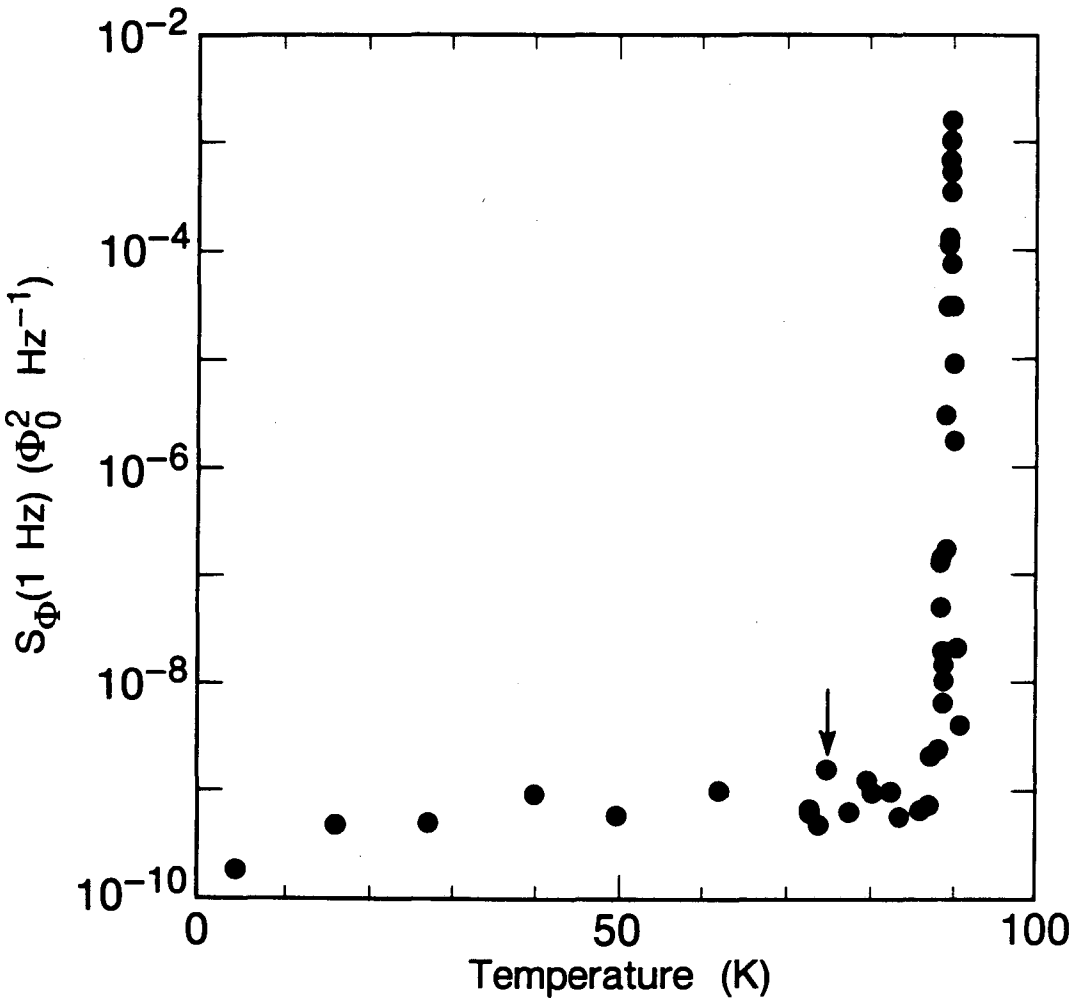

FIG. 4-5. Flux noise $S\Phi(1\ \mathrm{Hz})$ vs. temperature for YBCO(3). Values below $8 \times 10^{-10}\ \Phi_0^2/\mathrm{Hz}$ include large contributions from the measuring system, and therefore represent upper limits on noise from the film. A significant and reproducible maximum in noise from the film occurs near 75 K (arrow), and a large peak at $T_c = 89.8$ K.

Testing the Direct Noise Mechanism

The direct noise mechanism introduced in Chapter III is a local mechanism, in the sense that a fluctuating magnetic field linking the SQUID can arise in a region of the sample as small as a single vortex. Of course, the motion of even one vortex will cause a redistribution of screening currents to exclude magnetic fields from the bulk of the sample, but the only role these currents play in coupling the noise into the SQUID is to maintain the superconducting-groundplane boundary condition. I regard this local mechanism as a hypothesis which should be tested. Alternative mechanisms have been proposed [129] in which circulating currents play an essential role in the generation of the noise.

I made a single scratch through the "ring" sample YBCO(4) which prevented the flow of circulating currents, and then remeasured the noise. Figure 4-6 shows no significant change in the magnitude of the noise as a result of this altered geometry. There is some uncertainty in the value of α_s to be used in Eq. 2-2 for the slit-ring geometry, since the method for estimating the coupling outlined in Chapter II assumes that the sample inductance can support a shielding current. Inspection of the inset to Fig. 3-2 leads me to expect a decrease in the effective coupling since the flux in the ring is no longer quantized, and some of the field lines from a vortex will close through the hole in the sample. However, the uncertainty in α_s introduced by these considerations is small compared to the orders of magnitude over which the noise power varies in Fig. 4-6. I conclude that the generation of flux noise in "ring" samples is independent of the availability of a closed path for current around the ring. In Chapter VI it

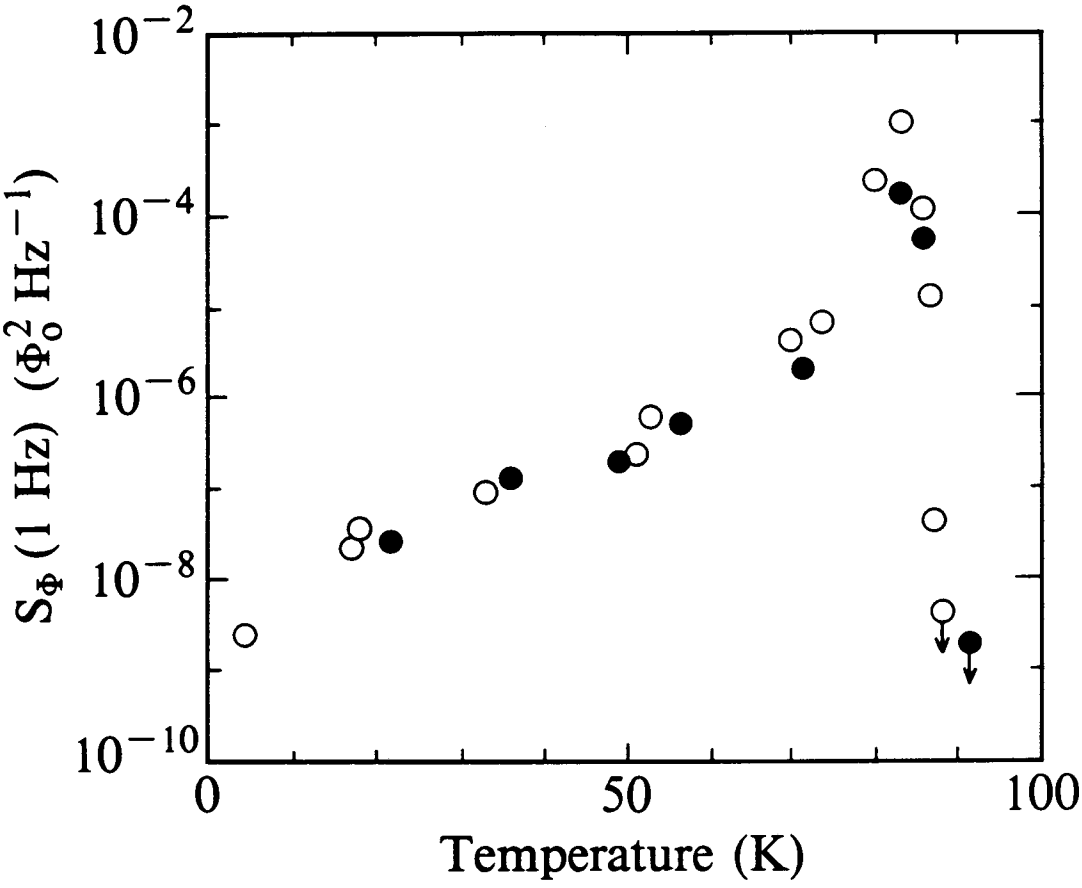

FIG. 4-6. Flux noise S_Φ(1 Hz) vs. temperature for YBCO(4). Open symbols represent measurements made with the ring intact as in Fig. 4-2, solid symbols with the ring slit to eliminate circulating currents. Noise is referred to sample as in Eq. 2-2 with the same value of α_s for both geometries. At 4.2 K, the open and solid symbols coincide.

will be shown that for other geometries, current fluctuations must be taken into account to calculate the coupling.

V. 1/*f* Noise as a Superposition of Random Telegraph Signals

> You may wish to skip over the following discussion – and any other discussion of the subject that you encounter in the next several years, until you hear that the whole thing has gotten sorted out.
>
> – Tom Weller, *Science Made Stupid* (1985)

My analysis of the 1/*f* noise is based on the Dutta-Dimon-Horn (DDH) model, which has also been applied successfully to noise in thin metal films [130,131], metallic constrictions [123], and tunnel junctions [132]. The derivation of Eq. (5-7) for the slope of the noise power spectrum by DDH [2] has subsumed decades of previous work under their name, tending to overshadow vital early contributions by Bernamont [133], van der Ziel [134], du Pré [135], and McWhorter [136]. However, since no one today objects to the phrase "Maxwell's equations," I will unashamedly refer to "the DDH model." The central assumption of this model is that 1/*f*-like noise arises from the incoherent superposition of many thermally activated switching processes, similar to those analyzed in Chapter III. Physically this assumption makes a great deal of sense; flux creep experiments [24,137,138] long ago demonstrated the thermally activated hopping of vortices, and vortex motion affects the flux linking the SQUID by the direct noise mechanism. An attempt has been made to explain the noise as a manifestation of universal conductance fluctuations [129], but the relevance of this theory to my experiment is disputed [139-

141]. Two principal extensions to the DDH model will be made in this dissertation. The first is the generalization to temperature-dependent activation energies, the necessity of which was demonstrated in Chapter III; this model is the subject of a previous publication [142]. The second modification, which I will postpone to Chapter VII, is the inclusion of a driving force which acts on the vortices.

Excellent reviews of the literature which has grown up around the DDH model are provided by Refs. [109,131,143]. Other more elegant theories of $1/f$ noise exist, but none has been as successful in explaining experimental data.

Extended Dutta-Dimon-Horn Model

The DDH model postulates an ensemble of two-state fluctuators, or hopping processes, which are identical except for their activation energy $U(T)$. In the absence of detailed knowledge of the pinning potential, the fluctuators are generally assumed [109] to be symmetrical, so that $U^{(1)}(T) = U^{(2)}(T) \equiv U(T)$ and $\tau_{A1} = \tau_{A2} \equiv 2\tau_0$ in the notation of Chapter III. Recall that for the RTSs previously analyzed, I showed that at worst the activation energies were slightly different, and the attempt times were of the same order. Since attempt times will enter the model only logarithmically, such small differences are not significant. Furthermore, I will demonstrate in Chapter VII that symmetrical processes are necessary to explain the current dependence of the noise. For a symmetrical

thermally activated process, Eq. (3-1) gives the temperature dependence of the correlation time

$$\tau(T) = \frac{1}{\tau_1^{-1} + \tau_2^{-1}} = \tau_0 \exp[\, U(T)/k_B T\,] \qquad (5\text{-}1)$$
$$= \tau_0 \exp[\, U_0 \beta(T)\,] \ ,$$

where U_0 is the activation energy at zero temperature and $\beta(T) \equiv U(T)/U_0 k_B T$. The spectral density of the noise from this single process depends on τ according to Eq. (3-2):

$$S_\Phi(f,T) = \frac{(\Delta\Phi)^2\, \tau}{1 + (2\pi f \tau)^2} \ . \qquad (5\text{-}2)$$

At this point it is useful to relate the amplitude $\Delta\Phi$ of one process to its hopping distance ℓ. I demonstrated in Chapter III that $\Delta\Phi \approx \alpha_s \Phi_0 \ell / w$ for radial vortex motion, which generalizes to

$$\Delta\Phi = \frac{\alpha_s \Phi_0}{w} \ell \cos\theta \equiv \Phi_\ell\, \ell \cos\theta \qquad (5\text{-}3)$$

for hopping at an angle θ from the radial direction. Equation (5-3) defines the relationship between hopping distance and flux change which I call the direct noise mechanism. I will introduce an indirect noise mechanism in Chapter VI, for which the geometrical coefficient Φ_ℓ is quite different.

Assuming that the noise from the processes in the ensemble combines incoherently, as will be demonstrated in Chapter VIII, the total noise is

$$S_\Phi(f,T) = \frac{1}{2} \int_0^\infty dU_0\, D(U_0) \frac{(\Phi_\ell\, \ell)^2\, \tau}{1 + (2\pi f \tau)^2} \ , \qquad (5\text{-}4)$$

where $D(U_0)\,dU_0$ is the number of processes with zero-temperature activation energies between U_0 and U_0+dU_0. I have removed the angular dependence from Eq. (5-2) by averaging over θ, taken to be uncorrelated with U_0. I assume that τ_0, $\beta(T)$, and ℓ are the same for all processes. Of these, $\beta(T)$ is the least likely to vary from process to process, since it is notoriously difficult to distinguish core pinning interactions from magnetic interactions, for example, on the basis of their temperature dependence [8]. The consequences of a distribution of characteristic times τ_0 will be explored at the end of this chapter, and an energy-dependent hopping distance $\ell(U_0)$ will be considered in Chapter VII.

The correlation time τ is an exponential function of U_0, so the kernel in Eq. (5-4) is sharply peaked at a characteristic energy

$$\tilde{U}_0(f,T) = \frac{\ln(1/2\pi f\tau_0)}{\beta(T)} \quad . \tag{5-5}$$

Assuming that the distribution of activation energies $D(U_0)$ varies slowly across the width of the kernel, $D(U_0)$ can be taken outside the integral, which then yields

$$D[\tilde{U}_0(f,T)] = \frac{8\beta(T)}{(\Phi_\ell\,\ell)^2}\, f\, S_\Phi(f,T) \quad . \tag{5-6}$$

This equation summarizes the physical content of the DDH model. By measuring $S_\Phi(f,T)$ and taking an appropriate functional form for $\beta(T)$, I can determine $D(U_0)$. I will plot $D(U_0)$ in arbitrary units because, without RTSs clearly resolved in the time domain, I have no information about the hopping distance ℓ in Eq. (5-6). However, in Chapter VII the current

dependence of the noise will yield values for ℓ, making it possible to obtain $D(U_0)$ in meaningful units.

Checking the Slope of the Noise Power Spectrum

The model makes an additional prediction, which serves as a consistency check. Since $D[\tilde{U}_0(f,T)]$ is weakly frequency dependent, Eq. (5-6) implies $S_\Phi(f,T) \propto 1/f^m$, where $m = -\partial \ln S_\Phi / \partial \ln f$ is close to unity but may depend somewhat on temperature and frequency. It is remarkable that the innocuous assumptions of thermal activation [Eq. (5-1)] and a broad distribution of activation energies are sufficient to generate a $1/f$ spectrum. From Eqs. (5-5) and (5-6) it can be shown that the slope m obeys

$$m(f,T) = 1 - \frac{1}{\ln(1/2\pi f \tau_0)}\left(1 + \frac{\partial \ln S_\Phi}{\partial \ln T} \Big/ \frac{\partial \ln \beta}{\partial \ln T}\right) . \qquad (5\text{-}7)$$

Since $\partial \ln\beta / \partial \ln T < 0$ and $\ln(1/2\pi f \tau_0) > 0$, Eq. (5-7) implies that in temperature ranges over which the noise is increasing, the power spectrum will be steep, but when the noise is decreasing, it will have a shallower slope. Provided that the measured values of $m(T)$ agree with the prediction of Eq. (5-7), the $1/f$-like noise I measure is consistent with an ensemble of random telegraph signals.

The flux noise measurements from which I extract the distribution of activation energies $D(U_0)$ are plotted in Fig. 5-1. The measurement frequency is $f = 1$ Hz. The noise is $1/f$-like at all temperatures below T_c, except for the RTSs observed above 78 K in YBCO(2) and above 87 K in BSCCO(1), as listed in Table 3-1. These events are obviously not included

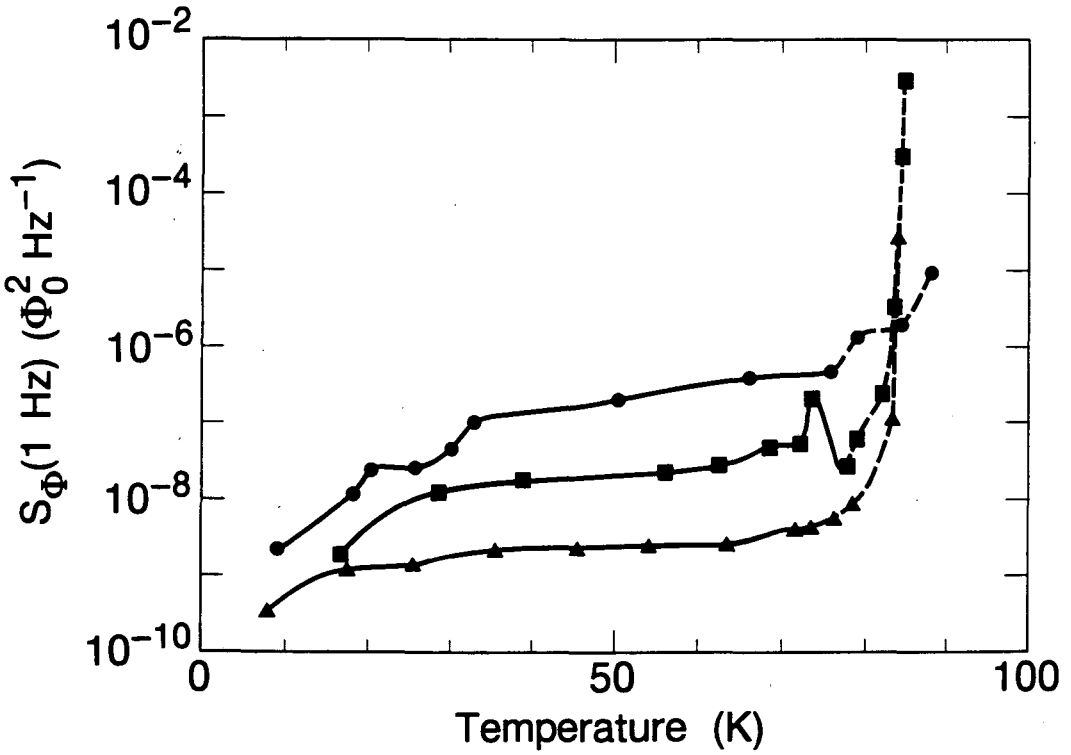

FIG. 5-1. Spectral density of flux noise at 1 Hz vs. temperature below T_c for three samples: squares, YBCO(1); triangles, YBCO(2); circles, BSCCO(1). SQUID noise has been subtracted. All data points show a $1/f$-like noise power spectrum. Curves are piecewise cubic interpolants used to calculate $m(T)$ (solid and dashed segments) and $D(U_0)$ (solid segment only).

in the following analysis. I am confident that the features in the temperature dependence of the noise are not the result of second superconducting phases with depressed T_c. Such phases are readily detected by their effect on the mutual inductance between the SQUID and the feedback coil, as exemplified by Fig. 2-5, and none were found at the temperatures in question.

Two parameters must to be specified to obtain quantitative results from the DDH model, the correlation time prefactor τ_0 and the temperature dependence $\beta(T)$. I choose $\tau_0 = 10^{-11}$ s because it falls near the middle of the range of physically reasonable values discussed in Chapter III. Since τ_0 appears in Eqs. (5-5) and (5-7) only within a logarithm, I can easily tolerate large uncertainties in its value; for example, Table 3-2 indicates that the deduced activation energies depend only very weakly on the attempt time. My choice of $\beta(T) = (1-t^4)/k_BT$ agrees with the $n = 2$ case in Chapter III [Eq. (3-3)], for the reasons presented there. For the value of T_c in $t = T/T_c$, I take the inductively measured value reported in Table 2-1(b).

A necessary condition for the validity of the DDH model is agreement between the measured and predicted slope of the noise power spectrum. Figure 5-2 shows the experimental values of $m(T)$ for each sample, and the values calculated from Eq. (5-7). The entire fit to $S_\Phi(T)$ in Fig. 5-1 (solid and dashed segments) is used, since Eq. (5-7) is relatively insensitive to the particular functional form of $\beta(T)$. Although the measured and predicted values of m can differ by 10%, the major trends are reproduced, making application of the DDH model credible. Note, for example, that in Fig. 5-2(a) the most extreme departures from

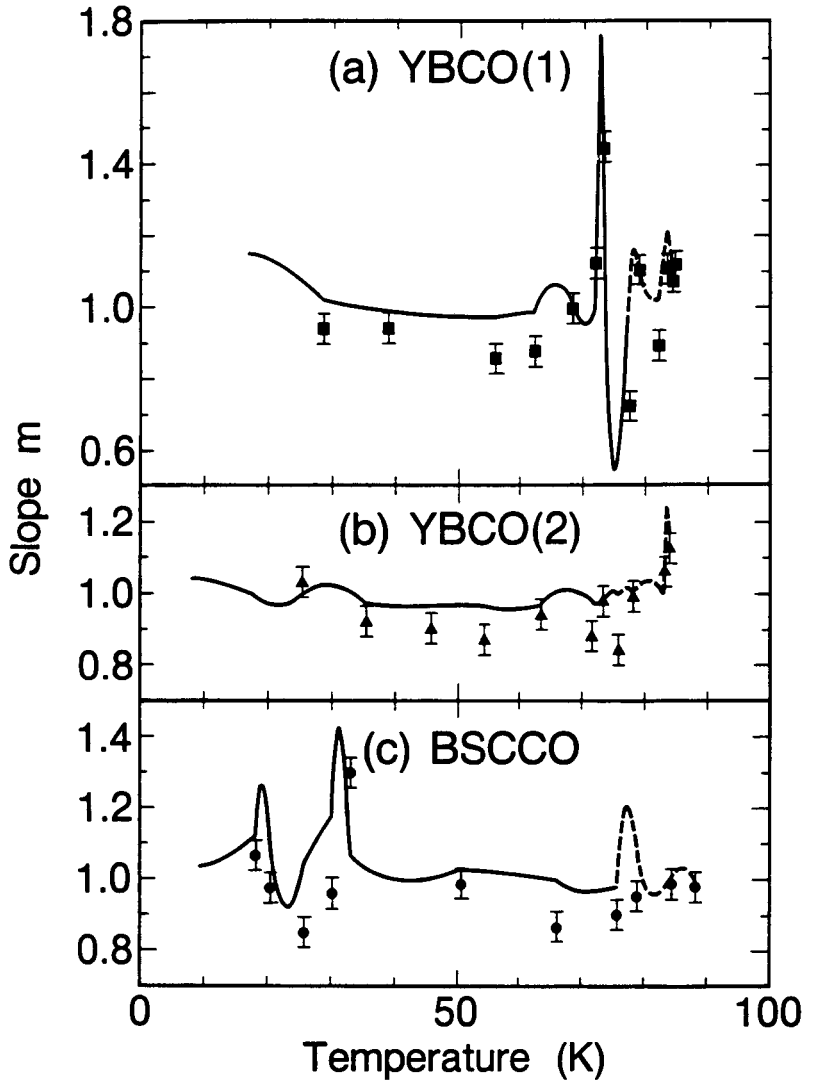

FIG. 5-2. Slope $m(T)$ of noise power spectrum vs. temperature for three samples: (a) YBCO(1), (b) YBCO(2), and (c) BSCCO(1). Points are experimental data. Curves are predictions of Eq. (5-7) from the fits to noise in Fig. 5-1, with $\tau_0 = 10^{-11}$ s and $\beta(T) = (1-t^4)/k_B T$.

$m = 1$ occur at 73 and 78 K. The predicted values of m correlate well with this behavior because $S_\Phi(T)$ exhibits a peak in this temperature range, as evident in Fig. 5-1. The distribution of activation energies will show structure corresponding to the noise peak, according to Eq. (5-6). Later in this chapter I will investigate another model for $1/f$ noise which is less successful in explaining the measured values of m.

Measuring the Distribution of Activation Energies

Figure 5-3 shows the distribution of zero-temperature activation energies computed from Eq. (5-6), using the fit to $S_\Phi(T)$ in Fig. 5-1. The dashed segment of the fit is not used in this calculation. For the YBCO samples, this is the region near T_c where $D(U_0)$ depends strongly on the exact temperature dependence of $\beta(T)$. For BSCCO(1), the dashed segment produces a peak in $m(T)$ according to Eq. (5-7) that is not reflected in the measured slope (Fig. 5-2), which could result from a noise process outside the DDH model. Both YBCO films show a peak in $D(U_0)$ below 0.1 eV, the origin of which is readily apparent from Eq. (5-6). Below $T_{peak} \approx 35$ K, $S_\Phi(T)$ increases rapidly, producing the onset of the peak in $D(U_0)$. For $T > T_{peak}$, $S_\Phi(T)$ levels off and the decrease of $\beta(T)$ dominates, rolling off $D(U_0)$. The energy at which $D(U_0)$ peaks is obtained from Eq. (5-5) with $(T_{peak}/T_c)^4 << 1$:

$$\tilde{U}_{0,peak} \approx \ln(1/2\pi f \tau_0)\, k_B T_{peak} \approx 0.07 \text{ eV} \quad . \qquad (5\text{-}8)$$

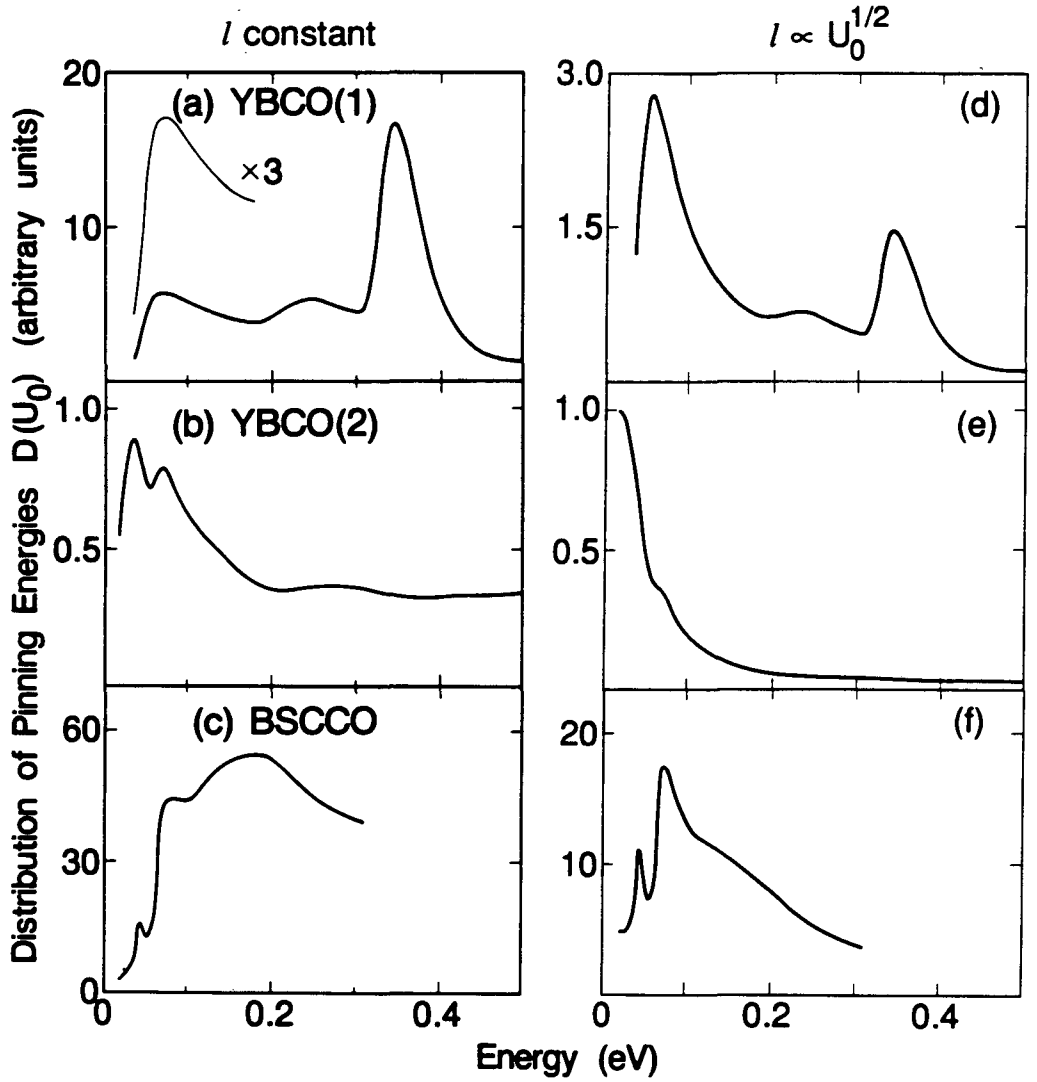

FIG. 5-3. Density of zero-temperature activation energies $D(U_0)$ vs. energy U_0 for three samples: (a) and (d), YBCO(1); (b) and (e), YBCO(2); (c) and (f), BSCCO(1). Two models of the hopping distance are shown: left column, constant ℓ according to Eqs. (5-5) and (5-6); right column, $\ell \propto U_0^{1/2}$ according to Eqs. (7-13) and (7-14). Arbitrary units on vertical scale are the same within each column. Curves depend slightly on the interpolation scheme chosen in Fig. 5-1 and the choice of parameters $\tau_0 = 10^{-11}$ s and $\beta(T) = (1-t^4)/k_BT$.

The distribution of activation energies for BSCCO(1) in Fig. 5-3 shows a broad peak because the noise increases steadily over the temperature range of the measurement.

In addition to the low-energy peak, YBCO(1) shows structure near 0.35 eV produced by the noise peak at 73 K. This structure is absent in the other samples I have measured, with the possible exception of YBCO(3) (Fig. 4-5). Note that according to Eq. (5-6) an increase in noise can correspond to a peak in $D(U_0)$ or to an increase in the hopping distance ℓ. The curve for YBCO(1) in Fig. 5-3(a) assumes the former explanation, but I can not rule out the possibility that noise near 73 K in this sample is dominated by a few processes with unusually large hopping distances. I will return to the question of hopping distance in Chapter VII, where I will present evidence that ℓ increases with energy in the ensemble. The distributions of activation energies extracted according to that variant of the DDH model [Eq. (7-13)] are shown in the right column of Fig. 5-3, and they also reveal a peak below 0.1 eV.

The idea of a distribution of pinning energies in copper oxide superconductors has been taken seriously by many workers [111,144-149], but others dismiss it as an artifice on the grounds that any measured temperature dependence of the noise can be fit by an appropriate $D(U_0)$. Although that much is true, the prediction of the slope m by Eq. (5-7) demonstrates that the DDH model accounts for the frequency dependence of the noise as well. There are also prior physical considerations which justify the model. The simple fact that the noise has a $1/f$ spectrum requires the correlation times for vortex motion to be distributed, and this arises most naturally from a distribution of activation energies. One

obvious alternative, a distribution of attempt times, will be shown to be unsatisfactory at the end of this chapter. Furthermore, the suppression of noise by current discussed in Chapter VII would not occur if the activation energies were not distributed. Thermally activated random telegraph signals, the fundamental entities in the DDH ensemble, have been observed directly as described in Chapter III. I contend that, given the reasonableness of its assumptions, the DDH model allows one to *measure* the distribution of activation energies by means of noise, rather than to *fit* the noise with an arbitrary $D(U_0)$.

When comparing my measured activation energies to the work of others, it is important to bear in mind that the noise measurements are insensitive to processes with larger values of U_0 than those plotted in Fig. 5-3. A vortex pinned at a high-energy "silent site" would be extremely unlikely to move during the time of the measurement. These silent sites might be of great importance, however, in an experiment performed far from equilibrium, such as flux creep near J_c or thermally activated resistivity near T_c. Nevertheless, there is remarkable agreement between the low-energy peak in $D(U_0)$ observed in my YBCO samples and the distributions derived by Hagen and Griessen [111] from flux creep measurements [26,27]. Zero-field critical current measurements on YBCO by Mannhart *et al.* [150] and Tahara *et al.* [151], and current-voltage characteristics measured by Tahara *et al.* [152], have also yielded pinning energies of 0.02 to 0.2 eV. Some authors [153] have objected strenuously to such small values of U_0 on the grounds that they are incompatible with the large critical currents observed in YBCO, and that they predict unphysically large values for the flux-flow resistivity. More sophisticated

analyses [139,154] which include a distribution of activation energies are able to reconcile these observations, demonstrating that different experiments probe different ranges of $D(U_0)$. The suppression of noise by current described in Chapter VII is strong evidence for the existence of barriers much higher than those producing the noise.

For several reasons, I am reluctant to apply the DDH model to the very large peak in the noise in the vicinity of T_c. Calculation of $D(U_0)$ in this temperature range is problematic because Eqs. (5-5) and (5-6) become quite sensitive to the temperature dependence of $\beta(T)$, which I do not know exactly. Furthermore, it is possible that the noise generation mechanism close to T_c differs from that at lower temperatures. Possible additional mechanisms include the creation of vortex-antivortex pairs when their energy approaches k_BT, enthalpy fluctuations across the normal-superconducting phase boundary involving large regions of the sample, phase slips in the "intrinsically fragile" order parameter [128], or the appearance of cooperative vortex motion as $\lambda(T)$ diverges. There are two indications that the noise near T_c may be intrinsic to YBCO and independent of microstructure. First, the peak in the noise power is roughly 10^{-3} Φ_0^2/Hz at 1 Hz for all YBCO samples. This is true of the samples described in this dissertation, as well as of much thinner (d_s = 10 nm) samples measured by Nancy Missert in her two-SQUID McDLT [155]. Second, the maximum noise occurs at precisely the temperature where the dc diamagnetic susceptibility of the sample vanishes, as shown in Fig. 4-3. Close to T_c, the DDH model should not be expected to yield accurate values for the slope of the noise power spectrum, but $m(T)$ plotted in Fig. 4-3(c) behaves qualitatively as Eq. (5-7) would predict, suggesting

that the notion of an ensemble of fluctuators may remain valid even in this temperature range.

An *a*-Axis Sample

The observation of the peak near 0.35 eV in the distribution of activation energies for YBCO(1) led me to suspect that this energy might be characteristic of the *a*-axis grains present in the sample. Sample YBCO(2), which shows no evidence of such grains, lacks the high-energy peak. Although my suspicion turned out to be wrong, the measurements which disproved it illuminate other aspects of the DDH model.

Figure 5-4(a) plots the noise measured in sample YBCO(6), a thin film with the *a*-*b* plane oriented perpendicular to the substrate in more than 90% of its grains. According to Table 2-1(b), this sample is not very different in transition temperature, critical current density, and degree of orientation from YBCO(1), which is better than 90% *c*-axis oriented. Despite these similarities, comparison of Figs. 5-1 and 5-4(a) shows YBCO(6) to be much noisier than YBCO(1) at all temperatures; apparently, crystalline orientation alone can significantly affect noise. This is accord with theoretical [156-158] and experimental [159,160] evidence that vortices parallel to the *a*-*b* plane move along the plane relatively freely, so that the magnitude of the noise is the result of longer hopping distances, lower pinning energies, or both.

The slope $m(T)$ of the noise power spectrum measured in YBCO(6) is plotted in Fig. 5-4(b) together with $m(T)$ calculated from Eq. (5-7).

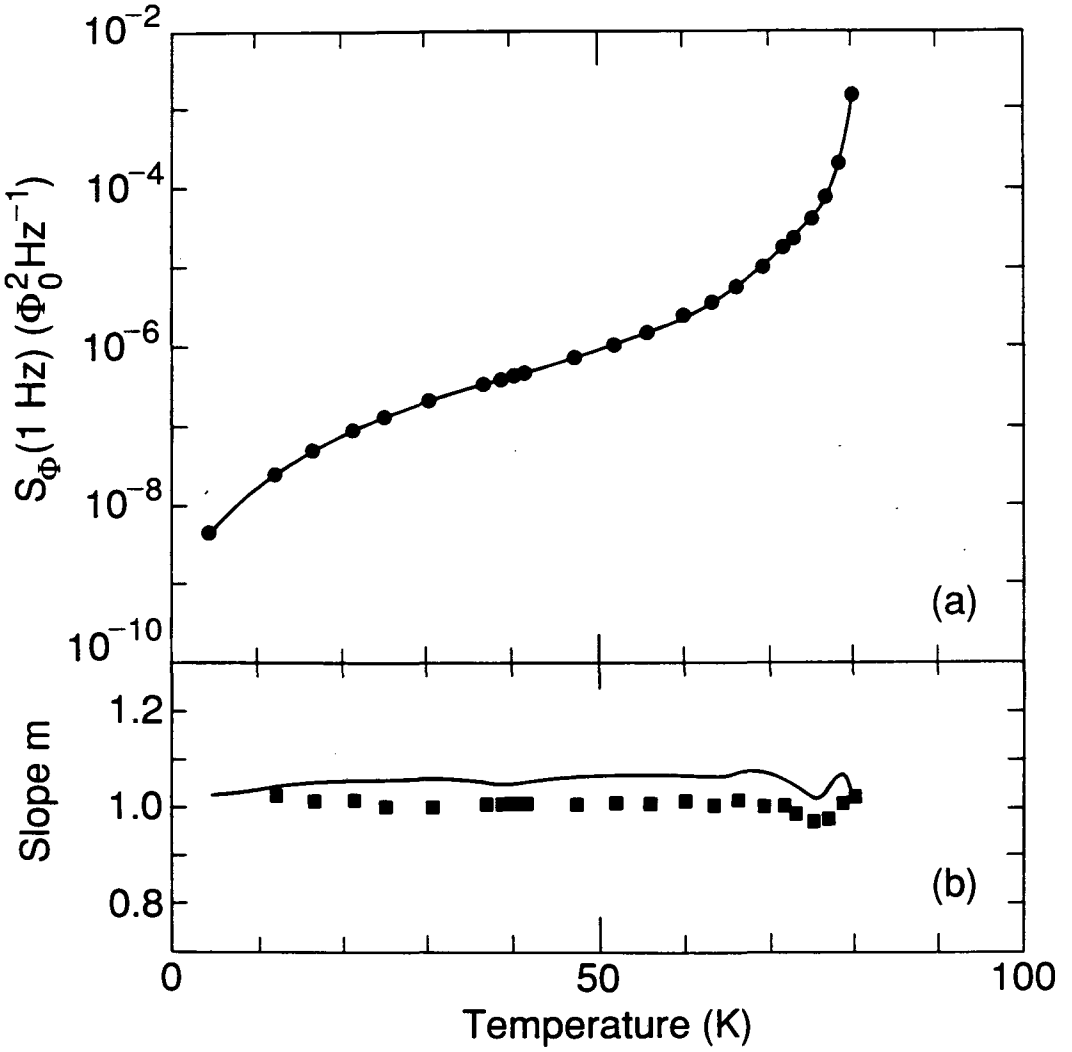

FIG. 5-4. Flux noise from *a*-axis sample YBCO(6). (a) Spectral density of noise at 1 Hz with SQUID noise subtracted vs. temperature below T_c. Curve is cubic spline fit to data. (b) Slope $m(T)$ of noise power spectrum vs. temperature. Points are experimental data; statistical error does not exceed height of symbols. Curve is prediction of Eq. (5-7) from the fitted curve in (a), with $\tau_0 = 10^{-11}$ s and $\beta(T) = (1-t^4)/k_B T$. All data points show a $1/f$-like noise power spectrum.

The measured slope is remarkably independent of temperature, in contrast to the data in Fig. 5-2, except for a small dip between 70 K and 80 K which matches the prediction of the DDH model. This temperature independence makes obvious a trend suggested by Fig. 5-2, namely that the predicted slope consistently exceeds the measured value by 0.05 to 0.1. I have implicitly assumed in the derivation of Eq. (5-7) that the vortex hopping distance ℓ is temperature independent, so that the temperature dependence of the noise from each process [Eq. (5-2)] is due solely to $\tau(T)$. As plotted in Fig. 3-4, the RTSs I observed behave in accordance with this assumption, at least over narrow ranges of temperature. Nevertheless, if I were to postulate that the hopping distance of at least some processes in the ensemble increased with temperature, then the curves in Figs. 5-2 and 5-4(b) would be displaced downward, improving their agreement with the experimental data. More generally, the fact that Eq. (5-7) overestimates m indicates an additional mechanism, unaccounted for in the model, which causes the noise to increase with temperature.

Because $S_\Phi(T)$ exhibits such a smooth temperature dependence, I expect $D(U_0)$ for YBCO(6) to be relatively featureless. This is true regardless of the model chosen for the hopping distance ℓ; Fig. 5-5(a) shows $D(U_0)$ calculated for the constant-ℓ model developed in this chapter, and Fig. 5-5(b) for the energy-dependent $\ell(U_0)$ introduced in Chapter VII. Neither model gives a distribution with the type of structure evident in Figs. 5-3 and 7-1 for c-axis samples. In particular, there is no peak which can explain the 0.35 eV feature in YBCO(1). I conclude that an a-axis film is a particularly simple system as a result of the confinement of vortices to channels parallel to the a-b planes, perhaps simple enough that

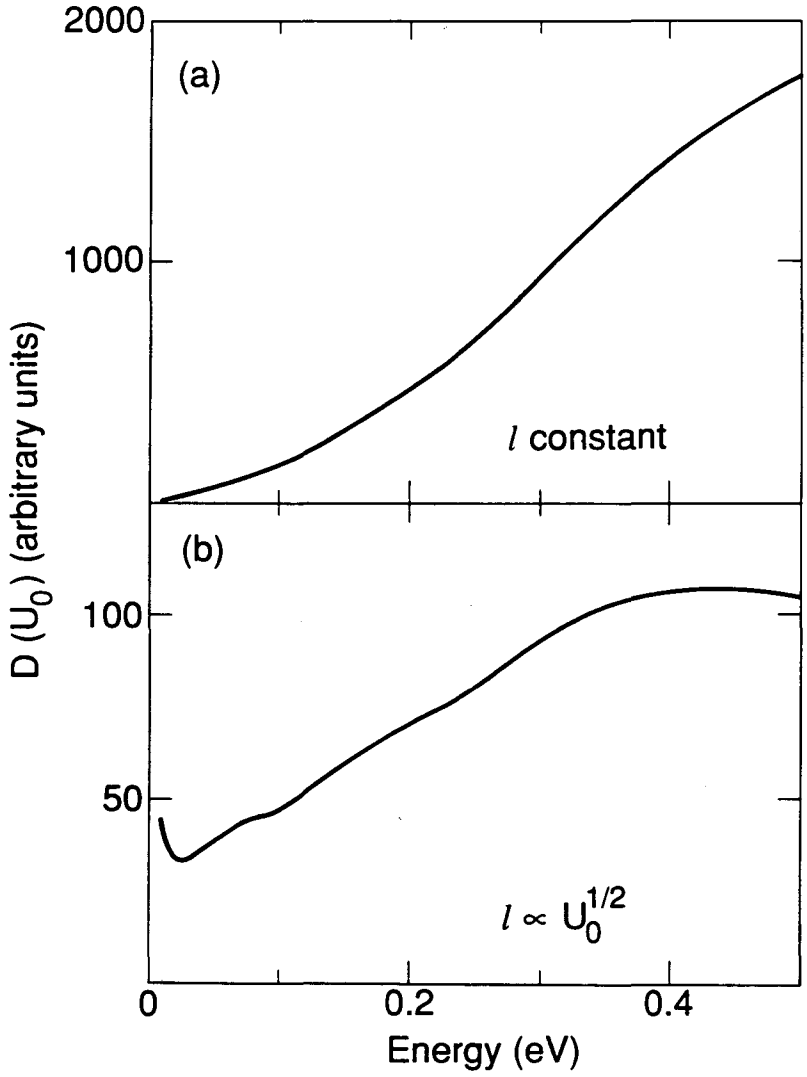

FIG. 5-5. Density of zero-temperature activation energies $D(U_0)$ vs. energy U_0 for *a*-axis sample YBCO(6) according to two models of the hopping distance ℓ. Both models employ $\tau_0 = 10^{-11}$ s and $\beta(T) = (1-t^4)/k_BT$, and give $D(U_0)$ in the same arbitrary units as Fig. 5-3. (a) Constant ℓ, generated by Eqs. (5-5) and (5-6). (b) $\ell \propto U_0^{1/2}$ from Eqs. (7-13) and (7-14).

its flux noise properties could be calculated directly from materials parameters.

Why Not a Distribution of Attempt Times?

To produce a $1/f$ spectrum from an ensemble of Lorentzians, one requires a distribution in the correlation time τ. This can arise from a distribution of activation energies, as I have assumed up to now, but a distribution in the prefactor τ_0 has also been suggested by Scofield *et al.* [161]. Clearly these are two limiting cases of a more general model in which both prefactors and activation energies are distributed, but such a model contains too many free parameters to have much predictive power. Ideally, a given noisy system will be found to be in one limit or the other, based either on knowledge of the physical origin of the distribution [136] or on the success of a consistency relation such as Eq. (5-7). Unfortunately, in many systems such as thin Ag films exhibiting resistance fluctuations [161], the noise is consistent with either limit and no meaningful distribution can be extracted. I will demonstrate that my experiment does not suffer from this problem.

In the Scofield model, τ is still given by Eq. (5-1), but U_0 is taken to be the same for all processes and τ_0 to vary with distribution $D(\tau_0)$. The analog of Eq. (5-7) for the slope of the noise power spectrum is then

$$m(f,T) = 1 - \frac{1}{U_0\beta(T)} \frac{\partial \ln S_\Phi}{\partial \ln T} \Big/ \frac{\partial \ln \beta}{\partial \ln T} \ . \qquad (5\text{-}9)$$

The temperature dependence of the activation energy for vortex motion in YBCO provides a crucial test of the Scofield model, one which is not available in most other systems. Note that $\beta(T)$ vanishes as $T \rightarrow T_c$, so Eq. (5-9) predicts that the slope will diverge near the transition temperature, in contrast to the result of Eq. (5-7) and contrary to the experimental data. Even if this problem is avoided by applying the model only to noise measurements well below T_c, the activation energy required for Eq. (5-9) to reproduce approximately the solid segment of the curve in Fig. 5-2(a) is $U_0 = 0.4$ eV. This implies that the processes contributing to the noise measured at $T = 4.2$ K and $f = 1$ Hz are those for which $\tau_0^{-1} = 2\pi f \exp[U_0\beta(T)] \sim 10^{480}$ Hz, which is unreasonable to say the least.

Assuming that the observed $1/f$ noise arises from a distribution in the prefactor τ_0 leads to difficulties at both ends of the experimental temperature range. In contrast, a distribution in the activation energy U_0 is consistent with all of my measurements. I certainly expect a real material to contain various values of both τ_0 and U_0, but the failure of the Scofield model shows that the latter is more relevant to the explanation of the noise power spectrum. Other idealizations implicit in the DDH model are the symmetry of each hopping process, and the fact that no process contains more than two states. I will make an attempt to justify these assumptions in Chapter VII.

VI. Flux Transformers

> On one of the chips is a superconducting quantum interference device (SQUID). . . . On the other chip is a flux transformer, a sort of hearing aid for SQUIDs. . . .
>
> – Judith Goldhaber, *LBL Currents* (7 December 1990)

As described in Chapter I, a flux transformer is a closed superconducting circuit used to increase the magnetic field sensitivity of a SQUID to the level required by many applications. Flux transformers with gradiometer pickup loops are also useful for rejection of distant spurious sources [76]. High-T_c magnetometers are attractive for applications such as magnetocardiography and magnetoencephalography because they require much less thermal shielding than their low-T_c counterparts, allowing pickup loops to be brought closer to the subject and thereby improving spatial resolution. At present, the $1/f$ noise of high-T_c SQUIDs is too high for the more demanding of these applications [74,75]. Even if this noise were substantially reduced, by improvements in high-T_c SQUIDs or by construction of hybrid magnetometers with low-T_c SQUIDs and high-T_c flux transformers, noise from the transformer itself would still unacceptably limit the field sensitivity. This motivated me to assemble a hybrid magnetometer on the McDLT apparatus to study the source of noise in YBCO flux transformers. As reported in a previous publication [107], vortex motion proved to be the source of the noise in transformers, as it is in thin films, but the mechanism by which it couples into the SQUID is very different.

Fabrication

A schematic of the YBCO flux transformers on which I made noise measurements appears in Fig. 6-1. They were designed and fabricated by Fred Wellstood and Jack Kingston, as detailed in Refs. [95,96,162]. For maximum field responsivity, the pickup loop was made as large as the substrate permitted, approximately 70 mm^2. The input coil is optimized when its inductance L_i matches that of the pickup loop, and when it is the same size as the SQUID, allowing efficient coupling. These two conflicting goals were realized by making a multiturn ($N = 10$) input coil, which necessitated an insulated superconducting crossunder to make contact to the innermost turn of the coil without shorting the turns together.

The transformer was fabricated by pulsed laser deposition as follows. First, a shadow mask defining the crossunder was affixed to the MgO substrate. The substrate was heated to 690°C and 300 nm of YBCO was deposited in the presence of 45 mTorr of O_2 and an rf plasma. The substrate was cooled to room temperature in O_2, the chamber was opened, and a second shadow mask was placed to define the insulating layer, depicted as a rectangle in Fig. 6-1. Through this mask was deposited 300 nm of $SrTiO_3$ with the substrate at 680°C and an O_2 pressure of 190 mTorr. Finally, after opening the chamber again to remove the mask, 300 nm of YBCO was deposited at 740°C and 190 mTorr, and then patterned by photolithography and an Ar ion mill into the input coil and pickup loop.

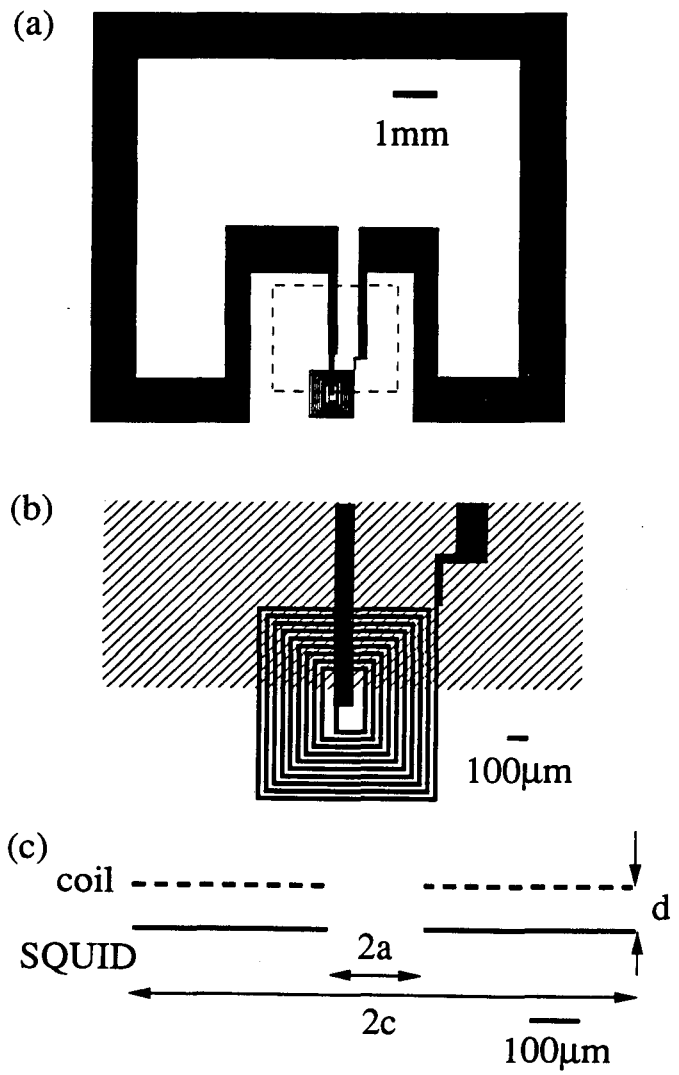

FIG. 6-1. YBCO flux transformer. (a) Pickup loop formed by wide lines, input coil centered on bottom edge, insulating $SrTiO_3$ layer indicated by dashed box. (b) Enlargement of input coil: $SrTiO_3$ is shaded region, crossunder is vertical strip connected to center of coil. (c) Cross section of input coil on McDLT hot side placed a distance *d* from Nb-PbIn SQUID on cold side.

The three flux transformers on which I made noise measurements, denoted T0, T1, and T2, are characterized in Table 2-1. The state of the art has advanced considerably since these transformers were fabricated. It is now possible to produce flux transformers with photolithographic patterning of all layers [75,163], and even integrated YBCO magnetometers with the SQUID and the flux transformer on the same substrate [164]. The noise in all recently reported magnetometers is dominated by that in the high-T_c measuring SQUID, so it is not known whether transformer noise has been reduced since I made the measurements described here.

The intrinsic noise in a flux transformer was measured by attaching it to the hot side of the McDLT apparatus as described in Chapter II and centering its input coil above the SQUID as illustrated in Fig. 6-1(c). The mutual inductance between the SQUID and the input coil is given by $M_i = \alpha_i(LL_i)^{1/2}$, where the self inductance L_i of the input coil is difficult to estimate because the SQUID acts as a superconducting groundplane. If the input coil were perfectly coupled to the SQUID ($\alpha_i = 1$), then $L_i = N^2L \approx$ 40 nH. Alternatively, if the input coil were far from the SQUID ($\alpha_i = 0$), its geometrical inductance would be $L_i \approx 100$ nH. With $d \approx 100$ μm the hybrid magnetometer is clearly in an intermediate regime, for which I estimate $L_i \approx 75$ nH, $\alpha_i \approx 0.5$, and $M_i \approx 3$ nH. The geometrically determined self inductance of the pickup loop is $L_p \approx 20$ nH.

Indirect Noise Mechanism

Consider a vortex hopping in a segment of the input coil shown in Fig. 6-1(c). One might expect this process to produce very little noise because the magnetic field lines from the vortex can close around the segment without significantly linking the SQUID. Unlike the direct noise geometry depicted in the inset to Fig. 3-2, the width of the transformer line is too small to act as a superconducting groundplane for the SQUID. However, the ability of the flux transformer to support a circulating shielding current provides another mechanism by which vortex motion can produce flux noise in the SQUID. Fred Wellstood has coined the term "indirect noise" to describe this mechanism, and the arguments below leading to Eq. (6-4) are largely a reiteration of his ideas.

The magnetic field lines from a vortex close preferentially around the nearer edge of the transformer line, so displacing a vortex the entire width w_j of the line would change the flux applied to the transformer by one flux quantum. Here, the subscript j labels the various segments of the transformer: input coil, pickup loop, and crossunder. In the same linear approximation invoked in Chapter III, a small displacement ℓ across the line produces an applied flux change $\Phi_0\ell/w_j$. Because the transformer is a closed superconducting circuit, a current $\Delta I = \Phi_0\ell/w_j(L_i+L_p)$ flows to oppose this flux. This current changes the flux through the SQUID by $\Delta\Phi = M_i\Delta I$, or

$$\Delta\Phi = \frac{\Phi_0 M_i}{w_j(L_i+L_p)}\ell \cos\theta \equiv \Phi_\ell\, \ell \cos\theta \ . \qquad (6\text{-}1)$$

Here, as in Eq. (5-3), I have included the dependence on the angle θ [see Fig. 7-3(a)]. Note that the geometrical coefficient Φ_ℓ defined by Eq. (6-1) for the indirect noise mechanism differs from the direct noise value in Eq. (5-3), and that it depends on position within the transformer through the width w_j.

In the previous chapter I considered an ensemble of hopping processes with different activation energies, and therefore different hopping rates, but identical direct coupling coefficients Φ_ℓ. The case of the flux transformers is more complicated; since Φ_ℓ varies within the ensemble, I will first concentrate on elucidating the indirect noise mechanism, and postpone the reintroduction of the distribution of activation energies until Chapter VII. Let the component of vortex position parallel to $\theta = 0$ fluctuate with an average spectral density $<S_r(f,T)>$, where the average is taken over enough processes that it exhibits a $1/f$-like spectrum as in Chapter V. If vortices are uniformly distributed in the transformer with areal density n_v, and correlations among them can be neglected, then the power spectrum of the flux noise in the SQUID is

$$S_\Phi(f,T) = n_v \int_A dA\, \Phi_\ell^2 <S_r(f,T)> \quad , \tag{6-2}$$

where superposition of the noise from the processes in the ensemble is accomplished by integrating over the area A of the transformer. When $<S_r(f,T)>$ is independent of position, Eq. (6-2) becomes

$$S_\Phi(f,T) = \zeta n_v \Phi_0^2 <S_r(f,T)> \quad , \tag{6-3}$$

where ζ is a dimensionless geometrical parameter which depends on the mechanism by which the hopping of vortices causes flux noise in the

SQUID. For the indirect noise mechanism, Φ_ℓ is as defined in Eq. (6-1), and I obtain

$$\zeta^{(in)} = \frac{\alpha_i^2 L L_i}{(L_i+L_p)^2}\left(\frac{\ell_i}{w_i}+\frac{\ell_{cr}}{w_{cr}}+\frac{\ell_p}{w_p}\right) \approx 1.2 \ , \qquad (6\text{-}4)$$

where ℓ_i, ℓ_{cr}, and ℓ_p are the lengths of the input coil, crossunder, and pickup loop, respectively, and w_i, w_{cr}, and w_p are their widths. Most of the indirect noise is due to the input coil because of the large ratio $\ell_i/w_i \approx 1200$, as compared to $\ell_{cr}/w_{cr} \approx 30$ and $\ell_p/w_p \approx 40$.

The direct noise contribution from the transformer is more difficult to calculate from Eq. (6-2) because the appropriate transfer coefficient Φ_ℓ must take into account the distortion of the vortex field by the body of the SQUID and by the lines of the transformer. Consider a simpler case, that of the noise from an unpatterned film. A rough approximation for this geometry is to take $\Phi_\ell = \alpha_s\Phi_0/w$ from Eq. (5-3) with $\alpha_s \approx 0.7$, and to integrate Eq. (6-2) over the area of the SQUID. This yields $\zeta^{(u)} \approx 3$ for the direct noise from an unpatterned film. Fred Wellstood has used the method of images [107] to obtain a better approximation, $\zeta^{(u)} \approx 3.9$. Table 6-1 lists this result together with estimates from Ref. [107] of the direct and indirect noise from the flux transformer. Note that the indirect noise is only about a factor of three less than the direct noise from an unpatterned film. On the other hand, the direct noise from the input coil is much less; I am therefore justified in neglecting correlations between the direct and indirect contributions.

Noise source	ζ	$\zeta / \zeta^{(u)}$
Unpatterned film	$\zeta^{(u)} = 3.9$	1
Input coil	$\zeta^{(i)} = 0.0015$	0.00038
Crossunder	$\zeta^{(cr)} = 0.11$	0.03
Indirect	$\zeta^{(in)} = 1.2$	0.31

TABLE 6-1. Estimates of flux noise parameter ζ defined in Eq. (6-3). Values for an unpatterned film, and for the input coil and crossunder of a flux transformer, are direct noise. Direct noise from pickup loop is negligible because of its distance from SQUID. Total indirect noise from all transformer components is given by Eq. (6-4). Noise also shown as a fraction of $\zeta^{(u)}$, the value for an unpatterned film.

Testing the Indirect Noise Mechanism

The noise measured in the three flux transformers agrees well with the theory developed above. Figure 6-2 shows that the noise power spectrum $S_\Phi(f)$ measured in transformer T2 scales approximately as $1/f$ and increases with temperature below T_c, as expected for vortex motion (compare Fig. 4-1). One difference from the noise in unpatterned films is the flattening of the spectra towards the high-frequency end of the experimental bandwidth, which is even more pronounced in Fig. 7-1(a). This results from Johnson noise in the normal metal components of the hot side, which are located just above the pickup loop of the transformer; an unpatterned film would screen the SQUID from this noise, but a flux transformer couples it into the SQUID. Nevertheless, the shields surrounding the apparatus insure that the measured low-frequency noise is characteristic of the transformer, and not the result of environmental noise. The magnitude of S_Φ(1 Hz) and its temperature dependence were similar for transformers T1 and T2, as plotted in Fig. 6-3(a). Mechanical problems with the field coil degraded its thermal isolation during these runs; it became normal and generated excess noise when the temperature of the hot side was above 62 K, so noise measurements above this temperature are omitted from Fig. 6-3.

To test the indirect mechanism of noise generation, I scribed through the pickup loop of T2, thereby preventing the flow of screening current. Figure 6-3(b) illustrates the resulting order-of-magnitude decrease observed in the noise power. According to Table 6-1, this is consistent with noise in the intact transformer being dominated by indirect noise,

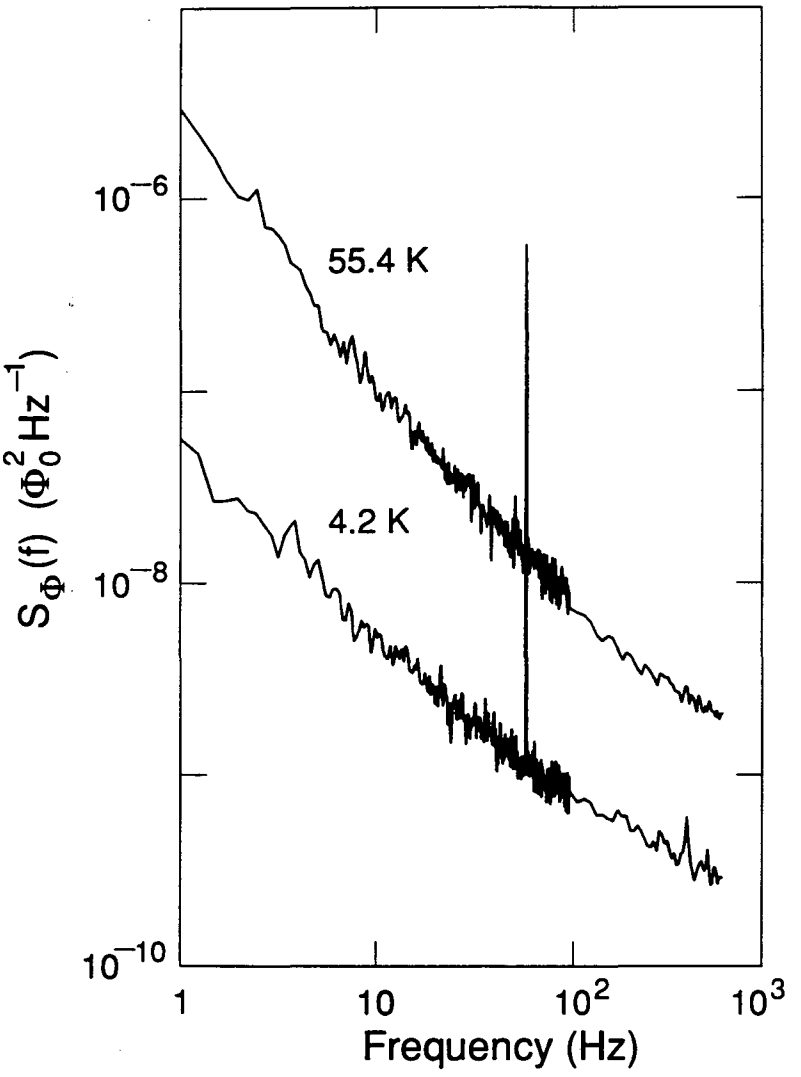

FIG. 6-2. Total noise power vs. frequency for transformer T2 at two temperatures in ambient field ($B < 1\mu T$). Noise in SQUID computed according to Eq. 2-1. Spike is 60 Hz pickup. Flattening at high frequencies caused by Johnson noise from normal metal components of apparatus.

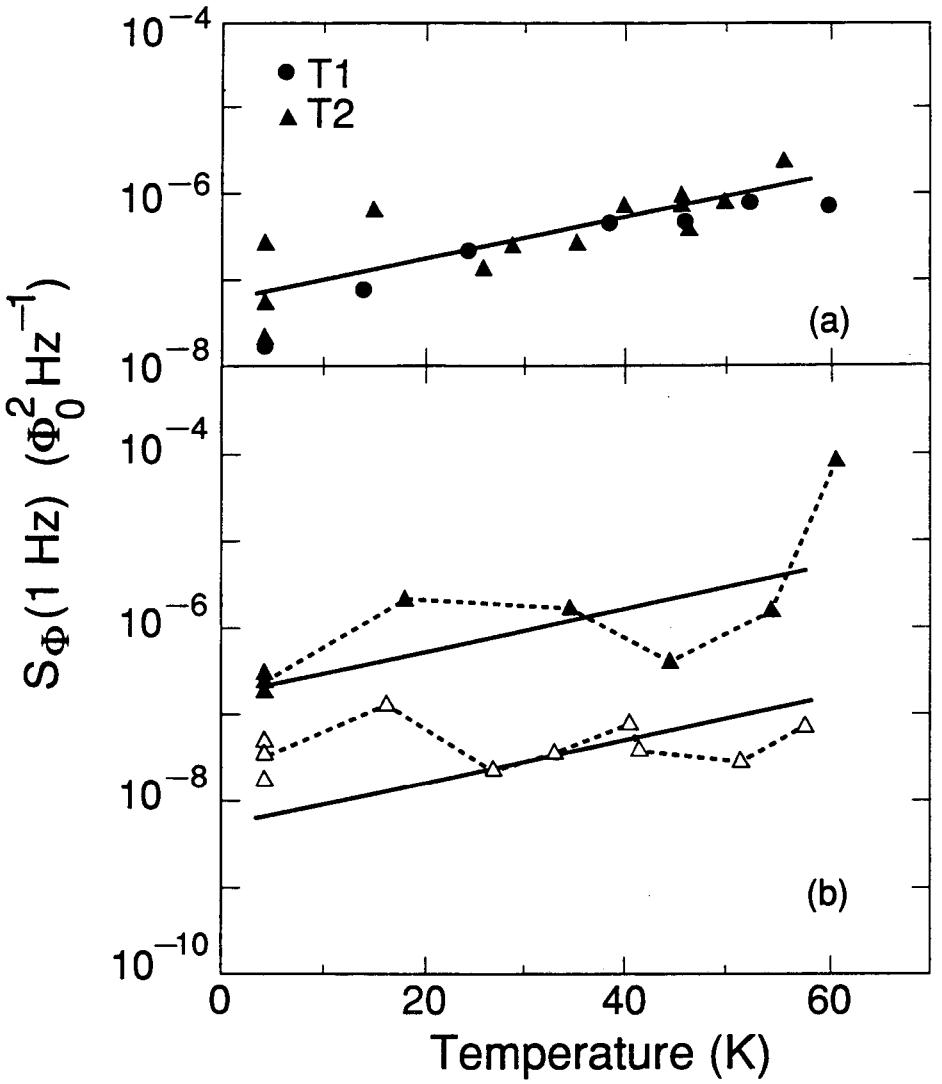

FIG. 6-3. Total noise power at 1 Hz vs. temperature in ambient field. Noise in SQUID computed according to Eq. 2-1. In (a), circles are for transformer T1, triangles for T2. In (b), noise from T2 is shown after transformer has been cut (open symbols) and after the SQUID has been moved beneath a 1-mm-wide line of the pickup loop (solid symbols). To facilitate quantitative comparison, a linear least-squares fit is made to the T2 data in (a), then replotted in (b) multiplied by 0.09 (lower line) and by 3 (upper line). The lines in (b) are the noise levels expected for the experimental geometries represented by the open and solid symbols, respectively, according to Table 6-1.

while in the cut transformer only direct noise from the crossunder is significant. Next I moved the 1-mm-wide strip of part of the pickup loop over the SQUID. Figure 6-3(b) shows that the noise from this wide portion of the film ("unpatterned film" geometry) is larger than that from the intact transformer by approximately a factor of three, as Table 6-1 predicts. Because the measured noise varies with the experimental geometry in accordance with the models of direct and indirect coupling, I am confident that I understand the mechanism by which vortex motion generates flux noise.

The agreement between the measured noise and the predictions of Table 6-1 implies that $<S_I(f,T)>$ is fairly uniform, because the noise in each case is generated by a different region of the transformer. When the transformer is intact, vortices moving in the input coil induce fluctuations in the screening current. The cut transformer lacks this noise mechanism, so its noise is dominated by vortex motion in the crossunder, a film deposited at a different time, and patterned in a different manner, than the input coil. Finally, the solid triangles in Fig. 6-3(b) represent noise generated by vortices in the pickup loop. These three regions must have similar microstructure and, judging from the similar levels of noise observed in T1 and T2, the microstructure may be reproducible from one fabrication run to the next. However, the different values of T_c for the two transformers, if not attributable to a single weak link uncharacteristic of the sample as a whole, indicate microstructural differences, a question to which I will return in Chapter VII.

Figure 6-3 indicates a dramatic decrease in the noise from a flux transformer after it is slit, while Fig. 4-6 shows that cutting a "ring"

sample has no discernable effect. This difference supports the idea that the flux transformer couples noise into the SQUID primarily by the indirect mechanism, and the ring by the direct mechanism. More precisely, when the geometry of the sample approximates that of the SQUID ($L_S \approx L$), the distinction between direct and indirect noise breaks down. Arguments analogous to those leading to Eq. 6-4 show the indirect noise parameter for the intact ring to be $\zeta^{(in)} \approx 4(c^2-a^2)\alpha_s^2 L/w^2 L_S \approx 3$, roughly the same value obtained by approximating the ring as an unpatterned film and taking the direct noise parameter $\zeta^{(u)}$ from Table 6-1.

Hybrid Magnetometer Performance

To quantify the performance of a magnetometer, one is interested not in the measured flux noise $S_\Phi(f)$, but in the total magnetic field noise

$$S_B(f) = \frac{S_\Phi^{(S)}(f) + S_\Phi^{(in)}(f)}{(gA_{eff})^2} , \tag{6-5}$$

where g is the factor by which the transformer enhances the magnetic field responsivity of the SQUID, $A_{eff} = 4ac$ is the sensing area of the SQUID determined by flux focusing, $S_\Phi^{(S)}(f)$ is the intrinsic flux noise in the SQUID, and $S_\Phi^{(in)}(f)$ is the indirect noise from the transformer. In writing Eq. (6-5), I have assumed that the indirect term dominates the transformer noise, as Table 6-1 indicates for my experimental geometry, and as the considerations outlined at the beginning of this chapter insure will be the case for most flux transformers. I obtained the best field sensitivity with transformer T1, for which $g = 9.5$ and $S_\Phi^{(S)}(10\text{ Hz}) << S_\Phi^{(in)}(10\text{ Hz}) \approx 9 \times$

$10^{-8}\ \Phi_0^2$/Hz, yielding $S_B^{1/2}(10\ \text{Hz}) \approx 0.3\ \text{pT Hz}^{-1/2}$ with the transformer at 60 K. This sensitivity is superior to the all-high-T_c devices [74,75] described in Chapter I, and approaches the values needed for clinical applications. In the next chapter I will describe a method which improves the sensitivity of the hybrid magnetometer by a factor of three.

VII. Current Dependence

"Use the Force, Luke!"

– George Lucas, *Star Wars* (1977)

In addition to improving the magnetic field sensitivity of the SQUID, the flux transformer provides a unique system for studying the dynamics of vortices, particularly their response to a driving force. The indirect noise mechanism makes noise from the input coil measurable, even though the direct coupling geometry is extremely unfavorable, and the narrow linewidth of the input coil means that even small currents in the transformer give large current densities and strong Lorentz forces. I find that a supercurrent suppresses the noise in the transformer, and that this suppression can be explained within the DDH model. From the effect of a driving force on the vortices producing the noise, I extract the hopping distance ℓ, the vortex number density n_V, and the pinning spring constant k_0. An earlier version of the model presented here appears in Ref. [141].

Reversible Suppression of 1/*f* Noise

This chapter will investigate the noise in flux transformers in the presence of a dc circulating current I, which I induced by applying a static magnetic field with the field coil. If a uniform field B were applied to the pickup loop of area A_p, then the transformer current would be simply $I =$

$BA_p/(L_i+L_p)$. However, the magnetic field produced by the field coil is not uniform across the flux transformer pickup loop, so the applied flux is not so easily calculated. I could have obtained a more uniform field by using the big coil, but the persistent current mode of the field coil avoids the noise and drift associated with a room-temperature current supply. Fortunately the transformer current I produced by a field coil current I_f is calculable with only one additional measurement according to $I = I_f \Delta M_f / M_i$, where $\Delta M_f \equiv M_f' - M_f = 51$ nH, M_f' is the mutual inductance measured between the field coil and the SQUID with the transformer below T_c, and M_f is the mutual inductance measured with the transformer normal. In the experiments described in this chapter, the largest current stored in the field coil is 0.16 mA, which corresponds to $I \approx 3$ mA and to a current density of 5×10^4 A/cm^2 in the input coil. In the next chapter I will demonstrate that the fields used, of order 10 μT, do not affect the noise measured in unpatterned YBCO films, so the phenomena I observe are most reasonably attributed to the induced supercurrent.

As shown in Fig. 7-1(a), inducing $I = 2$ mA causes the total low-frequency noise power from transformer T1 to decrease by an order of magnitude from its $I = 0$ value, and it returns to this value when the current is removed. This reversibility demonstrates that the number of mobile vortices in zero applied field has not been altered, and that the noise reduction can not be explained as the result of driving the vortices from shallow, noisy pinning sites into deeper, quieter ones, since they would then remain in the deeper sites after the removal of the current. The high-frequency regions of the spectra in Fig. 7-1(a) reveal the background noise sources discussed in Chapter VI, but the difference spectra in

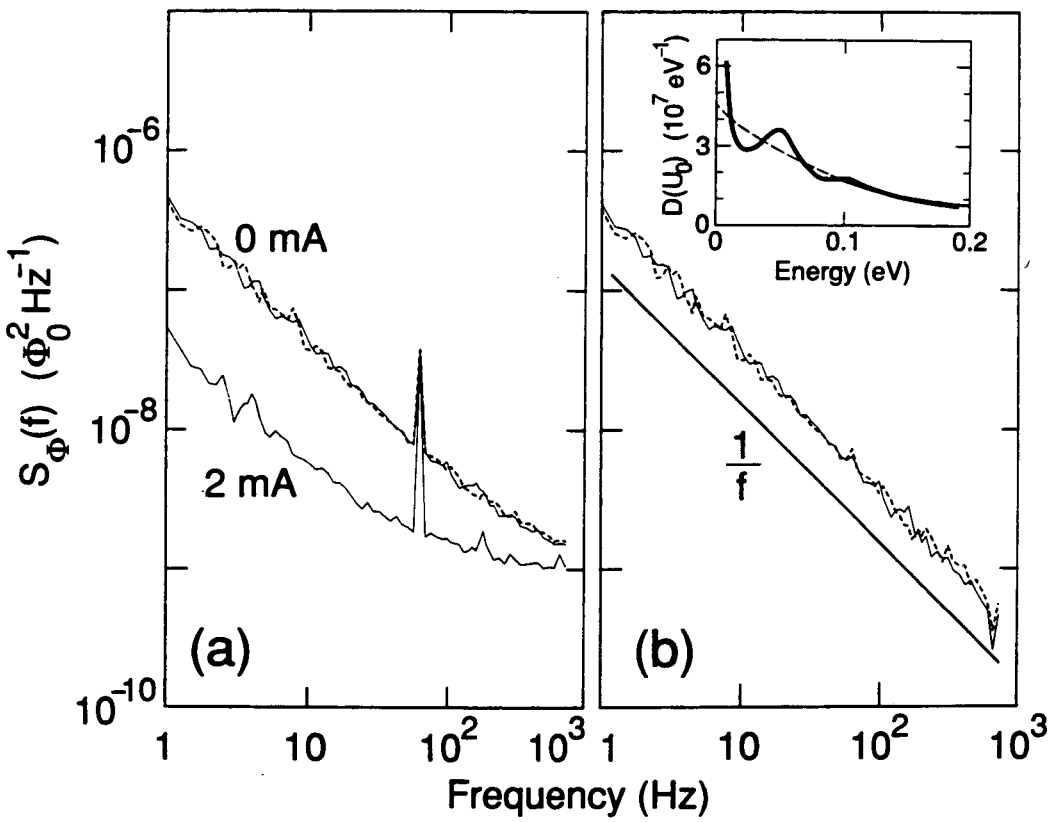

FIG. 7-1. (a) Total noise power vs. frequency for transformer T1 at 39 K. Noise in SQUID computed according to Eq. 2-1. Upper solid curve, initial spectrum ($I = 0$); lower solid curve, application of $I = 2$ mA; dashed curve, subsequent return to $I = 0$. Johnson noise and 60 Hz pickup are apparent as in Fig. 6-2. (b) Spectra for $I = 0$ with spectrum for $I =$ 2 mA subtracted. Note $1/f$ scaling. Inset: Solid curve, distribution of zero-temperature activation energies determined from noise measurements according to Eqs. (7-13) and (7-14). Peak near 0.05 eV is significant, weak 0.1 eV feature is not. Dashed curve, theoretical distribution from Eq. (7-12) with $k_0 = 6 \times 10^{-5}$ N/m, $N_p = 4 \times 10^6$, and $n_s = 600$ μm^{-2}.

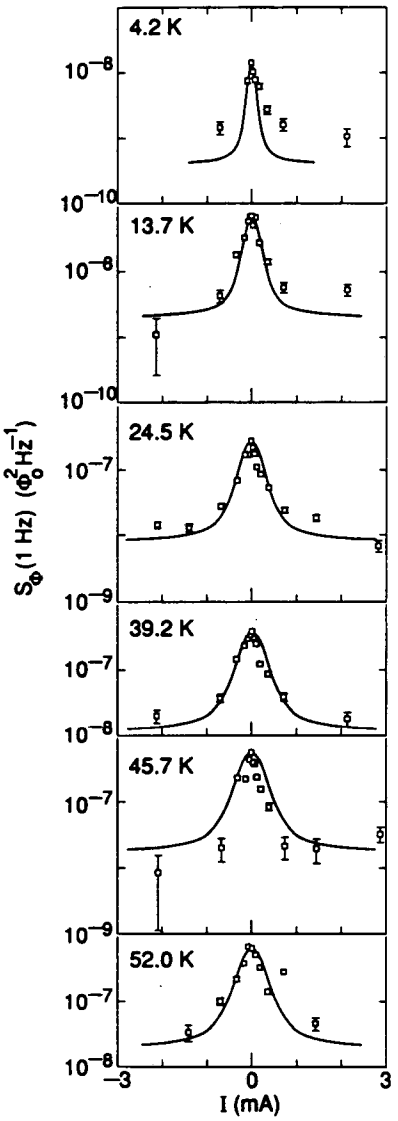

FIG. 7-2. Noise power $S\Phi$(1 Hz) in SQUID vs. current in transformer T1 for six temperatures. Points are experimental data, from which the least noise measured at each temperature has been subtracted to remove background. Curves are the prediction of Eqs. (6-2) and (7-3) with indirect noise transfer function from Eq. (6-1). Central peak is due to input coil, shoulders to pickup loop.

Fig. 7-1(b) scale as $1/f$; in other words, the effect of the current is to remove a source of $1/f$ noise. From the DDH model for $1/f$ noise developed in Chapter V, I will show that a sufficiently large current suppresses indirect noise, the dominant source of noise in the transformer. The residual noise at $I = 2$ mA is then explained as direct noise from the crossunder, consistent with the order-of-magnitude reduction observed when indirect noise was eliminated by cutting transformer T2 (Fig. 6-3). Subtracting the large-current background from the noise measurements at each temperature, I obtain the current dependence of the indirect noise power S_Φ(1 Hz) which is plotted in Fig. 7-2. The noise peaks symmetrically about $I = 0$ and the width of the peaks increases slightly with temperature.

Dutta-Dimon-Horn Model with Lorentz Force Terms

To find an explanation for the suppression of noise by current within the DDH model, I need to consider the effect of a Lorentz force on a single switching process as illustrated in Fig. 7-3(a). In a transformer segment of width w_j, a vortex hops between pinning sites 1 and 2, separated by a distance ℓ. As in Chapter V, the pinning potential [Fig. 7-3(b)] is assumed to be symmetric in the absence of a supercurrent, with zero-temperature activation energy U_0. I approximate the current I as uniformly distributed across the line, so that it exerts a Lorentz force $F = I\Phi_0/w_j$ on each vortex. Taking a more realistic current distribution [5] would only slightly improve the agreement between theory and experiment

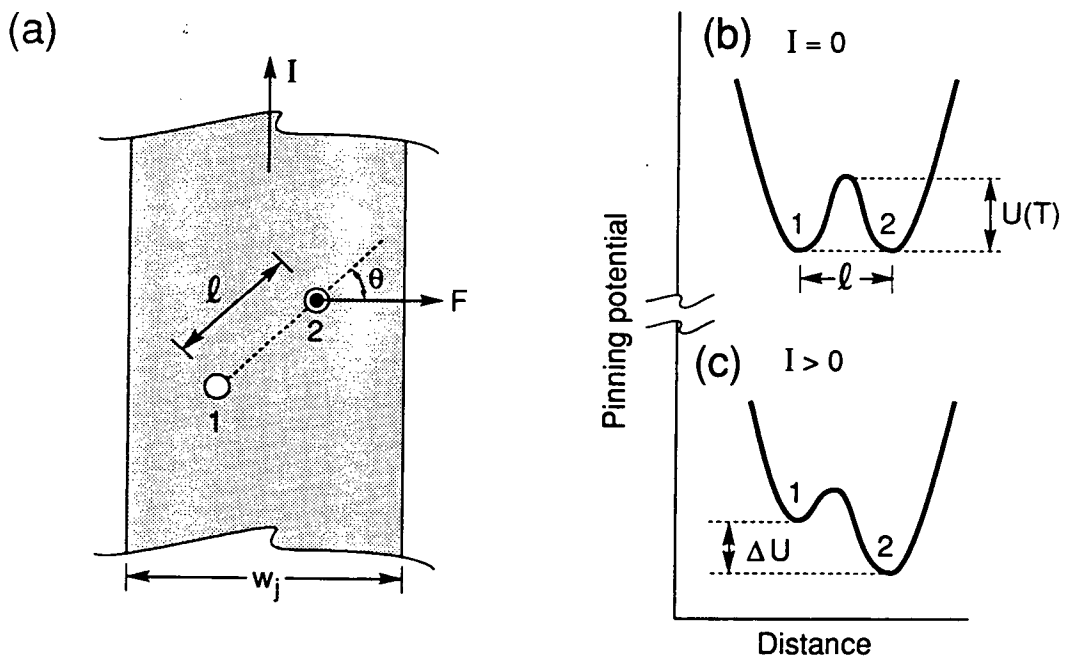

FIG. 7-3. (a) Schematic of single hopping process in transformer line of width w_j. Current I exerts force F on vortex which hops distance ℓ between pinning sites 1 and 2. Scale of ℓ exaggerated. (b) Schematic pinning potential for $I = 0$; (c) for $I > 0$.

in Fig. 7-2, while making integration of Eq. (6-2) more difficult and leaving the quantitative conclusions of this chapter substantially unchanged. Figure 7-3(c) indicates that the force introduces a misalignment $\Delta U = F\ell \cos\theta$ between the minima of the pinning potential, where θ is the angle between the Lorentz force and the vortex trajectory. Increasing current reduces the noise from this process because the vortex is less likely to be activated out of site 2 when the pinning potential is tipped strongly. This simple observation provides the physical basis for the suppression of indirect noise by current, and also reveals why direct noise is relatively unaffected in my geometry. According to Eq. (6-1), the noisiest indirect processes (largest $\Delta\Phi$) are those involving vortices in the input coil hopping across the line, in the direction of the Lorentz force. However, direct noise from the crossunder arises primarily from vortices hopping radially with respect to the SQUID, perpendicularly to the Lorentz force, which thus has little effect. In addition, the linewidth of the crossunder is five times that of the input coil, making the local Lorentz force significantly weaker.

In the presence of a supercurrent the barriers for thermal activation in states 1 and 2 are different, and Eq. (3-1) for the lifetime becomes

$$\tau_1(T,I) = 2\tau_0 \exp[\, U_0\beta(T) - \delta \,] \tag{7-1a}$$

$$\tau_2(T,I) = 2\tau_0 \exp[\, U_0\beta(T) + \delta \,] \;, \tag{7-1b}$$

where the characteristic time τ_0 and the temperature dependence $\beta(T)$ are defined as in Eq. (5-1), and $\delta = I\Phi_0\ell\cos\theta/2w_jk_BT$. The spectral density of radial motion for a single hopping process is a Lorentzian similar to Eq. (3-2):

$$S_r(f,T,I) = \frac{4(\ell \cos\theta)^2}{(\tau_1+\tau_2)[(\tau_1^{-1}+\tau_2^{-1})^2+(2\pi f)^2]} , \qquad (7\text{-}2)$$

where τ_1 and τ_2 are the lifetimes from Eq. (7-1). In order to evaluate the total flux noise in Eq. (6-2), I require the spectral density per vortex averaged over the ensemble of switching processes:

$$<S_r(f,T,I)> = \frac{1}{\pi n_v A}\int_0^{\pi} d\theta \int_0^{\infty} dU_0\, D(U_0)\, S_r(f,T,I) , \qquad (7\text{-}3)$$

Unlike Eq. (5-4), in which the angular dependence could be readily integrated out, Eq. (7-3) includes an explicit angular integral because processes with different values of θ will have different current dependences according to the factor of $\cos\theta$ in the dimensionless misalignment δ. Strictly speaking, the average should be taken over only those processes in the differential area dA of the transformer in Eq. (6-2), but w_j is constant over such large subsets of the ensemble that the result would differ only if the spatial distribution of processes were extremely nonuniform, a possibility ruled out by the results of Chapter VI.

At this point I have developed a theory which can explain the suppression of noise in the flux transformer by a supercurrent. Its essential elements are the current-dependent hopping of an ensemble of vortices given by Eq. (7-3), the indirect noise mechanism in Eq. (6-1) by which this motion produces flux noise in the SQUID, and the superposition of noise from all segments of the transformer in Eq. (6-2). Before proceeding, I would like to consider exactly which features of the pinning potential I expect the current dependence to reveal.

Two-Dimensional Pinning Model

In my discussion of the DDH model in Chapter V, I made as few assumptions as possible about the hopping distance ℓ, since results could be obtained without knowing its value. However, because the misalignment energy ΔU is proportional to ℓ, the current dependence of the noise provides a probe of the hopping distance, and these data demand a theory within which they can be interpreted. The first issue is whether ℓ is a single parameter characteristic of the sample, or a function which varies within the ensemble of hopping processes. I argue that the latter is the case, for two reasons. First, during crystal growth defects arise at random from interactions on length scales comparable to the dimensions of a unit cell. Therefore the resulting pinning potential on the larger scales relevant to vortex motion should be at least approximately self-similar [108,165], implying

$$\ell \propto U_0^{\nu} \tag{7-4}$$

for some exponent $\nu > 0$. Intuitively, Eq. (7-4) corresponds to the statement that when a vortex hops over a small barrier, it moves a small distance, while a large barrier implies a large distance, and the ratio of these distances depends only on the ratio of the barrier energies, not on their magnitudes.

The second argument for an energy-dependent hopping distance comes from the data in Fig. 7-2. Note that the width of the peak is only weakly dependent on temperature. From Eq. (5-5) I know that at temperatures not too close to T_c, the effective activation energy $\tilde{U}_0$ increases with

temperature roughly as $\tilde{U}_0 \propto T$. If the hopping distance, and therefore ΔU, were independent of temperature, then the fractional misalignment $\Delta U/\tilde{U}_0$ would decrease with increasing temperature, the current would suppress the noise less effectively, and the peaks would broaden. Since this does not occur, it is plausible that ℓ increases with energy in the ensemble.

The data do not constrain a particular functional form for $\ell(U_0)$, so I suggest a model related to the work of Marinari *et al.* [166,167] on random walks in random potentials, and to unpublished results due to Clem [108]. The model makes the following assumptions:

1. The problem is reduced to two dimensions by approximating the vortices as rigid rods normal to the surfaces of the film. This is reasonable since the thermal wandering of the vortex line over the thickness of the film is less than the distance between vortices and less than the hopping distance ℓ [168], and since the elastic energy required to tilt the vortex by a distance equal to ℓ is comparable to $\tilde{U}_0$ [117]. Certainly my noise measurement is sensitive only to the two-dimensional configuration of points at which the vortices emerge from the surface of the sample facing the SQUID; motion of internal segments does not generate noise. The areal density of vortices is n_V.

2. Pinning sites are randomly distributed with areal density n_S, and the "center" of a pinning site is a well-defined concept (see assumption 5 below). Essentially, I am assuming that the pinning which underlies $1/f$ noise is provided by localized features such as point defects [145,169] or screw dislocations [170,171], rather than by extended structures such as the twin or grain boundaries that lead to random telegraph signals.

3. Vortices do not interact with each other. This is a good approximation in my experiment because the mean distance between vortices $n_v^{-1/2}$ is greater than the penetration depth λ.

4. Each vortex interacts with only the nearest pinning site. This assumption buys a large amount of computational simplicity at the price of only a little generality.

5. The potential energy $u(|\boldsymbol{r}_v - \boldsymbol{r}_s|, T)$ of a vortex at position $\boldsymbol{r}_v$ due to a pinning site at $\boldsymbol{r}_s$ is the same for all pinning sites. This potential corresponds to an attractive central force which depends only on the distance between the centers of the vortex and the pinning site.

The model described above seems quite different from the ensemble of bistable hopping processes which I have employed previously, but I believe they can be related in a very simple manner. I suggest that each hopping process in the ensemble corresponds to a pair of pinning sites in the two-dimensional model. This is certainly a valid identification at temperatures low enough such that $\ell[\tilde{U}_0(T)] << n_s^{-1/2}$. In this limit, most vortices can not escape from their pinning sites on the time scale of the experiment, and the only ones which produce a measurable amount of noise are those which happen to be located at one of a pair of sites which are unusually closely spaced. The analogy is certainly invalid when $\ell[\tilde{U}_0(T)] >> n_s^{-1/2}$, since all hopping events will be fast compared to the experimental bandwidth and the noise will appear nearly white. Interestingly enough, this is what is observed just above T_c in my experiment (see Figs. 4-2 and 4-3) and in that of Nancy Missert [155]. Data presented later in this chapter imply that transformer T1 is in the always-troublesome intermediate regime, $\ell[\tilde{U}_0(T)] \approx n_s^{-1/2}$. In this case I can not rigorously

justify the identification of a process with each pair of pinning sites in the two-dimensional model, but the issue may be amenable to further theoretical analysis or to numerical simulation.

Although I have assumed that the shape of the pinning potential is the same at each site in the two-dimensional model, the activation energies for vortex motion will be distributed nevertheless, because the distances between pinning sites differ as a result of their random distribution in the plane. Since I expect the density of pinning sites to greatly exceed the density of vortices, most of the pinning sites will be unoccupied and the number of processes in the ensemble will be determined by the number of vortices. However, two dimensions allow a vortex to hop to any of several sites, so there will be some number P_V of processes for each vortex in the two-dimensional model.

Multiplicity and Distribution of Activation Energies

The multiplicity of processes P_V can be calculated exactly. Consider a pair of pinning sites, separated by a distance ℓ. This pair will constitute a process provided that a vortex moving along the line connecting the sites is never more strongly attracted to a third site than it is to the nearer of the pair. Thus, the two sites in a process are located at opposite ends of a diameter of a circle which contains no other sites. The area of this circle is $A_\ell = \pi\ell^2/4$. In a sample of total area A, there will be $n_S A-2$ other sites, and the probability that none of them falls within the circle is $p(\ell) = (1 - A_\ell/A)^{n_S A-2}$. In the limit $A >> \ell^2, n_S^{-1}$ this becomes

$$p(\ell) = \exp[-\pi n_s \ell^2/4] \ . \tag{7-5}$$

For a vortex at a given site, the number of available hopping processes P_V is given by the number of sites at a distance ℓ, multiplied by $p(\ell)$ and integrated over all possible hopping distances:

$$P_V = \int_0^\infty d\ell \ 2\pi\ell \ n_s p(\ell) = 4 \ . \tag{7-6}$$

This result depends on the dimensionality of the problem and on my definition of what constitutes a process in the two-dimensional model, but not on the number density of pinning sites or the functional form of their interaction with the vortices.

I would now like to calculate the distribution of activation energies for the two-dimensional model. Since there is a one-to-one correspondence between activation energy and hopping distance, I begin by considering the number of available processes with hopping distances in the range from ℓ to $\ell+d\ell$:

$$D(\ell)\, d\ell = \frac{n_s A}{2} 2\pi\ell \ d\ell \ n_s p(\ell) \ , \tag{7-7}$$

where the factor of one-half eliminates double counting. The familiar distribution of activation energies is then given by

$$D(U_0) \propto D(\ell) \frac{d\ell}{dU_0} \ . \tag{7-8}$$

Equation (7-8) is a proportionality, rather than an equality, because not all of the available processes will be occupied by vortices. The constant of proportionality can be determined from the normalization condition

$$\int_0^\infty dU_0\, D(U_0) \;=\; P_v n_v A \;\equiv\; N_p \;, \tag{7-9}$$

where N_p is the number of processes in the ensemble.

In order to obtain an explicit formula for the distribution of activation energies, it is necessary to assume a functional form for the single-site pinning potential $u(r,T)$. A common assumption in theories of vortex dynamics [10] is that vortices are connected to their pinning sites by Hooke's law springs, with a force constant known as the Labusch parameter α [172]. In the absence of detailed knowledge of the physical origin of the pinning, I will adopt this assumption, which would of course also result from the Taylor series expansion of a general potential:

$$u(r,T) \;=\; \tfrac{1}{2}k(T)r^2 \;. \tag{7-10}$$

All pinning sites are assumed identical, so no constant term is necessary in Eq. (7-10). Note that the temperature dependence of the spring constant $k(T)$ will be the same as that of the activation energy in Eq. (3-3). I define $k_0 = k(0)$, and the relationship between hopping distance and activation energy is then simply

$$\ell(U_0) \;=\; \left(\frac{8U_0}{k_0}\right)^{1/2} \;, \tag{7-11}$$

which agrees with Eq. (7-4) for $\nu = 0.5$. Using Eq. (7-11), it becomes possible to evaluate Eq. (7-8) , yielding the distribution of activation energies for the two-dimensional model:

$$D(U_0) \;=\; N_p \frac{2\pi n_s}{k_0} \exp[\,-2\pi n_s U_0/k_0\,] \;, \tag{7-12}$$

which has been normalized as in Eq. (7-9). My simple two-dimensional model thus provides one possible physical basis for the exponential distribution assumed in the theories of Inui *et al.* [145] and Martin and Hebard [149].

I would like to extract the distribution of activation energies from my noise measurements, both for comparison with the distributions obtained in Chapter V and to test the theoretical prediction of Eq. (7-12). For $I = 0$ the integrals in Eqs. (6-2) and (7-3) can be evaluated analytically, subject to the usual condition that $D(U_0)$ is slowly varying, to yield

$$D[\tilde{U}_0(f,T)] = \frac{k_0 A}{\zeta^{(in)}\ln(1/2\pi f\tau_0)}\left(\frac{\beta(T)}{\Phi_0}\right)^2 f\, S_\Phi(f,T,0) \ , \qquad (7\text{-}13)$$

where $\zeta^{(in)}$ is defined in Eq. (6-4), $S_\Phi(f,T,0)$ is the noise from the transformer measured with zero circulating current, and the characteristic energy $\tilde{U}_0$ satisfies

$$\tilde{U}_0(f,T) = \frac{\ln(1/2\pi f\tau_0)}{\beta(T)} + \frac{1}{2\beta(T)}\ln\left(\frac{\tilde{U}_0(f,T)\beta(T) + 1}{\tilde{U}_0(f,T)\beta(T) - 1}\right) . \qquad (7\text{-}14)$$

These results look quite different from those obtained in Chapter V because the hopping distance ℓ is no longer assumed to be the same for all processes, but rather to increase with energy according to Eq. (7-11). For $f\tau_0 = 10^{-11}$, however, the second term on the right side of Eq. (7-14) introduces only a 0.2% correction to $\tilde{U}_0$; otherwise the result is the same as Eq. (5-5). The only qualitative difference between Eqs. (5-6) and (7-13) is the additional factor of $\beta(T)$ which appears in the latter, the consequences of which are apparent in Figs. 5-3 and 5-5. The distribution of

activation energies for transformer T1 obtained from the measured values of $S_\Phi(1\ \mathrm{Hz}, T, 0)$ is plotted in the inset to Fig. 7-1(b). It shows a broad peak near 0.05 eV similar to those observed in the single-layer films of Chapter V regardless of whether ℓ is taken to be constant or proportional to $U_0^{1/2}$. There is also a strong upturn at lower energies; note the remarkable similarity to Fig. 3 of Ref. [173].

Neglecting terms of the same order as the second term on the right side of Eq. (7-14), one can easily show that the consistency relation for the slope of the noise power spectrum in the absence of a supercurrent is unchanged from the constant-ℓ result in Eq. (5-7). Neither the predicted nor the measured values of the slope for transformer T1 show any significant departure from $m \approx 1$.

Hopping Distances and Restoring Forces

Having obtained the form of $D(U_0)$, I can solve for the noise in the presence of a supercurrent by integrating Eq. (7-3) numerically for each value of w_j and then summing over the components of the transformer as in Eq. (6-2). The resulting curves are shown in Fig. 7-2. The only fitting parameter is the zero-temperature spring constant $k_0 = 6 \times 10^{-5}$ N/m, which determines the width of the peaks and also sets the scale for $D(U_0)$ according to Eq. (7-13). The measured and calculated noise in Fig. 7-2 agree trivially at $I = 0$ because $D(U_0)$ was obtained from these data; the shape of the peaks for non-zero current depends only weakly on the form of $D(U_0)$, but is sensitive to k_0 and to the geometry of the transformer.

Knowing k_0 allows me to calculate the hopping distance ℓ from Eq. (7-11). Since $\tilde{U}_0$ increases from 8.5 meV to 190 meV over the temperature range from 4.2 K to 60 K, the hopping distance of processes which contribute to the measured noise ranges from 13 nm to 64 nm. These values are one or two orders of magnitude smaller than those given in Table 3-1 for the random telegraph signals in YBCO, consistent with my assertion that each RTS is a single long-range process, while $1/f$ noise results from many short-range hopping events. In order for the motion of a single vortex in a sample ring of area $A_S \approx 1$ mm^2 to dominate the noise from $N_V = n_V A_S/\tilde{U}_0\beta(T) \approx 10^3$ others, its hopping distance must be larger by at least a factor of $N_V^{1/2} \approx 30$, as is the case. Here I have used the value $n_V = 0.03$ μm^{-2} deduced below for transformer T1, and I have taken $1/\tilde{U}_0\beta(T) \approx 0.04$ as a rough estimate of the fraction of the ensemble in the bandwidth of the measurement at a fixed temperature.

As discussed in Chapter V, the DDH model assumes a symmetrical pinning potential, so that both sites in Fig. 7-3(b) have the same activation energy for $I = 0$. My simple two-dimensional model explains this as the result of the same type of defect being present at each site. I suggested in Chapter III that the equality of activation energies observed in RTSs is experimental evidence for symmetrical processes, but the unusually large hopping distances may cast doubt on the relevance of the RTSs to the ensemble of processes producing $1/f$ noise. Against this I can only argue that a short-range asymmetric process seems even more improbable than a long-range asymmetric process. Fortunately the suppression of noise by current provides convincing evidence on this issue. If the two activation energies in each double well were completely uncorrelated, then tipping

the pinning potential would bring as many processes into alignment as it brought out, and the noise would not depend on current. The sharpness of the peaks in Fig. 7-2 requires that the processes in the ensemble be approximately symmetrical, although a small random asymmetry could explain the discrepancy between theory and experiment at 4.2 K. This discrepancy might also be the result of a hopping distance smaller than that given by Eq. (7-11), or of vortex motion by configurational tunneling [33].

At 4.2 K the noise in transformer T2 was also suppressed by an induced supercurrent, giving a hopping distance of the order of 100 nm, many times the value for T1 at this temperature. This is difficult to reconcile with the similar levels of noise observed in the two transformers [Fig. 6-3(a)] unless there are fewer mobile vortices in T2 than T1. Furthermore, I was unable to detect any current dependence in T2 at 28 K or 46 K, except for the RTS discussed at the end of this chapter. A possible explanation for this is that processes with $\ell > 100$ nm tend to be less symmetric than those with short hopping distances. This asymmetry would also reduce the number of vortices which are mobile in T2 at a given temperature and current, compensating for the greater noise per process resulting from larger values of ℓ.

The suppression of noise in each bistable process requires that there be no pinning site to the right of site 2 in Fig. 7-3(c) into which the vortex can hop. In terms of the two-dimensional model, this means that the next site in that direction is more distant than site 1, so that the barrier is relatively large. Even if this were not the case, however, the vortex would simply move under the influence of the Lorentz force until it encountered

such a barrier. The idea of a distribution of activation energies is given powerful support by the data in Fig. 7-2, since there must exist both small barriers over which vortex hopping occurs ("hoppers") and large barriers ("stoppers") over which the Lorentz force is unlikely to drive a vortex. Thus I believe that my noise measurements probe the low-energy region of the distribution of activation energies, as explained in Chapter V. Experiments such as flux creep [25-31] employing current densities orders of magnitude larger than in my experiment, or thermally activated resistivity [34-37] measured closer to T_c where $U(T) << U_0$, may well involve vortex motion over the "stoppers." Experiments such as these are also generally performed in magnetic fields 10^5 times larger than the residual field in my experiment, and the resulting strong vortex-vortex repulsion may compete with the pinning forces.

Excess Vortices

Evaluating the distribution of activation energies for the two-dimensional model [Eq. (7-12)] requires two additional parameters, the number of processes in the ensemble N_p and the density of pinning sites n_s. I choose $N_p = 4 \times 10^6$ to make the integral of the distribution over the experimental energy range (8.5 meV to 190 meV) equal to that of the measured distribution. The pinning site density is then adjusted to give the best fit, yielding $n_s = 600\ \mu m^{-2}$. This high value agrees with the limit set by Dolan *et al.* [174], $n_s > 100\ \mu m^{-2}$, for the areal density of an unidentified but uniformly spatially distributed pinning mechanism

inferred from images of decorated flux lattices in YBCO. The theoretical distribution of activation energies is plotted in the inset to Fig. 7-1(b). The qualitative agreement with the measured distribution is good, although the simple exponential in Eq. (7-12) does not reproduce the measured peak at $U_{0,peak} \approx 0.05$ eV. This peak may indicate that the defects which cause the pinning have a preferred intersite distance of $(8U_{0,peak}/k_0)^{1/2} \approx 30$ nm, or it may indicate a pinning mechanism beyond the scope of the two-dimensional model.

The number density of vortices in transformer T1 is given by $n_v = N_p/P_vA = 0.03\ \mu m^{-2}$, indicating that typically only one pinning site out of $n_s/n_v \approx 2 \times 10^4$ is occupied by a vortex. Integrating $D(U_0)$ from 8.5 meV to 190 meV indicates that almost 80% of the processes in the ensemble fall within the experimentally accessible energy range. Thus there are few silent sites, provided that the form of Eq. (7-12) is valid for $U_0 >$ 190 meV. However, I have no evidence that my two-dimensional model applies to the whole of the sample, but only to the regions producing the noise, and much larger barriers may well exist. For example, the pinning sites could be nonuniformly distributed, with hoppers in the regions where they cluster and large site-free areas acting as stoppers.

The vortex density can be expressed as an effective field $B_{eff} = n_v\Phi_0 = 60\ \mu T$, which is much larger than the field in which the sample was cooled. The actual magnetization of the sample may be near zero if there are approximately equal numbers of vortices and antivortices, but the number of fluctuators is too large to be explained by the ambient field in the dewar. Some other mechanism must generate vortices in the film, such as the freezing in of vortex-antivortex pairs as the film is cooled through

T_c. In the next chapter I will discuss further evidence for these excess vortices from field-cooling experiments.

Current Dependence of a Random Telegraph Signal

According to the results of this chapter, a supercurrent suppresses the total indirect noise because it reduces the correlation time τ of each process in the ensemble. The observation of a single RTS which is appropriately modulated by the supercurrent would be a striking confirmation of this idea. Although I often found knee-like features in the transformers' power spectra which appeared and disappeared reproducibly as a function of I, only one RTS was both clearly resolved in the time domain and sufficiently stable to allow detailed investigation of its current dependence. The typical behavior of this process, which appeared in transformer T2 at 45 K, is illustrated in Fig. 7-4. Subsequently increasing the temperature by 1 K caused the switching to vanish; either the process has moved out of the experimental bandwidth because its activation energy is actually larger than the value deduced below, or the vortex has simply escaped from the double well. I find the latter explanation more likely, since the observed RTSs tend to be quite sensitive to perturbations, as discussed in connection with Fig. 3-5.

As shown in Fig. 7-4(a), the flux through the SQUID in the absence of a supercurrent switches between two levels separated by $\Delta\Phi = 9 \times 10^{-3}\Phi_0$. Additional noise is present from the motion of other vortices in the film, including a second rare RTS which executes a single cycle in

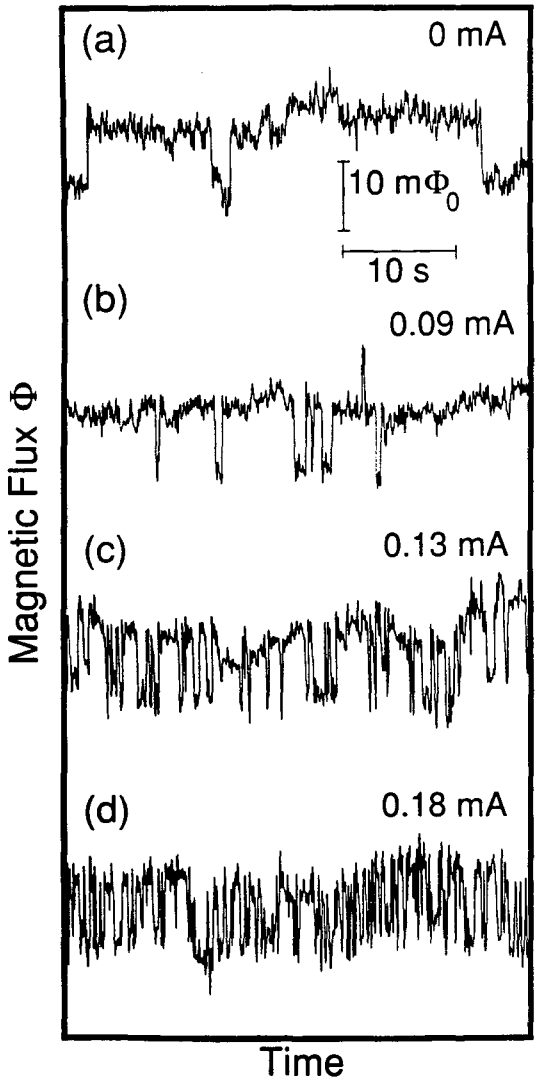

FIG. 7-4. Flux through SQUID vs. time generated by transformer T2 at 45 K for four different values of the circulating current *I*: (a) 0 mA, (b) 0.09 mA, (c) 0.13 mA, (d) 0.18 mA. Zeros of axes are arbitrary; traces are displaced for clarity.

Fig. 7-4(b). As the induced current in the transformer is increased, $\Delta\Phi$ remains constant but the switching rate of the dominant RTS increases; this is approximately reversible upon returning to zero current. The data are inconsistent with a symmetrical process like the one sketched in Fig. 7-3 because the switching rate increases with I instead of decreasing. One might be tempted to explain this as the result of an inherent misalignment in the pinning potential, so that increasing current tends to align the minima of the double well rather than tipping them further. However, according to Eq. (7-1) this would imply that one lifetime would increase and the other would decrease in a manner that kept their product $\tau_1\tau_2$ constant, and both lifetimes decrease with increasing I.

The RTS observed in transformer T2 is not as well-behaved as one might infer from the data in Fig. 7-4. The lifetime ratio γ at $I = 0$ varied apparently randomly among three separate measurements, each immediately following a noise measurement at higher current. The fluctuator also tended to alternate several seconds of inactivity with short bursts of switching in a decidedly non-Poisson manner. Nevertheless, it is obvious that this RTS is not representative of the processes which produce $1/f$ noise in transformer T1, and in T2 at 4.2 K, because its current dependence is not the same as theirs and because its hopping distance is much larger. The disparity is readily explained if the extended defects which produce RTSs differ from the localized defects relevant to $1/f$ noise. The data are consistent with an approximately symmetric process whose barrier $U(T,I)$ is current dependent, decreasing linearly from 0.11 eV at $I = 0$ to 0.09 eV at $I = 0.18$ mA according to Eq. (5-1) with $\tau_0 = 10^{-11}$ s. A possible extended defect is a high-angle grain boundary [175,176] acting as a

Josephson junction whose critical current [177] $I_0 \approx eU(T,0)/\hbar = 27\ \mu A$ is reduced by the imposition of a shielding current.

The hopping distance inferred for the process in Fig. 7-4 depends on the segment of the transformer in which it is located. For a vortex in the input coil, or one in the crossunder beneath a line of the input coil, Eq. (6-1) gives $\ell \cos\theta = 6\ \mu m$, indicated as a lower limit in Table 3-1. At the other extreme, a process in the pickup loop would require $\ell \cos\theta = 300\ \mu m$, large enough to make that location extremely unlikely.

VIII. Magnetic Field Dependence

> They had to evacuate the grade school on Tuesday. Kids were getting headaches and eye irritations, tasting metal in their mouths. . . . Denise and Steffie stayed home that week as men in Mylex suits and respirator masks made systematic sweeps of the building with infrared detecting and measuring equipment. Because Mylex is itself a suspect material, the results tended to be ambiguous and a second round of more rigorous detection had to be scheduled.
>
> – Don DeLillo, *White Noise* (1985)

The measurements which I have described thus far were all made in the ambient magnetic field within the mu-metal shield, $B < 1$ μT. I demonstrated in Chapter VII that at least for transformer T1, this field is too weak to explain the density of vortices n_v, and I hypothesized an additional mechanism to account for the excess. In order to bring n_v under experimental control, it is necessary to cool the sample through T_c in a larger applied field. This chapter describes the results of such experiments, some of which have been published previously [125,142], as well as measurements of noise in the presence of flux creep. I will present evidence that the processes in the DDH ensemble add incoherently, and that there is an intrinsic mechanism generating vortices in other samples besides T1.

Incoherent Vortex Motion

Increasing the number of vortices in samples YBCO(3) and BSCCO(1) increases their noise, as illustrated in Figs. 8-1 and 8-2. To make these measurements, I raise the temperature of the sample above T_c, store a current in the field coil which produces a field B parallel to the c axis, and then cool the sample to the temperature of interest. In the absence of an intrinsic mechanism for generating vortices, this produces a vortex density $n_V = B/\Phi_0$ proportional to the applied field, which remains constant during the noise measurement. According to Figs. 8-1 and 8-2, the noise power measured after field cooling increases linearly with B for fields of a few mT. Although not evident on the scale of these figures, the noise for $B < 0.1$ mT lies above the linear extrapolation, an effect which I will address below.

The linearity of the total noise power as a function of the number of fluctuators provides experimental justification for the neglect of correlations among the processes summed in Eq. (5-4). Contrary to the assertion of Ref. [142], however, it does not imply that no such correlations exist. The phenomenon of flux creep discussed later in this chapter, and the observation of vortex lattices in decoration experiments [178], are evidence for vortex-vortex interactions even in the small fields I apply. Nevertheless, it must be true that the vortices producing the noise exhibit both correlation and anticorrelation at random, so that when summed over the ensemble the noise is the same as if there were no correlation at all. I am indebted to Kristin Ralls for this observation. I do expect the interaction energies to be small, since the average vortex spacing

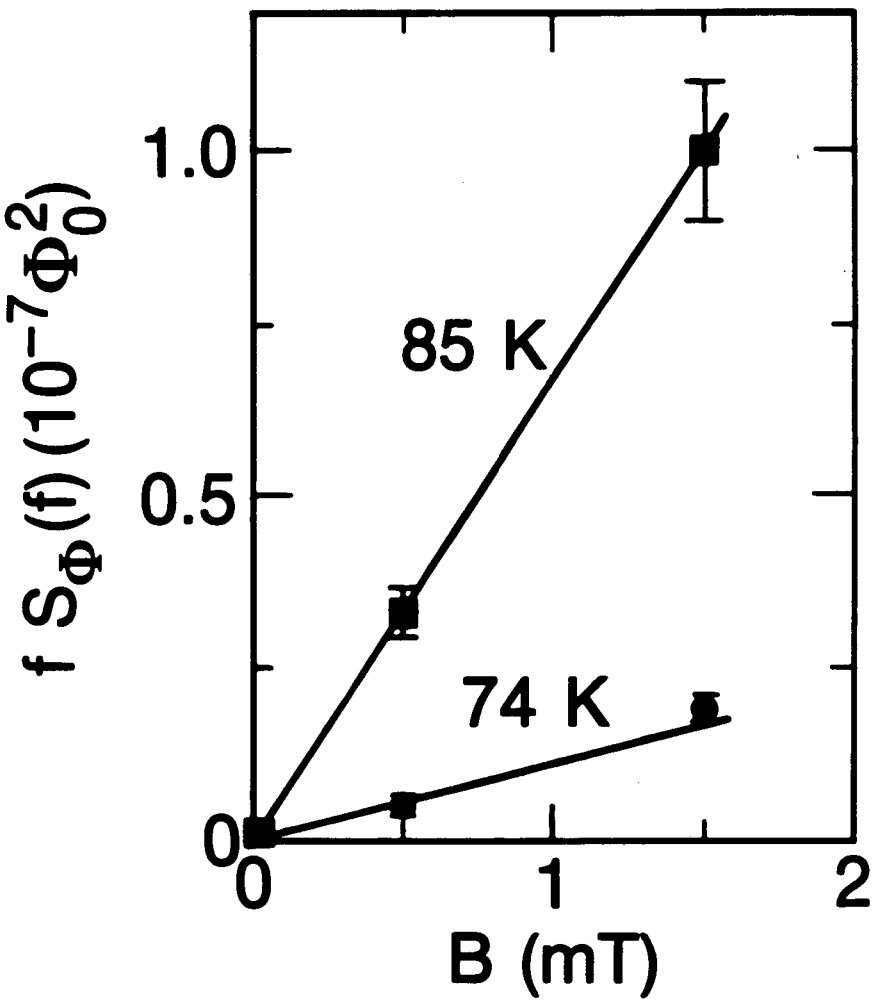

FIG. 8-1. Noise power $f\,S_\Phi(f)$ for YBCO(3) at two temperatures as a function of the magnetic field B in which the sample was cooled (3 Hz $\leq f \leq$ 30 Hz). Lines are guides to the eye which intercept the origin.

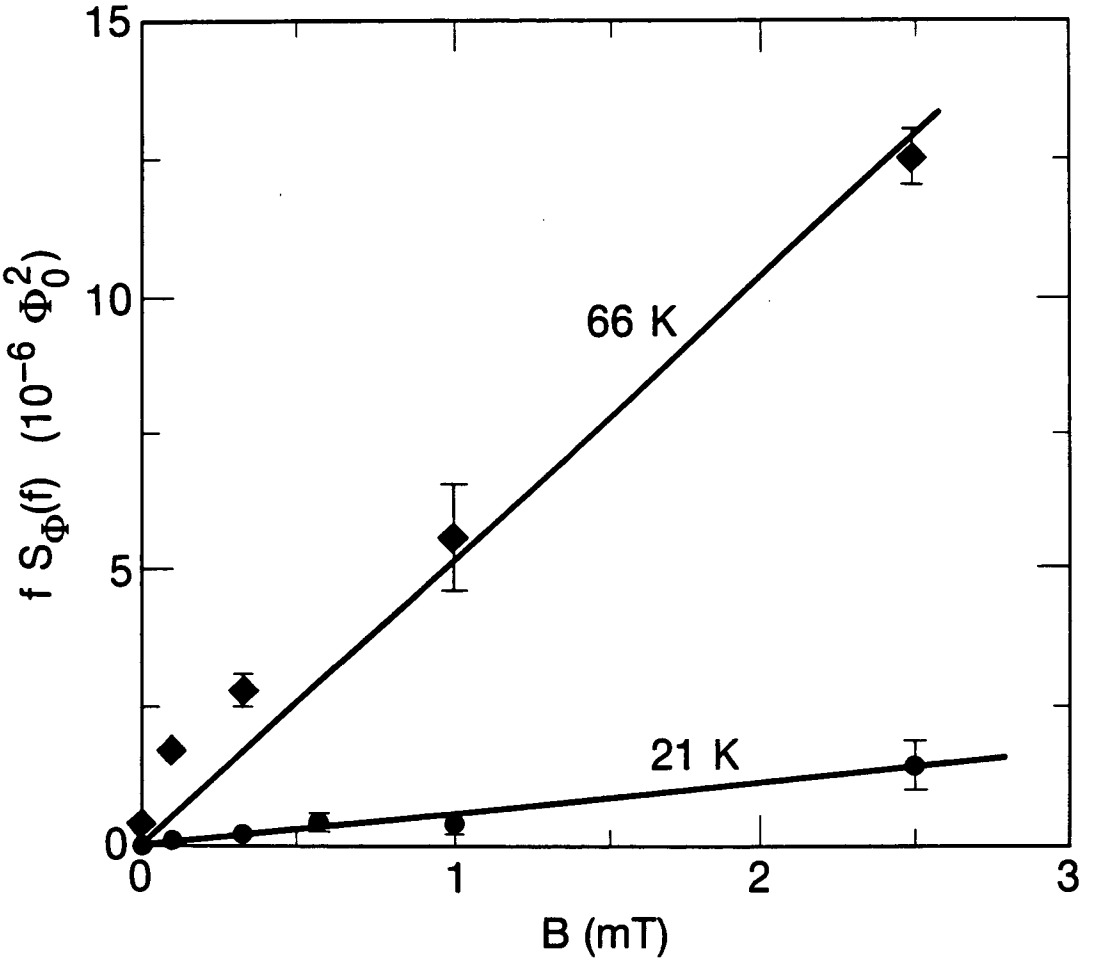

FIG. 8-2. Noise power $f\,S_\Phi(f)$ for BSCCO(1) at two temperatures as a function of the magnetic field B in which the sample was cooled (1 Hz $\leq f \leq$ 100 Hz). Lines are guides to the eye which intercept the origin.

$a_0 \approx (\Phi_0/B)^{1/2} \gtrsim 1$ μm exceeds the penetration depth [29,114,115], even at the elevated temperatures in Figs. 8-1 and 8-2.

Excess Vortices Revisited

The existence of a mechanism which produces a vortex density B_{eff}/Φ_0 even in the absence of an applied magnetic field implies that the proportionality between $S_\Phi(f)$ and B should break down as $B \rightarrow B_{eff}$ from above. Thus the noise power should become independent of field for values of B much less than those plotted in Figs. 8-1 and 8-2. I expect the field dependence of the noise to obey

$$S_\Phi(B) = S_\Phi(0)\left(1 + \frac{B}{B_{eff}}\right), \tag{8-1}$$

where B_{eff} and $S_\Phi(0)$ parametrize the vortex density and the resulting noise, respectively, according to the hypothetical intrinsic mechanism. At the time of this writing, this idea is being tested by Tim Shaw in a series of measurements of noise after cooling in small magnetic fields. Very preliminary results [179] are consistent with Eq. (8-1), with effective fields at least as large as the value $B_{eff} = 60$ μT deduced for T1 in Chapter VII.

Glyantsev *et al.* [180] have found that the $1/f$ magnetic flux noise generated near T_c by bulk samples of YBCO is independent of field over the range 10^{-10} T $< B < 10^{-5}$ T. Although they claim that this result rules out vortex motion as the source of the noise, it is also consistent with an intrinsic vortex density comparable to those discussed in this dissertation.

Flux Creep

A number of groups [25-31] have studied vortex motion in copper oxide superconductors by means of flux creep, usually in magnetic fields greater than 0.1 T. The sensitivity of the SQUID and its intimate coupling to the sample in the McDLT apparatus allow me to observe this phenomenon in fields two orders of magnitude smaller. Before each flux creep measurement, I raise the temperature of the sample above T_c, apply a magnetic field $B = 1$ mT perpendicular to the film, and then cool to the temperature of interest. After waiting for temperature stabilization, I release the current in the field coil, place the SQUID in feedback, and record the flux linking the SQUID as a function of time t for several hours. Figure 8-3 shows the decaying magnetization observed in YBCO(1) at 81 K, which appears linear when plotted on a logarithmic time axis as expected for thermally activated flux creep [126,127]. I have occasionally observed nonlogarithmic relaxation, but all the data presented here are well fitted by the usual creep equation for the change in the flux linking the SQUID,

$$\Phi(t) = -\Phi_1 \ln(t/t_0) \ , \tag{8-2}$$

where Φ_1 is the temperature-dependent creep rate and t_0 is the time at which I define $\Phi = 0$.

A plot of Φ_1 as a function of temperature for YBCO(1) is shown in Fig. 8-4. I interpret the sharp peak at 79 K as a manifestation of the famous irreversibility line observed in copper oxides [25,181] as well as low-T_c Type-II materials [182], although it could also be evidence of

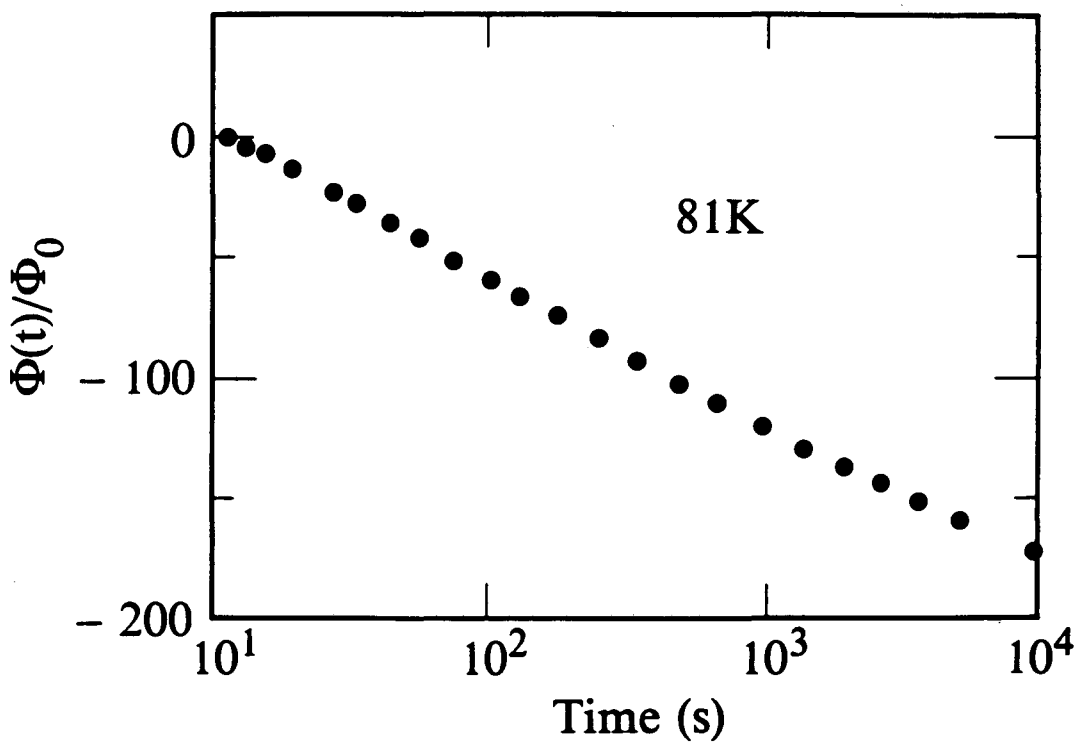

FIG. 8-3. Change in flux linking the SQUID in units of the flux quantum, $\Phi(t)/\Phi_0$, vs. time for YBCO(1) at 81 K. Sample was cooled through T_c in a magnetic field of 1 mT. Measurement made in zero applied field, and $t = 0$ is time at which the field was removed.

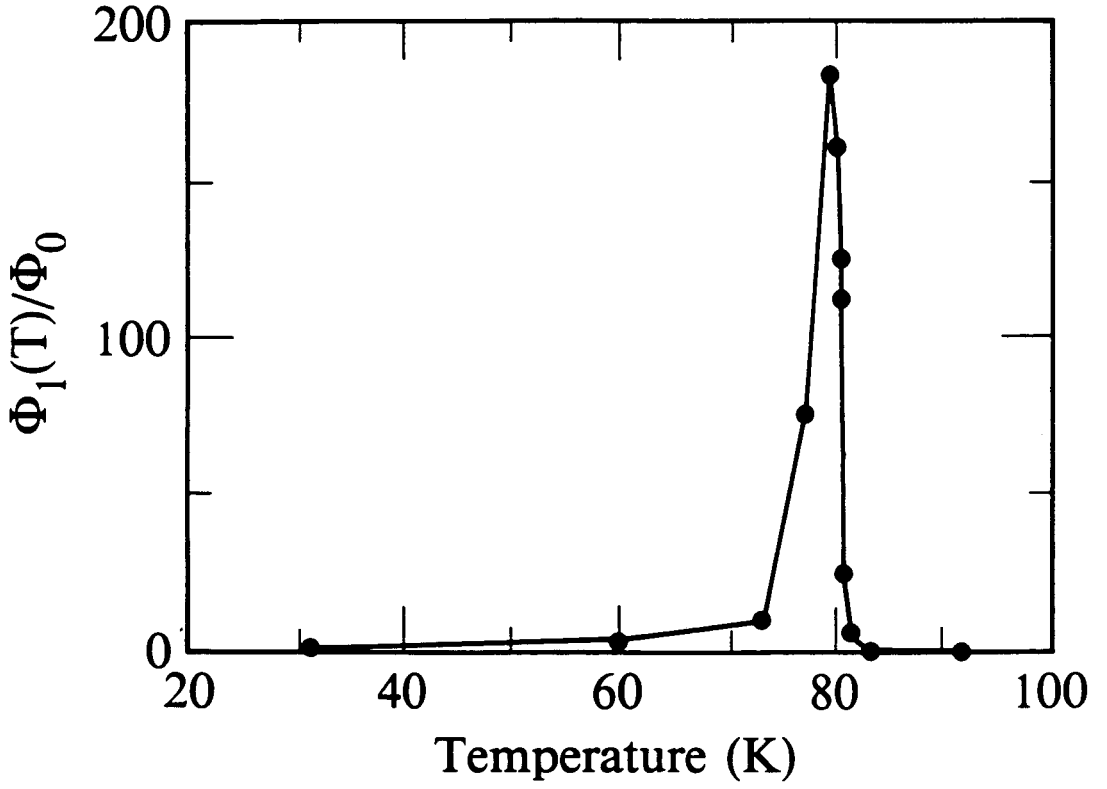

FIG. 8-4. Flux creep rate Φ_1 in units of the flux quantum vs. temperature for YBCO(1) after cooling in B = 1 mT. Greatest creep rate was measured at 79 K, well below T_c = 85 K. Curve is a guide to the eye.

parallel relaxation [111]. At temperatures below the peak, the creep is so slow that there is little vortex motion during the time of the experiment, while above the peak it is so fast that most of the relaxation occurs before the measurement begins. At $t = 0$ the number of vortices in the sample is $N_V = BA_S/\Phi_0 = 5 \times 10^5$, so the creep rate $\Phi_1 = 10\Phi_0$ measured at 73 K corresponds to an average radial displacement of only $w\ln(10)\Phi_1/N_V\alpha_S\Phi_0 \approx 30$ nm per vortex per decade of time.

Time Dependence of Field Cooled Noise

The existence of noisy and quiet metastable flux configurations was demonstrated in Chapter III. Vortices were observed to switch between these states, presumably by hopping over a larger intervening barrier, both spontaneously and under the influence of a small applied magnetic field. In a flux creep measurement there is net motion of vortices across the sample, driven by their mutual repulsion, and I expect that they will encounter noisy and quiet regions of the pinning potential as they traverse it. This is precisely the phenomenon illustrated in Fig. 8-5. These spectra were taken with sample TCBCO(1) at 77 K, after cooling through T_c in $B = 0.1$ mT. The field was removed at $t = 0$ and the noise measured subsequently with an averaging time of 40 s to 120 s, during which the time-averaged flux through the SQUID drifted by $d\langle\Phi\rangle/dt < 6 \times 10^{-3}\ \Phi_0$/s as a result of flux creep. This rate is too small to contribute measurably the noise, which appears as quasistationary fluctuations superimposed on the monotonic drift. It is conventional in theories of flux creep to neglect

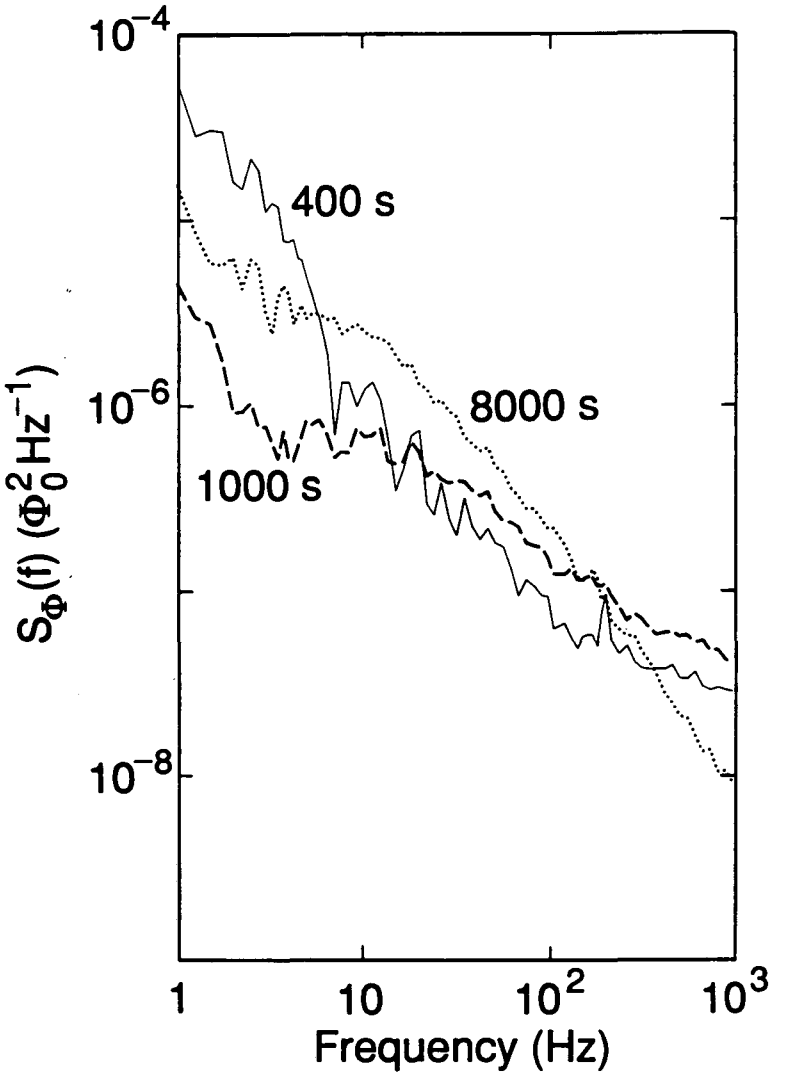

FIG. 8-5. Noise spectral density $S\Phi(f)$ vs. frequency for TCBCO(1) at three different times after cooling to 77 K in $B = 0.1$ mT. Measurements made after field was removed at $t = 0$: solid spectrum, $t = 400$ s; dashed spectrum, $t = 1000$ s; dotted spectrum, $t = 8000$ s. Increasing smoothness of spectra with increasing t is an artifact caused by longer averaging times.

hopping in the direction opposite the driving force because most experiments are insensitive to it, but a noise measurement reveals vortex motion in both directions.

From 1 Hz to 1 kHz the noise power spectra in Fig. 8-5 all scale roughly as $1/f$, but on a finer scale the slope shows significant variations. These features are reminiscent of those seen in the voltage noise of metal-insulator-metal tunnel junctions [132] when a small number of traps are active in the barrier, producing a few superposed Lorentzians in the experimental bandwidth. I seems reasonable that a few vortex hopping processes dominate the noise at a given time. Subsequent spectra exhibit different features; vortices may have moved out of some processes and into others, or enduring processes may be shifted as a result of interactions with vortices that have moved. The noise power at a given frequency evolves apparently at random, with no discernable trend over more than a decade in time, 400 s $\leq t \leq$ 8000 s. I was unable to measure the noise for $t <$ 400 s because the drift during the averaging time of the spectrum analyzer exceeded its dynamic range.

Zero-field-cooled noise measurements on TCBCO(1) often fell in the same range as the spectra in Fig. 8-5, but they did not exhibit noticeable time dependence. Apparently cooling in $B = 0.1$ mT does not greatly increase the number of mobile vortices, but it does tend to trap them in metastable states. Cooling in $B = 1$ mT before switching off the field increases the low-frequency noise by the expected factor of ten for $t \lesssim$ 3000 s, but after that time the noise begins to relax to its zero-field-cooled value. Since it is unlikely that a significant fraction of the vortices is

expelled from the sample, I believe this reduction results from vortices being driven against stoppers by their density gradient.

IX. Summary and Prospects

Well I was out in my four door
with the top down
And I looked up and there they were:
Millions of tiny teardrops
just sort of hanging there
And I didn't know whether to laugh or cry
And I said to myself:
What next big sky?

– Laurie Anderson, *Strange Angels* (1989)

Conclusions

In this dissertation I have described a new method for detecting the motion of Abrikosov vortices in Type-II superconductors. This technique is related to, and was in fact motivated by, the sensitivity of a SQUID to the hopping of vortices pinned in its washer. What makes the McDLT apparatus unique is that the superconductor generating the flux noise and the device detecting it are not the same, so that, for example, the temperature of the sample can be varied independently of that of the SQUID. It is also possible to use the same SQUID to make noise measurements on a large number of as-fabricated samples. Patterning of the sample, with its attendant risk of damage, is eliminated.

Noise measurements are sensitive to vortices in thermal equilibrium. Unlike measurements of flux creep or thermally activated resistivity, in which strong driving forces are necessary to produce measurable vortex motion, the McDLT can detect stationary noise from vortices hopping

among the minima of the unperturbed pinning potential. Thus the pinning energies extracted are more likely to represent intrinsic materials properties, undistorted by current or inhomogeneous vortex density. When I do deliberately apply a driving force in my experiment, its effects can be understood as a perturbation on the model previously developed to explain the noise.

My experiment is also distinguished from flux creep and transport measurements by its very small applied magnetic field, usually < 1 μT. The resulting large vortex spacing implies that vortex-vortex interactions are weak in comparison to interactions with pinning sites, allowing the effects of these two types of forces to be clearly distinguished. In contrast, experiments in large magnetic fields involve strongly correlated vortex motion, and issues of bundle size and collective pinning complicate their analysis.

I am able to detect random telegraph signals (RTSs) caused by the thermally activated motion of a single vortex in YBCO, BSCCO, and TCBCO, and to explore their dependence on temperature and current. These measurements yield the vortex hopping distance and activation energy. Such RTSs are fairly uncommon, because they require one vortex to have a hopping distance on the order of 1 μm; typically the noise from the sample exhibits a $1/f$ spectrum produced by the motion of many vortices over much smaller distances.

A key concept in this dissertation is the distribution of activation energies which, according to the Dutta-Dimon-Horn model, explains the $1/f$ spectrum. Because my measurements of $1/f$ noise are sensitive only to activation energies below 0.5 eV, I probe the low-energy end of this

distribution, and the pinning potential can be approximated by an ensemble of symmetrical double wells. In YBCO with its *c*-axis oriented perpendicularly to the substrate, the distribution of activation energies shows a broad peak below 0.1 eV. The suppression of noise by a supercurrent described in Chapter VII is further evidence that activation energies in the samples are distributed, and that the processes tend to be symmetrical. Different experiments are sensitive to different regimes in the distribution of activation energies, explaining the disparity between the energies deduced from flux creep and from transport measurements, for example.

The noise power produced by the sample is linear in the magnetic field in which the sample was cooled, and therefore linear in the number of vortices, for 0.1 mT $< B <$ 3 mT. This implies that correlations among vortices may be neglected when calculating their total noise, as assumed in the Dutta-Dimon-Horn model. In magnetic fields below this range the noise shows signs of crossing over to a field-independent regime, which would require some number of vortices to be trapped in the film even in the absence of an applied field. This hypothesis is borne out by integrating the distribution of activation energies measured for transformer T1, which shows an areal density of vortices two orders of magnitude larger than could be explained by the ambient field.

The work reported in this dissertation has implications for the design and fabrication of practical magnetometers from copper oxide superconductors. The decrease of noise with increased film quality shows that intrinsically quiet films are a necessary (but not sufficient) condition for sensitive SQUIDs and flux transformers. The noise in a YBCO flux

transformer is dominated by fluctuations in the screening current, driven by vortex motion in the input coil. This indirect noise could be minimized by intelligent design, such as choosing the greatest possible input coil linewidth, and by the use of a dc supercurrent to suppress vortex motion as demonstrated in Chapter VII.

Unanswered Questions

Only an exceptionally uninteresting experiment would fail to raise more questions than it answers. In this respect, my experiment has been interesting indeed. The following list of questions suggests research directions that I believe will be fruitful.

Which materials parameters determine the noise? Table 2-1 contains too few samples to establish more than a rough correlation between sample parameters and flux noise power. Many additional measurements on well-characterized samples will be necessary to separate the effects of deposition technique, crystalline orientation, critical current, and so forth.

Which microstructural properties determine the noise? Provided that a definitive correlation could be found between a materials parameter and the flux noise power, the microstructural cause of the correlation would remain to be demonstrated. One possibility would be to produce known defects in the sample in a controlled manner, and to measure their effect on the noise.

Why does the DDH slope equation slightly overestimate the measured slope of the noise power spectrum? An effect which causes the

noise to increase with temperature has been overlooked, such as an increase in the number of mobile vortices, or individual processes with temperature dependent hopping distances.

What produces peak in $D(U_0)$ below 0.1 eV in YBCO? The simple two-dimensional model of Chapter VII predicts a featureless exponential distribution of activation energies. Clearly the pinning potential contains additional structure which requires explanation.

When does the two-dimensional model break down? The Hooke's law approximation in Eq. (7-10) my be valid only for $r \lesssim \xi$, or it may hold for all distances $r \lesssim \lambda$, depending on the nature of the pinning interaction. The latter has been assumed in this dissertation, but some scaling between hopping distance and activation energy seems inevitable in either case. Also, the identification of one process in the DDH ensemble with each unobstructed pair of pinning sites in the two-dimensional model may not be valid for $\ell[\tilde{U}_0(T)] \gtrsim n_s^{-1/2}$, when vortices can circumvent large barriers by a series of short hops around them. Numerical simulations should be able to resolve this issue.

What causes intrinsic vortices? I hypothesize that the number of vortices pinned in the sample, which far exceeds the density corresponding to the ambient field in my experiment, results from the freezing-in of fluctuations when cooling through T_c. A theoretical prediction of the expected magnitude of this effect would be very useful. Experimental tests should be possible, such as the dependence of the excess vortex density on sample thickness (and hence vortex self-energy), degree of anisotropy (dimensionality of fluctuations), and cooling rate.

How does the intrinsic number of vortices vary with sample parameters? Again, many well-characterized samples are needed, and the observed correlations might shed light on the mechanism by which these vortices are generated. A method for reducing the flux noise in real devices might result.

What causes noise peak at T_c? I have argued that the magnitude of this peak is intrinsic to YBCO and relatively independent of materials parameters. If so, it should be possible to address it theoretically.

Is there a simple explanation for the distribution of activation energies in Fig. 5-5? The behavior of the *a*-axis sample YBCO(6) is so featureless that it begs to be explained by some simple model derived from the highly anisotropic pinning potential present in *a*-axis films.

Do conventional superconductors reproduce any of the phenomena discussed in this dissertation? Vortex motion has long been suspected of causing flux noise in SQUIDs fabricated from Nb and PbIn, but there are no definitive experiments in this area, especially in the region near T_c.

References

[1] J. Bardeen, L. N. Cooper and J. R. Schrieffer, "Theory of Superconductivity," *Phys. Rev.* **108,** 1175 (1957).

[2] P. Dutta, P. Dimon and P. M. Horn, "Energy Scales for Noise Processes in Metals," *Phys. Rev. Lett.* **43,** 646 (1979).

[3] V. L. Ginzburg and L. D. Landau, *Zh. eksper. teor. Fiz.* **20,** 1064 (1950).

[4] A. A. Abrikosov, "On the Magnetic Properties of Superconductors of the Second Group," *Sov. Phys. JETP* **5,** 1174 (1957).

[5] T. Van Duzer and C. W. Turner, *Principles of Superconductive Devices and Circuits* (Elsevier, New York, 1981).

[6] D. S. Fisher, "Flux-Lattice Melting in Thin-Film Superconductors," *Phys. Rev. B* **22,** 1190 (1980).

[7] J. W. P. Hsu and A. Kapitulnik, "Flux Motion in a Two-Dimensional Single-Crystal Nb Film," *Appl. Phys. Lett.* **57,** 1061 (1990).

[8] H. Ullmaier, *Irreversible Properties of Type II Superconductors* (Springer-Verlag, Berlin, 1975).

[9] L. Civale, A. D. Marwick, T. K. Worthington, M. A. Kirk, J. R. Thompson, L. Krusin-Elbaum, Y. Sun, J. R. Clem and F. Holtzberg, "Vortex Confinement by Columnar Defects in $YBa_2Cu_3O_7$ Crystals: Enhanced Pinning at High Fields and Temperatures," *Phys. Rev. Lett.* **67,** 648 (1991).

[10] A. M. Campbell and J. E. Evetts, "Flux Vortices and Transport Currents in Type II Superconductors," *Adv. Phys.* **21,** 199 (1972).

[11] E. H. Brandt and U. Essmann, "The Flux-Line Lattice in Type-II Superconductors," *Phys. Stat. Sol. B* **144,** 13 (1987).

[12] The work of H. Kamerlingh Onnes is reviewed by R. de Bruyn Ouboter, "Superconductivity: Discoveries During the Early Years of Low Temperature Research at Leiden 1908-1914," *IEEE Trans. Mag.* **23,** 355 (1987).

[13] M. D. Lemonick, "Superconductors," *Time* **129** (19), 64 (11 May 1987).

[14] J. R. Gavaler, "Superconductivity in Nb-Ge Films above 22 K," *Appl. Phys. Lett.* **23,** 480 (1973).

[15] S. Foner, E. J. McNiff Jr., J. R. Gavaler and M. A. Janocko, "Upper Critical Fields of Nb_3Ge Thin Film Superconductors," *Phys. Lett. A* **47,** 485 (1974).

[16] J. G. Bednorz and K. A. Müller, "Possible High T_c Superconductivity in the Ba-La-Cu-O System," *Z. Phys. B* **64,** 189 (1986).

[17] J. G. Bednorz, M. Takashige and K. A. Müller, "Susceptibility Measurements Support High-T_c Superconductivity in the Ba-La-Cu-O System," *Europhys. Lett.* **3,** 379 (1987).

[18] M. K. Wu, J. R. Ashburn, C. J. Torng, P. H. Hor, R. L. Meng, L. Gao, Z. J. Huang, Y. Q. Wang and C. W. Chu, "Superconductivity at 93 K in a New Mixed-Phase Y-Ba-Cu-O Compound System at Ambient Pressure," *Phys. Rev. Lett.* **58,** 908 (1987).

[19] H. Maeda, Y. Tanaka, M. Fukutomi and T. Asano, "A New High-T_c Oxide Superconductor without a Rare Earth Element," *Jpn. J. Appl. Phys.* **27,** L209 (1988).

[20] Z. Z. Sheng and A. M. Hermann, "Superconductivity in the Rare-Earth-Free Tl-Ba-Cu-O System above Liquid-Nitrogen Temperature," *Nature* **332,** 55 (1988).

[21] Z. Z. Sheng and A. M. Hermann, "Bulk Superconductivity at 120 K in the Tl-Ca/Ba-Cu-O System," *Nature* **332,** 138 (1988).

[22] T. K. Worthington, W. J. Gallagher and T. R. Dinger, "Anisotropic Nature of High-Temperature Superconductivity in Single-Crystal $Y_1Ba_2Cu_3O_{7-x}$," *Phys. Rev. Lett.* **59,** 1160 (1987).

[23] U. Welp, W. K. Kwok, G. W. Crabtree, K. G. Vandervoort and J. Z. Liu, "Magnetic Measurements of the Upper Critical Field of $YBa_2Cu_3O_{7-\delta}$ Single Crystals," *Phys. Rev. Lett.* **62,** 1908 (1989).

[24] M. R. Beasley, R. Labusch and W. W. Webb, "Flux Creep in Type-II Superconductors," *Phys. Rev.* **181,** 682 (1969).

[25] Y. Yeshurun and A. P. Malozemoff, "Giant Flux Creep and Irreversibility in an Y-Ba-Cu-O Crystal: An Alternative to the Superconducting-Glass Model," *Phys. Rev. Lett.* **60,** 2202 (1988).

[26] Y. Yeshurun, A. P. Malozemoff and F. Holtzberg, "Magnetic Relaxation and Critical Current in an YBaCuO Crystal," *J. Appl. Phys.* **64,** 5797 (1988).

[27] M. Tuominen, A. M. Goldman and M. L. Mecartney, "Time-Dependent Magnetization of a Superconducting Glass," *Phys. Rev. B* **37,** 548 (1988).

[28] M. Tuominen, A. M. Goldman and M. L. Mecartney, "Superconducting Glass Behavior of $YBa_2Cu_3O_{7-x}$," *Physica C* **153-155,** 324 (1988).

[29] B. D. Biggs, M. N. Kunchur, J. J. Lin, S. J. Poon, T. R. Askew, R. B. Flippen, M. A. Subramanian, J. Gopalakrishnan and A. W. Sleight, "Flux Creep and Critical-Current Anisotropy in $Bi_2Sr_2CaCu_2O_{8+\delta}$," *Phys. Rev. B* **39,** 7309 (1989).

[30] C. Rossel, Y. Maeno and I. Morgenstern, "Memory Effects in a Superconducting Y-Ba-Cu-O Single Crystal: A Similarity to Spin-Glasses," *Phys. Rev. Lett.* **62,** 681 (1989).

[31] J. Z. Sun, B. Lairson, C. B. Eom, J. Bravman and T. H. Geballe, "Elimination of Current Dissipation in High Transition Temperature Superconductors," *Science* **247,** 307 (1990).

[32] P. L. Gammel, L. F. Schneemeyer, J. V. Waszczak and D. J. Bishop, "Evidence from Mechanical Measurements for Flux-Lattice Melting in Single-Crystal $YBa_2Cu_3O_7$ and $Bi_{2.2}Sr_2Ca_{0.8}Cu_2O_8$," *Phys. Rev. Lett.* **61,** 1666 (1988).

[33] S. Gregory, C. T. Rogers, T. Venkatesan, X. D. Wu, A. Inam and B. Dutta, "Evidence for a Vortex-Glass State from Mechanical Measurements of Flux-Line-Induced Energy Dissipation in $YBa_2Cu_3O_{7-x}$ Thin Films," *Phys. Rev. Lett.* **62,** 1548 (1989).

[34] T. T. M. Palstra, B. Batlogg, L. F. Schneemeyer and J. V. Waszczak, "Thermally Activated Dissipation in $Bi_{2.2}Sr_2Ca_{0.8}Cu_2O_{8+\delta}$," *Phys. Rev. Lett.* **61,** 1662 (1988).

[35] T. T. M. Palstra, B. Batlogg, R. B. van Dover, L. F. Schneemeyer and J. V. Waszczak, "Dissipative Flux Motion in High-Temperature Superconductors," *Phys. Rev. B* **41,** 6621 (1990).

[36] E. Zeldov, N. M. Amer, G. Koren, A. Gupta, R. J. Gambino and M. W. McElfresh, "Optical and Electrical Enhancement of Flux Creep in $YBa_2Cu_3O_{7-\delta}$ Epitaxial Films," *Phys. Rev. Lett.* **62,** 3093 (1989).

[37] E. Zeldov, N. M. Amer, G. Koren, A. Gupta and M. W. McElfresh, "Flux Creep Characteristics in High-Temperature Superconductors," *Appl. Phys. Lett.* **56,** 680 (1990).

[38] M. P. A. Fisher, "Vortex-Glass Superconductivity: A Possible New Phase in Bulk High-T_c Oxides," *Phys. Rev. Lett.* **62,** 1415 (1989).

[39] D. S. Fisher, M. P. A. Fisher and D. A. Huse, "Thermal Fluctuations, Quenched Disorder, Phase Transitions, and Transport in Type-II Superconductors," *Phys. Rev. B* **43,** 130 (1991).

[40] R. H. Koch, V. Foglietti, W. J. Gallagher, G. Koren, A. Gupta and M. P. A. Fisher, "Experimental Evidence for Vortex-Glass Superconductivity in Y-Ba-Cu-O," *Phys. Rev. Lett.* **63,** 1511 (1989).

[41] P. L. Gammel, L. F. Schneemeyer and D. J. Bishop, "SQUID Picovoltometry of $YBa_2Cu_3O_7$ Single Crystals: Evidence for a Finite-Temperature Phase Transition in the High-Field Vortex State," *Phys. Rev. Lett.* **66,** 953 (1991).

[42] H. K. Olsson, R. H. Koch, W. Eidelloth and R. P. Robertazzi, "Observation of Critical Scaling Behavior in the ac Impedance at the Onset of Superconductivity in a Large Magnetic Field," *Phys. Rev. Lett.* **66,** 2661 (1991).

[43] G. J. Dolan, F. Holtzberg, C. Feild and T. R. Dinger, "Anisotropic Vortex Structure in $Y_1Ba_2Cu_3O_7$," *Phys. Rev. Lett.* **62,** 2184 (1989).

[44] C. A. Bolle, P. L. Gammel, D. G. Grier, C. A. Murray, D. J. Bishop, D. B. Mitzi and A. Kapitulnik, "Observation of a Commensurate Array of Flux Chains in Tilted Flux Lattices in Bi-Sr-Ca-Cu-O Single Crystals," *Phys. Rev. Lett.* **66,** 112 (1991).

[45] S. Martin, A. T. Fiory, R. M. Fleming, G. P. Espinosa and A. S. Cooper, "Vortex-Pair Excitation near the Superconducting Transition of $Bi_2Sr_2CaCu_2O_8$ Crystals," *Phys. Rev. Lett.* **62,** 677 (1989).

[46] N.-C. Yeh and C. C. Tsuei, "Quasi-Two-Dimensional Phase Fluctuations in Bulk Superconducting $YBa_2Cu_3O_7$ Single Crystals," *Phys. Rev. B* **39,** 9708 (1989).

[47] S. N. Artemenko, I. G. Gorlova and Y. I. Latyshev, "Vortex Motion and Kosterlitz-Thouless Transition in Superconducting Single Crystals $Bi_2Sr_2CaCu_2O_x$," *Phys. Lett. A* **138,** 428 (1989).

[48] M. Ban, T. Ichiguchi and T. Onogi, "Power Laws in the Resistive State in High-T_c Superconductors," *Phys. Rev. B* **40,** 4419 (1989).

[49] D. H. Kim, A. M. Goldman, J. H. Kang and R. T. Kampwirth, "Kosterlitz-Thouless Transition in $Tl_2Ba_2CaCu_2O_8$ Thin Films," *Phys. Rev. B* **40,** 8834 (1989).

[50] J. G. Bednorz and K. A. Müller, "Perovskite-Type Oxides -- The New Approach to High-T_c Superconductivity," *Rev. Mod. Phys.* **60,** 585 (1988).

[51] M. Tinkham and C. J. Lobb, "Physical Properties of the New Superconductors," *Solid State Phys.* **42,** 91 (1989).

[52] J. Friedel, "The High-T_c Superconductors: A Conservative View," *J. Phys. Condens. Matter* **1**, 7757 (1989).

[53] A. S. Davydov, "Theoretical Investigation of High-Temperature Superconductivity," *Phys. Rep.* **190**, 191 (1990).

[54] C. P. Poole Jr., T. Datta and H. A. Farach, *Copper Oxide Superconductors* (John Wiley, New York, 1988).

[55] J. C. Phillips, *Physics of High-T_c Superconductors* (Academic Press, San Diego, 1989).

[56] J. W. Lynn, *High Temperature Superconductivity* (Springer-Verlag, New York, 1990).

[57] R. Beyers and T. M. Shaw, "The Structure of $Y_1Ba_2Cu_3O_{7-\delta}$ and Its Derivatives," *Solid State Phys.* **42**, 135 (1989).

[58] A. M. Stoneham and L. W. Smith, "Defect Phenomena in Superconducting Oxides and Analogous Ceramic Oxides," *J. Phys. Condens. Matter* **3**, 225 (1991).

[59] K. C. Hass, "Electronic Structure of Copper-Oxide Superconductors," *Solid State Phys.* **42**, 213 (1989).

[60] W. E. Pickett, "Electronic Structure of the High-Temperature Oxide Superconductors," *Rev. Mod. Phys.* **61**, 433 (1989).

[61] R. C. Jaklevic, J. Lambe, A. H. Silver and J. E. Mercereau, "Quantum Interference Effects in Josephson Tunneling," *Phys. Rev. Lett.* **12**, 159 (1964).

[62] R. C. Jaklevic, J. Lambe, J. E. Mercereau and A. H. Silver, "Macroscopic Quantum Interference in Superconductors," *Phys. Rev.* **140A**, 1628 (1965).

[63] B. D. Josephson, "Possible New Effects in Superconductive Tunneling," *Phys. Lett.* **1**, 251 (1962).

[64] B. D. Josephson, "Coupled Superconductors," *Rev. Mod. Phys.* **36**, 216 (1964).

[65] R. H. Koch, C. P. Umbach, G. J. Clark, P. Chaudhari and R. B. Laibowitz, "Quantum Interference Devices Made from Superconducting Oxide Thin Films," *Appl. Phys. Lett.* **51**, 200 (1987).

[66] C. D. Tesche and J. Clarke, "dc SQUID: Noise and Optimization," *J. Low Temp. Phys.* **29**, 301 (1977).

[67] J. Clarke, C. D. Tesche and R. P. Giffard, "Optimization of dc SQUID Voltmeter and Magnetometer Circuits," *J. Low Temp. Phys.* **37**, 405 (1979).

[68] R. H. Koch, W. J. Gallagher, B. Bumble and W. Y. Lee, "Low-Noise Thin-Film TlBaCaCuO dc SQUIDs Operated at 77 K," *Appl. Phys. Lett.* **54**, 951 (1989).

[69] J. Clarke, W. M. Goubau and M. B. Ketchen, "Tunnel Junction dc SQUID: Fabrication, Operation, and Performance," *J. Low Temp. Phys.* **25**, 99 (1976).

[70] M. Kawasaki, P. Chaudhari and A. Gupta, "1/*f* Noise in $Y_1Ba_2Cu_3O_{7-\delta}$ Superconducting Bicrystal Grain Boundary Junctions," *Phys. Rev. Lett.* (submitted).

[71] J. E. Zimmerman and N. V. Frederick, "Miniature Ultrasensitive Superconducting Magnetic Gradiometer and Its Use in Cardiography and Other Applications," *Appl. Phys. Lett.* **19**, 16 (1971).

[72] F. Wellstood, C. Heiden and J. Clarke, "Integrated dc SQUID Magnetometer with a High Slew Rate," *Rev. Sci. Instrum.* **55**, 952 (1984).

[73] D. Drung, R. Cantor, M. Peters, H. J. Scheer and H. Koch, "Low-Noise High-Speed dc Superconducting Quantum Interference Device Magnetometer with Simplified Feedback Electronics," *Appl. Phys. Lett.* **57**, 406 (1990).

[74] A. H. Miklich, J. J. Kingston, F. C. Wellstood, J. Clarke, M. S. Colclough, K. Char and G. Zaharchuk, "Sensitive $YBa_2Cu_3O_{7-x}$ Thin-Film Magnetometer," *Appl. Phys. Lett.* **59**, 988 (1991).

[75] B. Oh, R. H. Koch, W. J. Gallagher, R. P. Robertazzi and W. Eidelloth, "Multi-Level YBaCuO Flux Transformers with High-T_c SQUIDs: A Prototype High-T_c SQUID Magnetometer Working at 77 K," *Appl. Phys. Lett.* **59,** 123 (1991).

[76] J. Clarke, "SQUID Concepts and Systems," in *NATO ASI Series Vol. F59: Superconducting Electronics,* edited by H. Weinstock and M. Nisenoff (Springer-Verlag, Berlin, 1989), p. 87.

[77] T. Ryhänen, H. Seppä, R. Ilmoniemi and J. Knuutila, "SQUID Magnetometers for Low-Frequency Applications," *J. Low Temp. Phys.* **76,** 287 (1989).

[78] J. Clarke and R. H. Koch, "The Impact of High-Temperature Superconductivity on SQUID Magnetometers," *Science* **242,** 217 (1988).

[79] M. Tinkham, *Introduction to Superconductivity* (McGraw-Hill, New York, 1975).

[80] P. G. de Gennes, *Superconductivity of Metals and Alloys* (W. A. Benjamin, New York, 1966).

[81] F. C. Wellstood, *Excess Noise in the dc SQUID: 4.2 K to 20 mK* (Ph. D. thesis, University of California at Berkeley, 1988).

[82] C. P. Bean, "Magnetization of High-Field Superconductors," *Rev. Mod. Phys.* **36,** 31 (1964).

[83] K. P. Daly, W. D. Dozier, J. F. Burch, S. B. Coons, R. Hu, C. E. Platt and R. W. Simon, "Substrate Step-Edge $YBa_2Cu_3O_7$ rf SQUIDs," *Appl. Phys. Lett.* **58,** 543 (1991).

[84] C. L. Jia, B. Kabius, K. Urban, K. Herrman, G. J. Cui, J. Schubert, W. Zander, A. I. Braginski and C. Heiden, "Microstructure of Epitaxial $YBa_2Cu_3O_7$ Films on Step-Edge $SrTiO_3$ Substrates," *Physica C* **175,** 545 (1991).

[85] A. Ramirez, "Fast Food Lightens Up But Sales Are Often Thin," *New York Times* **140** (48544), D1(L) (19 March 1991).

[86] J. R. Clem, "Johnson Noise from Normal Metal near a Superconducting SQUID Gradiometer Circuit," *IEEE Trans. Mag.* **23**, 1093 (1987).

[87] R. J. Cava, B. Batlogg, C. H. Chen, E. A. Rietman, S. M. Zahurak and D. Werder, "Oxygen Stoichiometry, Superconductivity and Normal-State Properties of $YBa_2Cu_3O_{7-\delta}$," *Nature* **329**, 423 (1987).

[88] S. Yamaguchi, K. Terabe, A. Imai and Y. Iguchi, "High-Temperature Resistivity Measurements of $YBa_2Cu_3O_{7-x}$," *Jpn. J. Appl. Phys.* **27**, L220 (1988).

[89] K. Char, M. R. Hahn, T. L. Hylton, M. R. Beasley, T. H. Geballe and A. Kapitulnik, "Growth and Properties of Sputtered High-T_c Oxide Thin Films," *IEEE Trans. Mag.* **25**, 2422 (1989).

[90] C. B. Eom, J. Z. Sun, K. Yamamoto, A. F. Marshall, K. E. Luther, T. H. Geballe and S. S. Laderman, "*In Situ* Grown $YBa_2Cu_3O_{7-d}$ Thin Films from Single-Target Magnetron Sputtering," *Appl. Phys. Lett.* **55**, 595 (1989).

[91] A. Inam, M. S. Hegde, X. D. Wu, T. Venkatesan, P. England, P. F. Miceli, E. W. Chase, C. C. Chang, J. M. Tarascon and J. B. Wachtman, "As-Deposited High T_c and J_c Superconducting Thin Films Made at Low Temperatures," *Appl. Phys. Lett.* **53**, 908 (1988).

[92] T. Venkatesan, X. D. Wu, B. Dutta, A. Inam, M. S. Hegde, D. M. Hwang, C. C. Chang, L. Nazar and B. Wilkens, "High-Temperature Superconductivity in Ultrathin Films of $Y_1Ba_2Cu_3O_{7-x}$," *Appl. Phys. Lett.* **54**, 581 (1989).

[93] M. Naito, R. H. Hammond, B. Oh, M. R. Hahn, J. W. P. Hsu, P. Rosenthal, A. F. Marshall, M. R. Beasley, T. H. Geballe and A. Kapitulnik, "Thin-Film Synthesis of the High-T_c Oxide Superconductor $YBa_2Cu_3O_7$ by Electron-Beam Codeposition," *J. Mater. Res.* **2**, 713 (1987).

[94] C. B. Eom, A. F. Marshall, S. S. Laderman, R. D. Jacowitz and T. H. Geballe, "Epitaxial and Smooth Films of *a*-Axis $YBa_2Cu_3O_7$," *Science* **249,** 1549 (1990).

[95] J. J. Kingston, F. C. Wellstood, P. Lerch, A. H. Miklich and J. Clarke, "Multilayer $YBa_2Cu_3O_x$-$SrTiO_3$-$YBa_2Cu_3O_x$ Films for Insulating Crossovers," *Appl. Phys. Lett.* **56,** 189 (1990).

[96] F. C. Wellstood, J. J. Kingston, M. J. Ferrari and J. Clarke, "Superconducting Thin-Film Flux Transformers of $YBa_2Cu_3O_{7-x}$," *Appl. Phys. Lett.* **57,** 1930 (1990).

[97] D. B. Mitzi, L. W. Lombardo, A. Kapitulnik, S. S. Laderman and R. D. Jacowitz, "Growth and Properties of Oxygen- and Ion-Doped $Bi_2Sr_2CaCu_2O_{8+\delta}$ Single Crystals," *Phys. Rev. B* **41,** 6564 (1990).

[98] W. Y. Lee, V. Y. Lee, J. Salem, T. C. Huang, R. Savoy, D. C. Bullock and S. S. P. Parkin, "Superconducting Tl-Ca-Ba-Cu-O Thin Films with Zero Resistance at Temperatures of up to 120 K," *Appl. Phys. Lett.* **53,** 329 (1988).

[99] M. J. Kirton and M. J. Uren, "Noise in Solid-State Microstructures: A New Perspective on Individual Defects, Interface States and Low-Frequency (1/*f*) Noise," *Adv. Phys.* **38,** 367 (1989).

[100] M. Matsuda and S. Kuriki, "Telegraph-Like Noise in Y-Ba-Cu Oxide Thin-Film dc SQUID's," *Appl. Phys. Lett.* **53,** 621 (1988).

[101] R. H. Ono, J. A. Beall, M. W. Cromar, P. M. Mankiewich, R. E. Howard and W. Skocpol, "Switching Noise in $YBa_2Cu_3O_x$ 'Macrobridges,'" *IEEE Trans. Mag.* **25,** 976 (1989).

[102] G. Jung, M. Bonaldi, S. Vitale and J. Konopka, "Random Telegraph Signals and Low Frequency Voltage Noise in Y-Ba-Cu-O Thin Films," *J. Appl. Phys.* (submitted).

[103] M. Johnson, M. J. Ferrari, F. C. Wellstood, J. Clarke, M. R. Beasley, A. Inam, X. D. Wu, L. Nazar and T. Venkatesan, "Random Telegraph Signals in High Temperature Superconductors," *Phys. Rev. B* **42,** 10792 (1990).

[104] C. E. Gough, M. S. Colclough, S. P. Harrop, M. N. Keene and C. M. Muirhead, "The Development of SQUID Magnetometers Using Bulk Ceramic Superconductors," *J. Less-Common Met.* **151,** 461 (1989).

[105] S. G. Hammond, S. P. Harrop, C. M. Muirhead, C. E. Gough, N. M. Alford and T. W. Button, "Noise Properties of Bulk 2-Hole SQUIDs of YBCO and BSCCO," *Physica C* **162-164,** 395 (1989).

[106] M. B. Ketchen, W. J. Gallagher, A. W. Kleinsasser, S. Murphy and J. R. Clem, "DC SQUID Flux Focuser," in *SQUID '85: Superconducting Quantum Interference Devices and their Applications,* Berlin, 1985, edited by H. Hahlbohm and H. Lübbig (Walter de Gruyter).

[107] M. J. Ferrari, J. J. Kingston, F. C. Wellstood and J. Clarke, "Flux Noise from Superconducting $YBa_2Cu_3O_{7-x}$ Flux Transformers," *Appl. Phys. Lett.* **58,** 1106 (1991).

[108] J. Clem, personal communication.

[109] M. B. Weissman, "1/*f* Noise and Other Slow, Nonexponential Kinetics in Condensed Matter," *Rev. Mod. Phys.* **60,** 537 (1988).

[110] S. Machlup, "Noise in Semiconductors: Spectrum of a Two-Parameter Random Signal," *J. Appl. Phys.* **25,** 341 (1954).

[111] C. W. Hagen and R. Griessen, "Distribution of Activation Energies for Thermally Activated Flux Motion in High-T_c Superconductors: An Inversion Scheme," *Phys. Rev. Lett.* **62,** 2857 (1989).

[112] J. Blezius, R. Akis, F. Marsiglio and J. P. Carbotte, "Penetration of a Magnetic Field in a Very Strong Coupling Superconductor," *Phys. Rev. B* **38,** 179 (1988).

[113] J. Rammer, "Magnetic Penetration Depth in $YBa_2Cu_3O_{9-\delta}$: Evidence for Strong Electron-Phonon Coupling?," *Europhys. Lett.* **5,** 77 (1988).

[114] D. R. Harshman, G. Aeppli, E. J. Ansaldo, B. Batlogg, J. H. Brewer, J. F. Carolan, R. J. Cava, M. Celio, A. C. D. Chaklader,

W. N. Hardy, S. R. Kreitzman, G. M. Luke, D. R. Noakes and M. Senba, "Temperature Dependence of the Magnetic Penetration Depth in the High-T_c Superconductor $Ba_2YCu_3O_{9-\delta}$: Evidence for Conventional *s*-Wave Pairing," *Phys. Rev. B* **36**, 2386 (1987).

[115] L. Krusin-Elbaum, R. L. Greene, F. Holtzberg, A. P. Malozemoff and Y. Yeshurun, "Direct Measurement of the Temperature-Dependent Magnetic Penetration Depth in Y-Ba-Cu-O Crystals," *Phys. Rev. Lett.* **62**, 217 (1989).

[116] M. Tinkham, "Resistive Transition of High-Temperature Superconductors," *Phys. Rev. Lett.* **61**, 1658 (1988).

[117] A. Sudbø and E. H. Brandt, "Flux-Line Tilt Moduli in Anisotropic Superconductors," *Phys. Rev. Lett.* **66**, 1781 (1991).

[118] T. P. Orlando, J. E. Mooij and H. S. J. van der Zant, "Phenomenological Model of Vortex Dynamics in Arrays of Josephson Junctions," *Phys. Rev. B* **43**, 10218 (1991).

[119] H. S. J. van der Zant, F. C. Fritschy, T. P. Orlando and J. E. Mooij, "Dynamics of Vortices in Underdamped Josephson-Junction Arrays," *Phys. Rev. Lett.* **66**, 2531 (1991).

[120] M. W. Coffey and J. R. Clem, "Unified Theory of Effects of Vortex Pinning and Flux Creep upon the rf Surface Impedance of Type-II Superconductors," *Phys. Rev. Lett.* **67**, 386 (1991).

[121] D. H. Wu and S. Sridhar, "Pinning Forces and Lower Critical Fields in $YBa_2Cu_3O_y$ Crystals: Temperature Dependence and Anisotropy," *Phys. Rev. Lett* **65**, 2074 (1990).

[122] K. R. Farmer, C. T. Rogers and R. A. Buhrman, "Localized-State Interactions in Metal-Oxide-Semiconductor Tunnel Diodes," *Phys. Rev. Lett.* **58**, 2255 (1987).

[123] K. S. Ralls and R. A. Buhrman, "Defect Interactions and Noise in Metallic Nanoconstrictions," *Phys. Rev. Lett.* **60**, 2434 (1988).

[124] M. J. Ferrari, M. Johnson, F. C. Wellstood, J. Clarke, P. A. Rosenthal, R. H. Hammond and M. R. Beasley, "Magnetic Flux

Noise in Thin-Film Rings of $YBa_2Cu_3O_{7-\delta}$," *Appl. Phys. Lett.* **53**, 695 (1988).

[125] M. J. Ferrari, M. Johnson, F. C. Wellstood, J. Clarke, A. Inam, X. D. Wu, L. Nazar and T. Venkatesan, "Low Magnetic Flux Noise Observed in Laser-Deposited *in situ* Films of $YBa_2Cu_3O_y$ and Implications for High-T_c SQUIDs," *Nature* **341**, 723 (1989).

[126] P. W. Anderson, "Theory of Flux Creep in Hard Superconductors," *Phys. Rev. Lett.* **9**, 309 (1962).

[127] P. W. Anderson and Y. B. Kim, "Hard Superconductivity: Theory of the Motion of Abrikosov Flux Lines," *Rev. Mod. Phys.* **36**, 39 (1964).

[128] M. Papoular, "On Dissipation and Noise in Weak Superfluidity: The Example of YBaCuO," *J. Phys. France* **50**, 1141 (1989).

[129] L. Wang, Y. Zhu, H. L. Zhao and S. Feng, "Theory of $1/f$ Magnetic Flux Noise in High-T_c Superconductors," *Phys. Rev. Lett.* **64**, 3094 (1990).

[130] J. Pelz and J. Clarke, "Dependence of $1/f$ Noise on Defects Induced in Copper Films by Electron Irradiation," *Phys. Rev. Lett.* **55**, 738 (1985).

[131] J. P. Pelz, *Flicker (1/f) Noise in Copper Films due to Radiation-Induced Defects* (Ph. D. thesis, University of California at Berkeley, 1987).

[132] C. T. Rogers and R. A. Buhrman, "Composition of $1/f$ Noise in Metal-Insulator-Metal Tunnel Junctions," *Phys. Rev. Lett.* **53**, 1272 (1984).

[133] J. Bernamont, "Fluctuations in the Resistance of Thin Films," *Proc. Phys. Soc. (London)* **49 (extra part)**, 138 (1937).

[134] A. van der Ziel, "On the Noise Spectra of Semi-Conductor Noise and of Flicker Effect," *Physica* **16**, 359 (1950).

[135] F. K. du Pré, "A Suggestion Regarding the Spectral Density of Flicker Noise," *Phys. Rev.* **78**, 615 (1950).

[136] A. L. McWhorter, "1/*f* Noise and Germanium Surface Properties," in *Semiconductor Surface Physics*, edited by R. H. Kingston (Univ. of Pennsylvania Press, Philadelphia, 1957), p. 207.

[137] Y. B. Kim, C. F. Hempstead and A. R. Strnad, "Critical Persistent Currents in Hard Superconductors," *Phys. Rev. Lett.* **9**, 306 (1962).

[138] Y. B. Kim, C. F. Hempstead and A. R. Strnad, "Flux Creep in Hard Superconductors," *Phys. Rev.* **131**, 2486 (1963).

[139] M. Johnson, M. J. Ferrari, F. C. Wellstood and J. Clarke, "Magnetic Flux Noise in High-T_c Superconductors," *Phys. Rev. Lett.* **66**, 1799 (1991).

[140] L. Wang, Y. Zhu, H. L. Zhao and S. Feng, "Wang *et al.* Reply," *Phys. Rev. Lett.* **66**, 1800 (1991).

[141] M. J. Ferrari, F. C. Wellstood, J. J. Kingston and J. Clarke, "Suppression of Magnetic Flux Noise in $YBa_2Cu_3O_{7-x}$ by a Supercurrent," *Phys. Rev. Lett.* **67**, 1346 (1991).

[142] M. J. Ferrari, M. Johnson, F. C. Wellstood, J. Clarke, D. Mitzi, P. A. Rosenthal, C. B. Eom, T. H. Geballe, A. Kapitulnik and M. R. Beasley, "Distribution of Flux-Pinning Energies in $YBa_2Cu_3O_{7-\delta}$ and $Bi_2Sr_2CaCu_2O_{8+\delta}$ from Flux Noise," *Phys. Rev. Lett.* **64**, 72 (1990).

[143] P. Dutta and P. M. Horn, "Low-Frequency Fluctuations in Solids: 1/*f* Noise," *Rev. Mod. Phys.* **53**, 497 (1981).

[144] R. H. Koch and A. P. Malozemoff, "Magnetic Properties of High Temperature Superconductors -- Implications for 1/*f* Noise in SQUIDs," in *Proceedings of the First International Symposium on Superconductivity*, Nagoya, Japan, 1988, edited by K. Kitazawa and T. Ishiguro (Springer-Verlag).

[145] M. Inui, P. B. Littlewood and S. N. Coppersmith, "Pinning and Thermal Fluctuations of a Flux Line in High-Temperature Superconductors," *Phys. Rev. Lett.* **63**, 2421 (1989).

[146] M. Foldeaki, M. E. McHenry and R. C. O'Handley, "Flux Expulsion and Penetration in Superconducting $YBa_2Cu_3O_{7-\delta}$," *Phys. Rev. B* **39,** 2883 (1989).

[147] A. Gurevich, "Distribution of Pinning Energies and the Resistive Transition in Superconducting Films," *Phys. Rev. B* **42,** 4857 (1990).

[148] V. A. Atsarkin, G. A. Vasneva, V. V. Demidov and N. E. Noginova, "Fast Magnetic Relaxation Detected by Transient rf and Microwave Absorption in High-T_c Oxides," *Solid State Commun.* **74,** 603 (1990).

[149] S. Martin and A. F. Hebard, "Hierarchically Occupied Pinning Distributions and Vortex Transport in Superconductors," *Phys. Rev. B* **43,** 6253 (1991).

[150] J. Mannhart, P. Chaudhari, D. Dimos, C. C. Tsuei and T. R. McGuire, "Critical Currents in [001] Grains and across their Tilt Boundaries in $YBa_2Cu_3O_7$ Films," *Phys. Rev. Lett.* **61,** 2476 (1988).

[151] S. Tahara, S. M. Anlage, C. B. Eom, D. K. Fork, T. H. Geballe and M. R. Beasley, "Critical Current Behavior in Narrow $YBa_2Cu_3O_{7-\delta}$ Thin Films," *Physica C* **162-164,** 1175 (1989).

[152] S. Tahara, S. M. Anlage, J. Halbritter, C. B. Eom, D. K. Fork, T. H. Geballe and M. R. Beasley, "Critical Currents, Pinning, and Edge Barriers in Narrow $YBa_2Cu_3O_{7-\delta}$ Thin Films," *Phys. Rev. B* **41,** 11203 (1990).

[153] E. Zeldov and N. M. Amer, "Flux-Pinning Energies in High-T_c Superconductors," *Phys. Rev. Lett.* **65,** 278 (1990).

[154] R. Griessen, "Resistive Behavior of High-T_c Superconductors: Influence of a Distribution of Activation Energies," *Phys. Rev. Lett.* **64,** 1674 (1990).

[155] N. Missert, personal communication.

[156] P. H. Kes, J. Aarts, V. M. Vinokur and C. J. van der Beek, "Dissipation in Highly Anisotropic Superconductors," *Phys. Rev. Lett.* **64,** 1063 (1990).

[157] S. Theodorakis, "Theory of Vortices in Weakly-Josephson-Coupled Layered Superconductors," *Phys. Rev. B* **42,** 10172 (1990).

[158] M. Tachiki and S. Takahashi, "Strong Vortex Pinning Intrinsic in High-T_c Oxide Superconductors," *Solid State Commun.* **70,** 291 (1989).

[159] S. Senoussi and C. Aguillon, "Anisotropy of the Irreversible Magnetization and the First Critical Field $H_{c1}(\theta)$ of $YBa_2Cu_3O_7$ Oriented Crystallites," *Europhys. Lett.* **12,** 273 (1990).

[160] W. K. Kwok, U. Welp, V. M. Vinokur, S. Fleshler, J. Downey and G. W. Crabtree, "Direct Observation of Intrinsic Pinning by Layered Structure in Single-Crystal $YBa_2Cu_3O_{7-\delta}$," *Phys. Rev. Lett.* **67,** 390 (1991).

[161] J. H. Scofield, J. V. Mantese and W. W. Webb, "Temperature Dependence of Noise Processes in Metals," *Phys. Rev. B* **34,** 723 (1986).

[162] F. C. Wellstood, J. J. Kingston and J. Clarke, "Superconducting Thin-Film Multiturn Coils of $YBa_2Cu_3O_{7-x}$," *Appl. Phys. Lett.* **56,** 2336 (1990).

[163] J. J. Kingston, F. C. Wellstood, D. Quan and J. Clarke, "Photolithographically Patterned Thin-Film Multilayer Devices of $YBa_2Cu_3O_{7-x}$," *IEEE Trans. Mag.* **27,** 974 (1991).

[164] R. Simon, "High-T_c Thin Films and Electronic Devices," *Physics Today* **44** (6), 64 (June 1991).

[165] M. Schroeder, *Fractals, Chaos, Power Laws: Minutes from an Infinite Paradise* (W. H. Freeman, New York, 1991).

[166] E. Marinari, G. Parisi, D. Ruelle and P. Windey, "Random Walk in a Random Environment and $1/f$ Noise," *Phys. Rev. Lett.* **50,** 1223 (1983).

[167] E. Marinari, G. Parisi, D. Ruelle and P. Windey, "On the Interpretation of $1/f$ Noise," *Commun. Math. Phys.* **89,** 1 (1983).

[168] D. R. Nelson, "Vortex Entanglement in High-T_c Superconductors," *Phys. Rev. Lett.* **60,** 1973 (1988).

[169] E. M. Chudnovsky, "Pinning by Oxygen Vacancies in High-T_c Superconductors," *Phys. Rev. Lett.* **65,** 3060 (1990).

[170] C. Gerber, D. Anselmetti, J. G. Bednorz, J. Mannhart and D. G. Schlom, "Screw Dislocations in High-T_c Films," *Nature* **350,** 279 (1991).

[171] M. Hawley, I. D. Raistrick, J. G. Beery and R. J. Houlton, "Growth Mechanism of Sputtered Films of $YBa_2Cu_3O_7$ Studied by Scanning Tunneling Microscopy," *Science* **251,** 1587 (1991).

[172] R. Labusch, "Calculation of the Critical Field Gradient in Type II Superconductors," *Crystal Lattice Defects* **1,** 1 (1969).

[173] R. Griessen, C. W. Hagen, J. Lensink and D. G. de Groot, "Distribution of Activation Energies in High Temperature Superconductors," *Physica C* **162-164,** 661 (1989).

[174] G. J. Dolan, G. V. Chandrashekhar, T. R. Dinger, C. Feild and F. Holtzberg, "Vortex Structure in $YBa_2Cu_3O_7$ and Evidence for Intrinsic Pinning," *Phys. Rev. Lett.* **62,** 827 (1989).

[175] D. Dimos, P. Chaudhari, J. Mannhart and F. K. LeGoues, "Orientation Dependence of Grain-Boundary Critical Currents in $YBa_2Cu_3O_{7-\delta}$," *Phys. Rev. Lett.* **61,** 219 (1988).

[176] J. Mannhart, R. Gross, K. Hipler, R. P. Huebener, C. C. Tsuei, D. Dimos and P. Chaudhari, "Spatially Resolved Observation of Supercurrents Across Grain Boundaries in YBaCuO Films," *Science* **245,** 839 (1989).

[177] C. J. Lobb, D. W. Abraham and M. Tinkham, "Theoretical Interpretation of Resistive Transition Data from Arrays of Superconducting Weak Links," *Phys. Rev. B* **27,** 150 (1983).

[178] P. L. Gammel, D. J. Bishop, G. J. Dolan, J. R. Kwo, C. A. Murray, L. F. Schneemeyer and J. V. Waszczak, "Observation of Hexagonally Correlated Flux Quanta in $YBa_2Cu_3O_7$," *Phys. Rev. Lett.* **59**, 2592 (1987).

[179] T. Shaw, personal communication.

[180] V. N. Glyantsev, I. M. Dmitrenko, V. V. Borzenets and V. I. Shnyrkov, "Inherent Magnetic Noise in HTS Ceramics in the Phase Transition Region," *Sov. J. Low Temp. Phys.* **15**, 554 (1989).

[181] K. A. Müller, M. Takashige and J. G. Bednorz, "Flux Trapping and Superconductive Glass State in La_2CuO_{4-y}:Ba," *Phys. Rev. Lett.* **58**, 1143 (1987).

[182] M. Suenaga, A. K. Ghosh, Y. Xu and D. O. Welch, "Irreversibility Temperatures of Nb_3Sn and Nb-Ti," *Phys. Rev. Lett.* **66**, 1777 (1991).

LAWRENCE BERKELEY LABORATORY
UNIVERSITY OF CALIFORNIA
INFORMATION RESOURCES DEPARTMENT
BERKELEY, CALIFORNIA 94720